APPLICATION OF DISSOLUTION DYNAMIC NUCLEAR POLARIZATION TO THE CHARACTERIZATION OF REACTIONS INVOLVING LARGE MOLECULES

A Dissertation

by

YOUNGBOK LEE

Submitted to the Office of Graduate Studies of
Texas A&M University
in partial fulfillment of the requirements for the degree of

DOCTOR OF PHILOSOPHY

Approved by:

Chair of Committee,	Christian Hilty
Committee Members,	David P. Barondeau
	Wenshe Liu
	Ryland Young
Head of Department,	David H. Russell

May 2013

Major Subject: Chemistry

ABSTRACT

Nuclear magnetic resonance (NMR) spectroscopy is one of the most important analytical tools for organic and biological chemistry. It provides not only detailed information on the structure of small molecules and macromolecules, but also on molecular interactions. Because of the inherent low sensitivity of NMR, a long signal averaging time or a high spin concentration is often required. A variety of methods have been explored to improve the sensitivity of NMR. Especially, large signal gains can be obtained by hyperpolarization of the nuclear spins. NMR signals of hyperpolarized samples are enhanced by several orders of magnitude. Dissolution Dynamic Nuclear Polarization (D-DNP) is a versatile technique capable of polarizing many different nuclei in the solid state, and subsequently providing a hyperpolarized liquid sample following a dissolution step. The resulting signal enhancement has made it possible to obtain detailed information in research fields as varied as metabolic imaging or enzyme catalysis. This dissertation aims to extend the applicability of D-DNP into new areas of chemistry, which involve the characterization of interactions and reactions involving large molecules.

In a first project, fluorine hyperpolarization is exploited to investigate protein-ligand interactions. The enhancement of ^{19}F signal allows for the detection of submicromolar concentrations of fluorinated ligands in the strong-, intermediate-, and weak-binding regimes. Several NMR parameters are utilized to observe ligand binding to the macromolecule, and to determine dissociation constants.

In a second project, competitive binding of ligands to the same binding pocket on a protein is investigated. Here, polarization flows from a first ligand hyperpolarized on protons to the protein, and then to the second ligand. The buildup in function of time of the signals due to this relayed nuclear Overhauser effect contains structural information on the binding epitope.

In a third project, the aim is to directly detect a larger molecule, a polymer, which has been synthesized starting from hyperpolarized monomers. Using DNP, single scan observation of ^{13}C, a common nucleus with large chemical shift dispersion, is possible. Time resolved ^{13}C NMR spectroscopy in combination with kinetic models permits the description of polymerization reaction of the living anionic polymerization of styrene. In summary, several approaches have been investigated for utilizing a large hyperpolarization initially produced on small molecules, for the benefit of characterizing properties of macromolecules. These developments extend the capabilities of D-DNP and demonstrate the potential for leading to new applications in fields as diverse as drug discovery and polymer science.

DEDICATION

To my parents and lovely wife

ACKNOWLEDGEMENTS

I would like to express the deepest appreciation to my advisor, Dr. Christian Hilty for his excellent guidance, patience, and providing me with an excellent atmosphere for doing research. Without his guidance and continuance help, this dissertation would not have been possible.

I would also like to thank my committee members, Dr. David P. Barondeau, Dr. Wenshe Liu, and Dr. Ryland Young for guiding my research and helping me to develop my background in chemistry.

I am thankful to Hilty group members, Hsuh-Ying Chen, Mukundan Ragavan, Giridhar Sekar, Guannan Zhang, Hlaing Min, Yaewon Kim, Chia-Hsiu Chen, Sean Bowen, and Soyoun Hwang, for sharing their idea and for comments on my work. Especially, I am grateful to Haifeng Zeng for numerous discussions and collaborations.

I am also grateful to my collaborators, Dr. Christian Giresinger, Dr. Donghan Lee, Dr. Alvar Gossert, Dr. Karen Wooley, and Gyu Seong Heo, for their valuable discussions and supports on many projects.

I am thankful to my Master advisor, Dr. Hoeil Chung for teaching me how to do research.

I would like to thank my parents. They were always supporting me an encouraging me with their best wishes.

Finally, I heartily thank my wife, Hyounju Kang. She was excellent as my loyal wife, standing by me through thick and thin.

NOMENCLATURE

1D	One Dimensional
2D	Two Dimensional
3D	Three Dimensional
BAEE	N_{α}-benzoyl-$_{L}$-arginine ethyl ester
BAME-d_3	N_{α}-benzoyl-$_{L}$-arginine methyl-d_3 ester
BBO	Broadband Observe
BDPA	α,γ-bisdiphenylene-β-phenylallyl
$CDCl_3$	Deuterated cholroform
CIDNP	Chemically Induced Dynamic Nuclear Polarization
CPMG	Carr-Purcell-Meibom-Gill
D-DNP	Dissolution Dynamic Nuclear Polarization
DMSO	Dimethyl Sulfoxide
DNP	Dynamic Nuclear Polarization
ESR	Electron Spin Resonance
EPR	Electron Paramagnetic Resonance
ESSI	Electron Spin-Spin Interaction
EZ	Electron Zeeman
FAXS	Fluorine chemical shift Anisotropy and eXchange for Screening
FID	Free Induction Decay

FMBC	3-fluoro-4-methylbenzenecarboximidamide hydrochloride
Gd(DTPA)	Gadolinium (III) diethyltriaminepentaacetic acid
HMQC	Heteronuclear Multiple-Quantum Correlation
HPLC	High-Performance Liquid Chromatography
HSQC	Heteronuclear Single Quantum Correlation
HYPER-BIOP-NOE	Hyperpolarized Binding Pocket NOE
INEPT	Insensitive Nuclei Enhanced by Polarization Transfer
INPHARMA	Interligand Polarization Transfer for Pharmacophore Mapping
IUPAC	International Union of Pure and Applied Chemistry
MALDI	Matrix Assisted Laser Desorption Ionization
MAS	Magic angle spinning
MOF	Metal-Organic Frameworks
MRI	Magnetic Resonance Imaging
MRS	Magnetic Resonance Spectroscopy
MW	Microwave
NMR	Nuclear Magnetic Resonance
NOE	Nuclear Overhauser Effect
NOESY	Nuclear Overhauser Effect Spectroscopy
NZ	Nuclear Zeeman
O-DNP	Overhauser Dynamic Nuclear Polarization
OX63	tris (8-carboxyl-2,2,6,6-tetra[2-(1-hydroxymethyl)]-benzo(1,2-d:4,5-d')bis(1,3)dithiole-4-yl) methyl sodium salt

PBS	Phosphate Buffered Saline
PEEK	Poly Ether Ether Ketone
PKA	Protein Kinase A
ppm	Parts per million
PHIP	Parahydrogen Induced Polarization
RF	Radio Frequency
RMSD	Root Mean Square Deviation
SABRE	Signal Amplification By Reversible Exchange
SE	Solid Effect
S.I.	Selective Inversion
SIOP	Spin Exchange Optical Pumping
SPINOE	Spin Polarization–Induced Nuclear Overhauser Effect
SS-DNP	Solid State Dynamic Nuclear Polarization
STD	Saturation Transfer Difference
TCEP	tris(2-carboxyethyl)phosphine
TEMPO	(2,2,6,6-Tetramethylpiperidin-1-yl)oxyl
TEMPOL	4-Hydroxy-2,2,6,6-tetramethylpiperidine-1-oxyl
THF	Tetrahydrofuran
TFA	Sodium trifluoroacetate
TFBC	4-(Trifluoromethyl)benzene-1-carboximidamide hydrochloride
TFMCPP	4-(trifluoromethyl)-1,5,6,7-tetrahydro-2*H*-cyclopenta[*b*]pyridin-2-One

TMSCl	Trimethylchlorosilane
TOTAPOL	1-(TEMPO-4-oxy)-3-(TEMPO-4-amino)propan-2-ol
TROSY	Transverse Relaxation-Optimized Spectroscopy
UV-VIS	Ultraviolet-Visible

TABLE OF CONTENTS

LIST OF FIGURES

FIGURE Page

FIGURE Page

FIGURE Page

FIGURE Page

LIST OF TABLES

CHAPTER I

INTRODUCTION

NMR Spectroscopy

Nuclear magnetic resonance (NMR) spectroscopy in the liquid state is an important analytical technique that provides not only structural information with atomic resolution but can also be used to study molecular interactions of small organic molecules and macromolecules.[1] The characteristics of molecules are reflected in the chemical shifts, which are dependent on the electronic structure around each nucleus (shielding effects), and which are the most prominent NMR observable parameters.[2-3] Different functional groups in small molecules can readily be identified with one dimensional (1D) NMR spectroscopy of ^{1}H, ^{13}C, ^{15}N, or other NMR observable nuclei. As the nuclear spins interact with each other either through bonds by scalar coupling (*J*-coupling)[4-5] or through space by dipolar coupling (Nuclear Overhauser Effect: NOE),[6-9] structural information about a molecule can be obtained. In addition, numerous NMR parameters including longitudinal relaxation rate, transverse relaxation rate, chemical shift change, and linewidth, are useful as probes to study molecular dynamics and interactions.[10-17] Due to these benefits, NMR is widely applied in fields, such as chemistry, and biochemistry.

Sensitivity of NMR

Despite the versatility of NMR spectroscopy, the use of this technique is often restricted by an intrinsically low sensitivity, which appears to be its most severe drawback. The sensitivity limitation is prompted by a small Zeeman energy splitting of nuclear spin states, which for a spin ½ nucleus such as ^{1}H, ^{13}C, ^{15}N are spin up (α: parallel to the external magnetic field) and spin down (β: anti-parallel). The small energy difference gives rise to only a slight population difference of the two energy levels. Unfortunately, the achievable NMR signal is proportional to this initial population difference, rather than the total number of spins. This property of the NMR signal is expressed with the concept of the spin polarization level, which is defined as

$$P = \frac{n_\alpha - n_\beta}{n_\alpha + n_\beta} = \tanh\left(\frac{\gamma \cdot \hbar \cdot B_0}{2 \cdot k \cdot T}\right) \qquad (-1)$$

where n_α, n_β is nuclear populations of the two states. The variables $\gamma, \hbar, B_0$ represent the gyromagnetic ratio, reduced Planck constant, and magnetic field. The variables k, T represent Boltzmann constant, and temperature, respectively. As pointed out in Equation (-1), the polarization level increases when the external magnetic field is increased, or when the temperature is decreased. Since the advent of the first commercial NMR spectrometer (Varian 30 MHz NMR) in 1952,[18] the approaches for enhancing the polarization level have mainly relied on building stronger superconducting magnets.[19] Nevertheless, the polarization level of ^{1}H, the most sensitive of the commonly used spins, at room temperature is just 8×10^{-5} even in a 23.5 T magnet (1000 MHz ^{1}H frequency). Alternatively, a high polarization level of ^{1}H spins can be achieved when the

NMR measurement is conducted at low temperature. For example, spectra of ^{1}H enhanced by a factor of 80 can be observed by solid state NMR measurement at ~ 7 K.[20] However, acquiring NMR spectra at the low temperature is still very technically challenging.

A variety of other experimental approaches have been developed to enhance the sensitivity of NMR spectroscopy. Ernst and Anderson suggested the pulsed Fourier transform (FT) NMR experiment.[21] A 10 times higher sensitivity in the FT technique compared with the previously available spectral sweep method was observed by reducing a spectral acquisition time.[21] Morris and Freeman proposed the enhancement of signals from insensitive nuclei such as ^{15}N, or ^{29}Si by polarization transfer from protons, which carry a higher polarization. This technique is called insensitive nuclei enhanced by polarization transfer (INEPT).[22] Subsequently, Bodenhausen and Ruben created the heteronuclear single quantum coherence (HSQC) spectroscopy, where the INEPT technique was applied to improve the sensitivity of ^{15}N nuclei.[23] For structural studies of large proteins, transverse relaxation-optimized spectroscopy (TROSY) was proposed by Wüthrich and coworkers.[24] This technique addresses a limitation of carrying out NMR spectroscopy of large molecules, where transverse relaxation rates are fast. With the TROSY scheme, linewidthes of ^{1}H and ^{15}N spins in proteins were reduced by 60% and 40% when compared with a conventional 2D correlation experiment by making use of a cancellation of two main relaxation mechanisms (dipole-dipole interactions and chemical shift anisotropy). Resulting signal enhancements were quoted as 2 to ~ 5 times.[24]

Several-fold improvements in signal strength have been achieved by improvements in NMR probe technology in the past several decades.[19] Styles et al. first proposed cryogenically cooled probe technology in which electrical noise is reduced by cooling the NMR coils and preamplifier with helium gas.[25] Using a cryogenically cooled probe, the sensitivity is enhanced by up to about four times when compared with the sensitivity of a conventional NMR probe at the same magnetic field strength.[25]

These efforts to improve sensitivity have made NMR spectroscopy an increasingly attractive and powerful analytical technique. Nevertheless, none of these approaches directly address the low initial polarization of nuclear spins at room temperature. As a consequence, further research to increase nuclear spin polarization in NMR experiments is important. Significant current effort is focused in the development and application of hyperpolarization techniques.[26-27] Hyperpolarization denotes a nuclear spin polarization far beyond that achievable under equilibrium conditions even in a strong magnet. Hyperpolarization techniques therefore represent some of the most powerful methods for signal enhancement in NMR spectroscopy.

Common Hyperpolarization Techniques

Hyperpolarized nuclear spin states have been produced in several different ways. In this section, four common hyperpolarization methods are discussed: parahydrogen induced polarization (PHIP), optical pumping, chemically induced dynamic nuclear polarization (CIDNP), and dynamic nuclear polarization (DNP).

Parahydrogen Induced Polarization

Parahydrogen induced polarization (PHIP) was first demonstrated by Bowers and Weitekamp in 1986. A reaction of acrylonitrile with parahydrogen was performed using Wilkinson's catalyst, resulting in increased spin polarization of the reaction product.[28-29] Hydrogen molecules exist in two isomeric spin states, a triplet state (total nuclear spin I=1; orthohydrogen) and a singlet state (total nuclear spin I=0; parahydrogen). The ratio between the former and the latter is ~ 3:1 at a thermal equilibrium and a room temperature.[30] Since the total nuclear spin of parahydrogen is zero, it cannot provide any NMR signals. However, the introduction of the parahydrogen into an unsaturated target molecule breaks the symmetry, resulting in enhanced population differences of the nuclear spin states. The parahydrogen-induced polarization technique has been utilized to investigate organometallic chemistry[31-34] as well as for magnetic resonance imaging.[35-38]

Separately from the previous approaches, where a molecule of hydrogen is directly incorporated into a target molecule, recent research indicates that a high level of nuclear polarization can also be achieved when a target molecule and parahydrogen make reversible coordination bonds with a metal center (SABRE; Signal Amplification By Reversible Exchange).[39] In the SABRE method,[39] the parahydrogen is first bound reversibly to the metal center, without a direct contact with the target molecule. At a subsequent time, the hyperpolarization derived from the parahydrogen with the metal center is transferred to the target molecule. Since the SABRE method does not require a

hydrogenation reaction, its use is not limited to specific substrates containing unsaturated functional groups.

Optical Pumping

In optical pumping, circularly polarized laser light is used to excite electron of alkali metals (typically rubidium, or cesium) from a lower energy state to a higher energy state. Nobel gas (^{129}Xe, or ^{3}He) and Quenching gas (normally N_2) transfer electrons of alkali metal between two sublevels of the excited state (collisional mixing), and deexcites the electrons from the higher energy states to the ground energy states (quenching) by collision. These collisional mixing and quenching processes make population differences between two sublevels of the ground state, resulting in enhanced electron spin polarization of the metal. Subsequently, the electron spin polarization of the alkali metal can then be transferred to nuclear spins of the noble gases through collisions. This process is known as spin exchange optical pumping (SIOP).[40] The optical pumping technique has been utilized for magnetic resonance imaging (MRI) of lungs and other organs, as well as for characterization of porous materials.[41-45] In addition to the spin exchange optical pumping process, the polarization level of nuclear spins in the solution state can be selectively increased through the spin polarization-induced NOE (SPINOE) effect that arises due to interaction with a polarized noble gas.[46] The SPINOE in combination with optical pumping has been applied to the study of protein surfaces,[47-48] and lipid membranes.[49]

Chemically Induced Dynamic Nuclear Polarization

Chemically induced dynamic nuclear polarization (CIDNP) was discovered by Ward and Lawler in 1967. Enhanced absorptive and emissive NMR signals were detected from chemical reactions with organolithium compounds.[50] The radical pair mechanism, which is a cyclic photochemical process, explained the most common cause of CIDNP.[51-54] CIDNP has been applied to the study of proteins. Here, flavin mononucleotide or its derivatives are used as a photosensitizer. The photo-excited dye in its triplet state induced by laser irradiation takes a single electron from a specific amino acid residue (normally tryptophan, histidine, or tyrosine). The residue is oxidized after the interaction with the dye, resulting in the formation of a transient triplet radical pair. Two competing reaction paths that are identified with the recombination (singlet-triplet mixing) product and the escape product (radical separation) affect the outcome of the transient radical pair.[55-56] Thus, the nuclear spin states of the residue can be controlled by the exchange rate between the two products, which gives rise to enhanced NMR intensities. CIDNP provides site specific enhancements, which have been used for the surface characterization of proteins,[57-60] protein folding,[61-62] and interactions proteins with oligonucleotide and carbohydrates.[63-64]

Dynamic Nuclear Polarization

Overhauser initially demonstrated the theoretical framework for the DNP mechanism in 1953 (Overhauser effect),[7] and Carver and Slichter proved it experimentally with metallic lithium in solid state and sodium ammonia solution in liquid.[65-67] In the DNP processes, electron spin polarization is transferred to the nuclear spin polarization by saturating EPR transitions of the metal, where maximum enhancement of nuclear spin polarization by DNP processes is determined by the ratio of gyromagnetic ratios between electron and nuclear spin (e.g. $\gamma_e / \gamma_{^1H} \sim 660$).

Since the Overhauser effect was first presented, additional DNP mechanisms have been identified by several researchers. Pound, Abragam, and Jeffries discovered a DNP mechanism in the solid state that is now known as the solid effect.[68-71] Borghini proposed spin temperature models for DNP (thermal mixing).[72-73] Kessenikh proposed a three-spin system with two electrons and one nucleus describing DNP polarization mechanism (cross effect), which was validated by Hwang, Hill, and Wollan later.[74-77] For these DNP processes, organic radicals, which are the source of the free electron spins, should be involved. Figure I-1 represents common radical structures. These radicals are stable and inert under most common conditions. DNP is a more generally useful technique than the other hyperpolarization techniques since most of the nuclear spins in molecules can be polarized by the DNP processes.

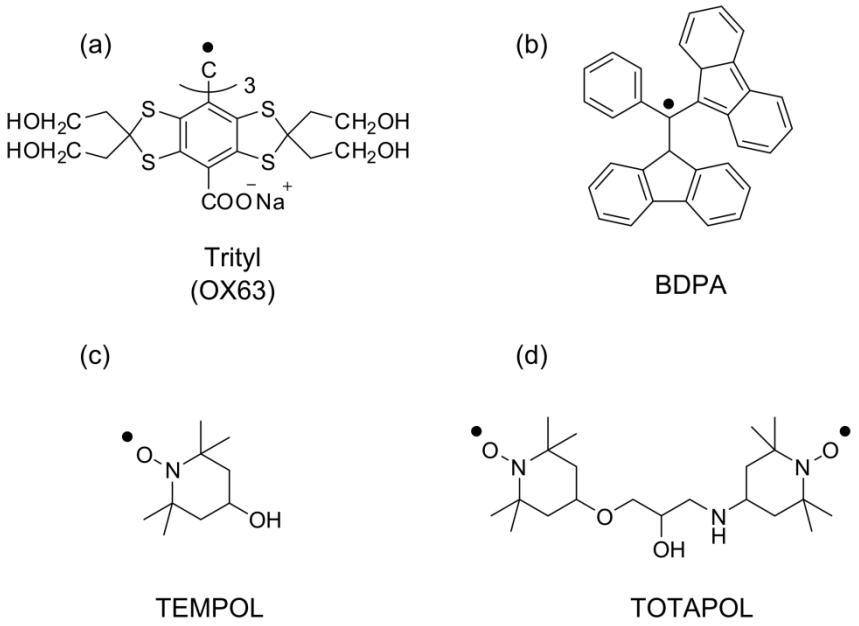

Figure I-1 : Common radical structures for the DNP experiments. (a) OX63; tris[8-carboxyl-2,2,6,6-tetra[2-(1-hydroxyethyl)]-benzo(1,2-d:4,5-d)bis(1,3)dithiole-4-yl]methyl sodium salt. (b) BDPA; α,γ-bisdiphenylene-β-phenylallyl. (c) TEMPOL; 4-Hydroxy-2,2,6,6-tetramethylpiperidine-1-oxyl. (d) TOTAPOL; 1-(TEMPO-4-oxy)-3-(TEMPO-4-amino)propan-2-ol.

DNP mechanisms

Overhauser Effect

The Overhauser effect is the only mechanism that polarizes nuclear spins directly in the liquid state. The polarization transfer in the liquid state results from cross relaxation processes (flip-flop (W_0) and flip-flip (W_2)), following a saturation of an EPR line of the electron (W_S).[78] The cross relaxation processes is due to the dipolar and scalar interactions between electron and nuclear spins, which are governed by rotational and translational molecular motions in the liquid state. These processes raise the population differences of the nuclear spins, giving rise to hyperpolarization of the nuclear spins.

Figure I-2 represents the energy diagram of a coupled system of an electron- and a nuclear spin. Electron and nuclear transitions are symbolized by W_S and W_I.

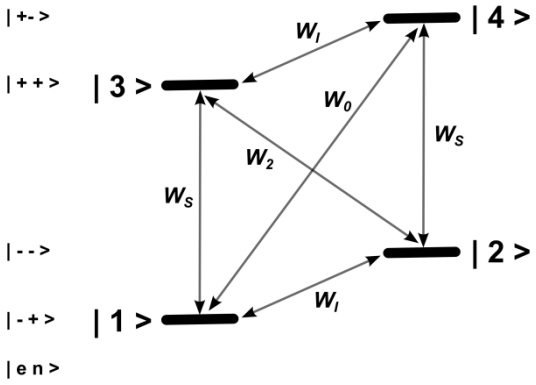

Figure I-2 : Energy level diagram for the Overhauser effect; *S* and *I* represent the electron spin and the nuclear spin, respectively. W_S and W_I are EPR and NMR transitions. W_0 and W_2 are zero and double quantum transitions.

The overall polarization enhancement (ε) is dependent on three parameters, ξ: coupling factor, f: leakage factor, s: saturation factor, as well as the ratio of gyromagnetic ratios between the electron and nucleus.

$$\varepsilon = \frac{\langle I_Z \rangle}{\langle I_{0,eq} \rangle} = 1 - \xi \cdot f \cdot s \cdot \frac{|\gamma_e|}{\gamma_N} \qquad (-2)$$

The elements $\langle I_Z \rangle$ and $\langle I_{0,eq} \rangle$ represent the expectation value of the nuclear polarization and the value in thermal equilibrium, respectively. The coupling factor (ξ) reflects the impact of the transition probability, which is described by a ratio between the cross-relaxation rates ($W_2 - W_0$) and auto-relaxation rates ($W_2 + 2W_I + W_0$). Since the coupling factor is almost zero at high magnetic fields (~ 10 T), the overall polarization enhancement (ε) is more efficient at low magnetic fields. The leakage factor (f) represents an influence of the electron spin on the nuclear spin relaxations. The

saturation factor (*s*) explains the degree of saturation of the electron transitions due to the influence of the microwave irradiation. When the electron transitions are fully saturated, the overall enhancement can be maximized. The saturation factor is governed by the microwave power and electron relaxations.

Solid Effect

In the solid effect, forbidden transitions (the flip-flip (W_2) and flip-flop (W_0) transitions) can directly enhance the nuclear polarization.[70] The hyperfine coupling leads to a mixing of spin states of the electron-nuclear coupled system under the influence of microwave irradiation. The mixed electronic and nuclear spin states make these forbidden transitions be allowed. As the hyperfine term becomes time-independent in the absence of molecular motions, the enhancement is directly obtained by saturating these forbidden transitions, using microwave irradiation at the frequency of $\omega_e - \omega_N$ (positive polarization, Figure I-3b), or $\omega_e + \omega_N$ (negative polarization, Figure I-3c). Under the proper assumptions—the relaxation rate of electrons (W_S) is much faster than the cross relaxation rates (W_2, W_0) and the nuclear relaxation rate (W_I), and the cross relaxation rates are much faster than the nuclear relaxation rate ($W_S \gg W_2$, $W_0 \gg W_I$)—, the theoretical enhancement becomes the gamma ratio (γ_e / γ_N). In order to obtain the maximum enhancement, frequencies of the forbidden transitions ($\omega_e \pm \omega_N$) should be completely resolved because simultaneous transitions with opposite enhancement signs may cancel each other when they are partially overlapped.

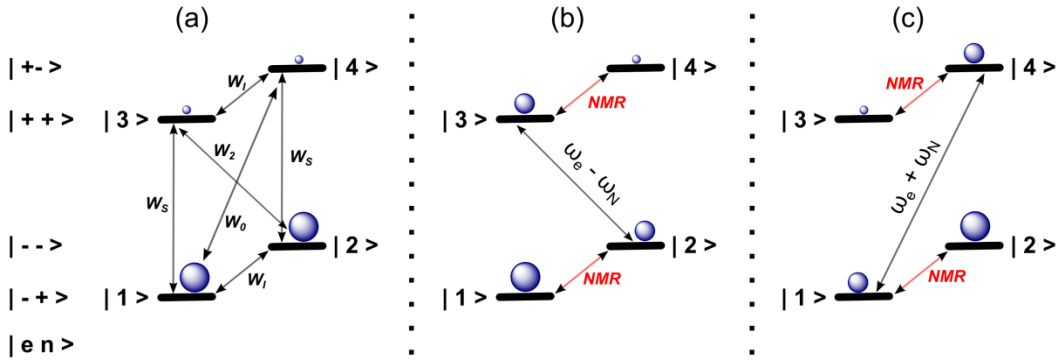

Figure I-3 : Energy level diagram for the solid effect. (a) two-spin system in thermal equilibrium condition. EPR and NMR transitions displayed with W_S and W_I. Transition frequencies for positive and negative enhancements are displayed in (b), and (c), respectively. Spin populations are represented with blue-colored circles.

Cross Effect

The cross effect was discovered in the 1960s by Kessenikh, Hwang, Hill, and Wollan.[74-77] This phenomenon was examined with polystyrene and a bis-phenly aroxyl radical. They observed that the two optimal microwave frequencies for positive and negative DNP enhancements moved closer together when the radical concentration was increased. The cross effect is explained by three-spin interactions, in which two dipolar coupled electrons $(\omega_{e1}, \omega_{e2})$ interact with one nuclear spin (ω_N). Since resonance frequencies of electron spins in solid state depend on their orientations and distances in an external magnetic field, proper radicals should be employed. In order to maximize the efficiency of the cross effect, the two EPR frequencies $(\omega_{e1}, \omega_{e2})$ should be split by the Larmor frequency of the nuclei ($\omega_{e1} - \omega_{e2} \approx \omega_N$). The energy level diagrams and possible transition lines for the three spin system are shown in Figure I-4. When the EPR transition is saturated with a microwave irradiation at the frequency of ω_{e1}, a positive

enhancement is observed (Figure I-4b). In the same manner, a negative enhancement is detected when applying the frequency of ω_{e2} (Figure I-4c). Maximum enhancement is obtained when the two energy levels |4> and |5> become degenerate ($\omega_{e1} - \omega_{e2} \approx \omega_N$) which is shown in Figure I-4b and c. It should be noted that the EPR frequencies (ω_{e1}, ω_{e2}) in the cross effect are different from the EPR frequency (ω_e) in the solid effect. Nitroxyl-based biradicals like TOTAPOL (Figure I-1), whose EPR spectra are inhomogeneously broadened by g-anisotropy, fulfill the conditions for the cross effect.[79] Unlike the solid effect, the mechanism of the cross effect relies on the allowed transitions resulting from electron spin-spin interactions. Thus, this condition induces much faster polarization build-up time compared to the time for the solid effect.[26]

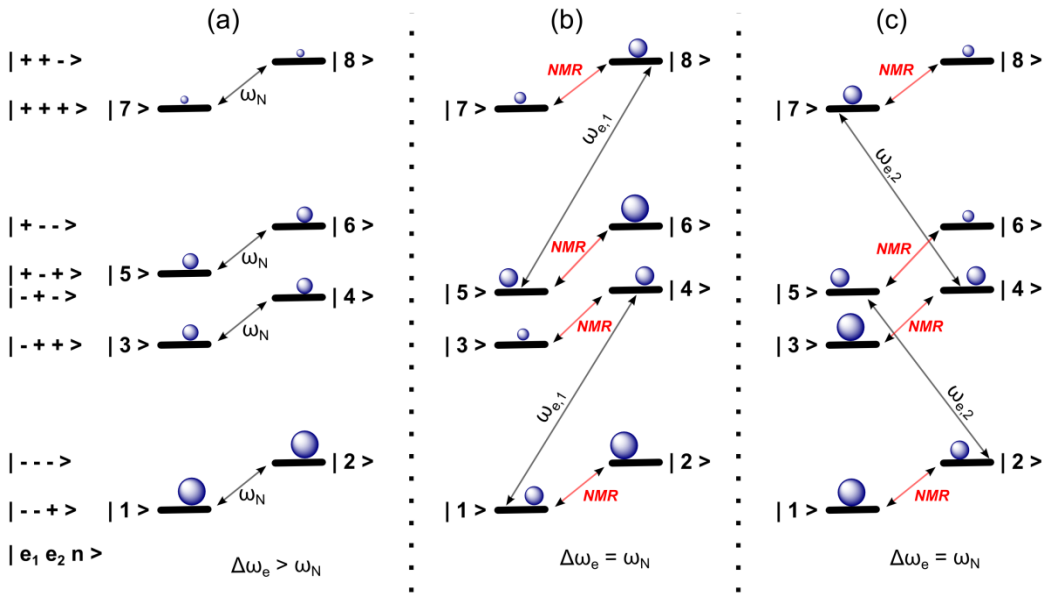

Figure I-4 : Energy level diagram for the cross effect. (a) three-spin system in a thermal equilibrium condition. Saturation of EPR transitions with microwave irradiation result in negative (b) or positive (c) enhancement of nuclear spin transitions. Spin populations are represented with blue-colored circles.

Thermal Mixing

In the thermal mixing, high radical concentrations, which cause homogeneously broadened EPR linewidth (δ) due to multiple dipolar coupled electrons, are involved, with the condition, $\delta > \omega_N$.[72, 80] As many electrons are involved in the DNP process, the spin temperature model with thermodynamic ensembles is a good explanation when the concept is too complex to define individual energy states. The theory describing thermal mixing (TM) was developed using the concept of thermodynamic ensembles of spin systems, based on the Provotov theory (spin temperature model).[81] The polarization transfer can be expressed with three interacting thermodynamic reservoirs: nuclear Zeeman (NZ), electron Zeeman (EZ), and electron spin-spin interaction (ESSI). The mechanism of thermal mixing is a consecutive two-step process. First, the spin temperature of the electron Zeeman reservoir (EZ) is cooled by irradiating at the microwave at a frequency of the allowed EPR transitions, leading to the cooling of the electron spin-spin interaction reservoir (ESSI). Second, the spin temperature of the nuclear Zeeman reservoir (NZ) is cooled by the three spins electrons-nuclear exchange process, since the nuclear Zeeman reservoir is in thermal contact with the electron spin-spin interaction reservoir (ESSI), giving rise to the hyperpolarization of the nuclear spin.

Experimental Arrangements and Applications

Overhauser DNP

Even though the Overhauser effect was initially discovered in metals, recently the main applications of Overhauser DNP (O-DNP) have been focused on polarizing molecules in liquid state. As the magnetic field is increased, the Overhauser effect becomes less efficient, resulting in two different experimental arrangements of potential benefit: i) polarize and measure the NMR spectrum at the same magnetic field, ii) polarize at a low magnetic field and measure the NMR spectrum at a high magnetic field by transferring the polarized sample. The first class of experimental setup was developed for the study of Overhauser magnetic resonance imaging by Wind and coworkers.[82] The Münnemann and Han groups used the experimental setup for a portable polarizer where relatively low magnetic fields (0.3 T ~ 1.4 T) were used to polarize water.[83-84] Hyperpolarization of water for an MRI contrast agent by the Overhauser DNP was investigated by the Han group.[85] The hyperpolarized water provided a contrast of signals from the background bulk water due to a substantial signal gain. Nuclear spin relaxation of the hyperpolarized water was utilized to study local water mobility on the surface of bio-macromolecules with site directed spin-labeling of water with nitroxide radicals.[86-87] Recently, the Han group also suggested *J*-coupling mediated ^{13}C O-DNP experiments for investigating the permeability of small molecules across phospholipid bilayers, an important consideration in drug delivery.[88] The second class of experimental setups has been developed by Dorn, Griesinger, and Bennati.[89-91] In this experimental setup, hyperpolarization first takes place in a low magnetic field (0.23 T ~ 0.34 T), and the

NMR spectrum is measured in a high magnetic field (4.7 T ~ 14.09 T) by way of shuttling of the polarized samples.

Solid-State DNP

Implementations of the DNP method for solid state NMR were described among others by Wind, Schaefer, and Griffin.[92-95] Solid state MAS spectroscopy in combination with the DNP technique (SS-DNP) has been used for signal enhancements for polymers, carbonaceous materials, diamonds[92-95] as well as biological macromolecules.[96] For the latter application, a new home-built gyrotron (cyclotron resonance maser) oscillator producing 100 W of 140 GHz irradiation was utilized.[95] Overall enhancements of 50 ~ 200 driven by thermal mixing were observed by employing cross polarization pulse sequences from the ^{1}H to ^{13}C or ^{15}N in the protein. In addition to the 1D SS-DNP experiments, SS-DNP enhanced 2D ^{13}C-^{13}C correlation spectroscopy provides nuclear spin connectivity. This method can be used for unambiguous chemical shift assignments in proteins. On the basis of Griffin's pioneering work in gyrotron-based DNP-MAS spectroscopy,[97-98] the SS-DNP technique has been extensively applied to study biological macromolecules and complexes, including amyloid fibers, peptides, membrane proteins, and bacteriophages.[99-103] Recently, the Griffin group determined the intermolecular structures of amyloid fibrils by using the 2D homonuclear ^{13}C-^{13}C and heteronuclear ^{15}N-^{13}C correlation experiments.[103] The Oschkinat group revealed a structure of a receptor-ligand-membrane complex in its natural condition without any sample purification.[101]

Solid-state DNP has also been utilized for materials characterizations. The Emsley group used DNP to enhance the NMR signal at the surface of a porous material.[104-105] The characteristics of surface adsorbed substrates, the distribution of surface bonding, and substrate-substrate interactions were studied by cross polarization spectroscopy (from ^{1}H to ^{13}C) or by 2D ^{1}H-^{29}Si correlation spectroscopy. The design of biradical, bis-cyclohexyl-TEMPO-bisketal helped to optimize signal enhancements.[106] The Emsley group also applied the SS-DNP technique to an analysis of powered microcrystalline solids and functionalized metal-organic frameworks (MOF).[107-108] In these work, 2D ^{13}C-^{13}C homonuclear and ^{1}H-^{13}C heteronuclear correlation experiments were conducted without any isotope labeling.[107-108]

Dissolution DNP

In 2003, Ardenkjær-Larsen and coworkers reported the first dissolution DNP (D-DNP) experiments in which ^{13}C-labeled urea was polarized in a glycerol-glassing agent with a trityl radical used as a free electron source.[109] In the D-DNP method, the polarization takes place at a cryogenic temperature (1.1 – 1.5 K). At this temperature, and in a moderate magnetic field (3.35 T), a high level of electron spin polarization persists, as illustrated in Figure I-5.

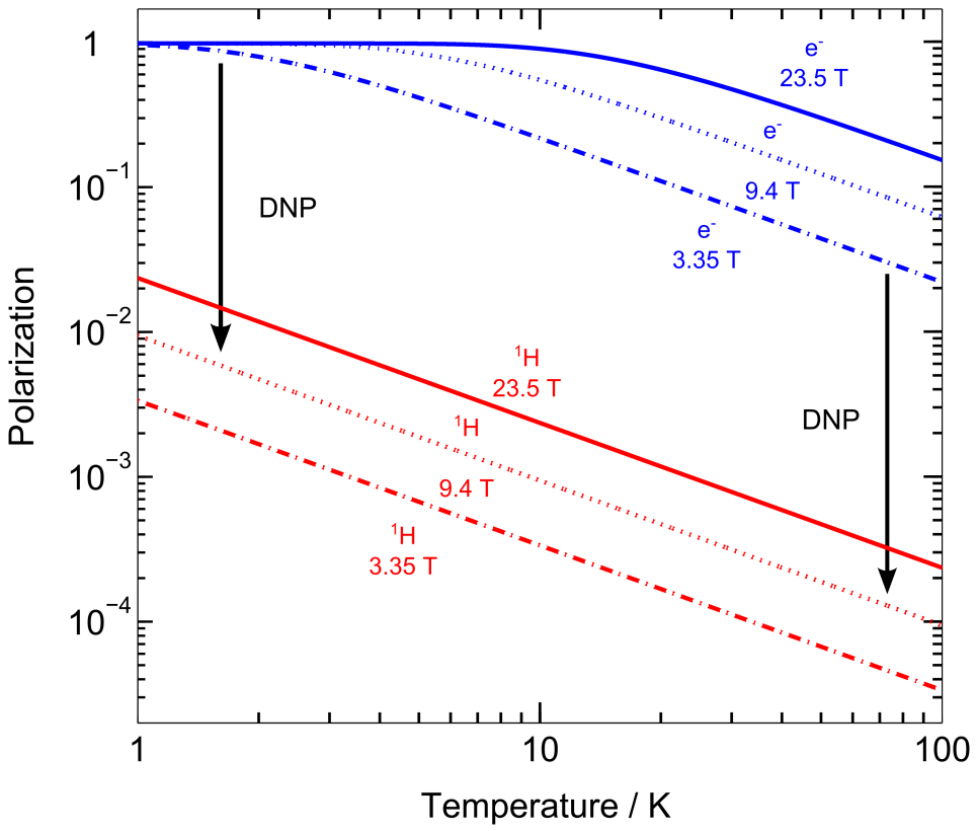

Figure I-5 : Temperature dependence of the polarization levels of electron and ^{1}H, which is defined in equation (I-1). Three different magnetic fields, 23.5 T (highest magnetic field to date), 9.4 T (magnetic field for experiments in this dissertation), and 3.35 T (magnetic field in DNP polarizer) are used for the calculations.

In the D-DNP method, the analyte solution is mixed with an organic free radical and a glassing solvent, typically a mixture of water, DMSO, glycerol, methanol, and ethylene glycol. During the polarization time, the sample is irradiated with microwaves (~ 94 GHz; $\omega_e \pm \omega_N$). Subsequently, the polarized sample is dissolved with a pre-heated solvent (~ 200 ℃ under 10 bar pressurization), and rapidly injected into the NMR spectrometer. Finally, the NMR spectra are acquired at room temperature. Figure I-6 represents a schematic diagram of the dissolution DNP processes.

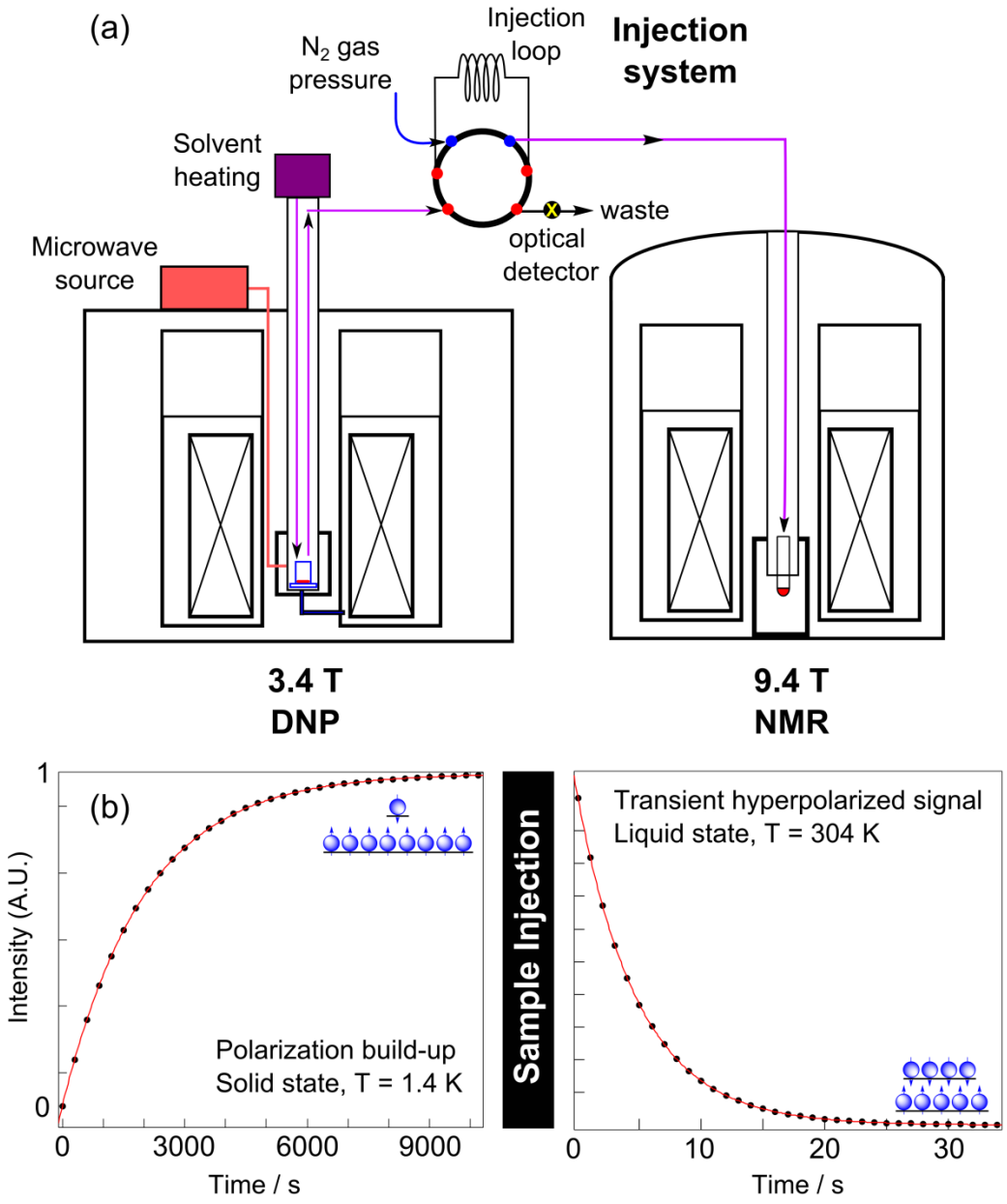

Figure I-6 : (a) Schematic diagram of the dissolution DNP setup. A small volume of the sample (1 ~ 20 μL) is polarized at a cryogenic temperature (typically, 1.1 ~ 1.5 K) by irradiating a microwave frequency in the 3.4 T DNP magnet. At a subsequent time, the frozen sample is dissolved in the pre-heated solvent, and transferred to a 1 mL injection loop (loading position; red ports in the injection system are connected together). When the polarized sample is detected in optical detector, the two-way valve is switched to injection position (red and blue ports are connected together). Subsequently, high pressure of nitrogen gas pushes the sample into the 5 mm NMR tube that is preinstalled in 9.4 T NMR spectrometer. (b) Solid state buildup (2,000 s buildup rate constant) and liquid state signal decay (6 s spin relaxation time) of DNP polarization level are represented.

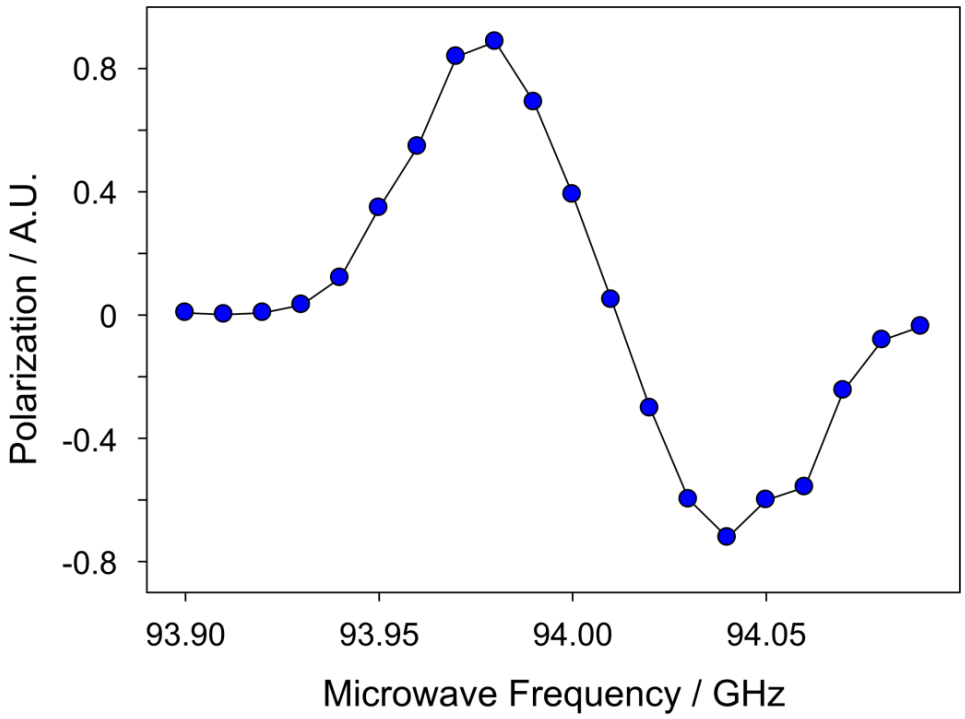

Figure I-7 : Microwave frequency dependence of nuclear spin polarization levels of Urea-^{13}C for the OX63 radical. For the measurement, 20 μL of 1.5 M Urea-^{13}C and 15 mM OX63 radical were mixed in glassing solvent (60% ethylene and 40 % water).

Optimal microwave frequencies of trityl radical (OX63) for ^{13}C polarization can be found from data shown in Figure I-7. Under these conditions, the frequency separation of maximum enhancement is consistent with both the thermal mixing and solid effect mechanisms. However, it is difficult to differentiate between the two DNP mechanisms in practical situations.[110]

The overall signal enhancement available through the dissolution DNP method is defined by

$$\varepsilon' = \varepsilon \cdot \frac{B_{DNP}}{B_{NMR}} \cdot \frac{T_{NMR}}{T_{DNP}} \qquad (-3)$$

where ε represent the actual DNP enhancement in solid state.[26] The enhancement can be higher than 10,000 due to the large temperature factor ($\frac{T_{NMR}}{T_{DNP}}$; ~250), compared to a conventional single scan NMR experiment. Experimentally, the polarization level of ^{13}C is accurately determined by acquiring a ^{15}N spectrum of ^{13}C-labeled urea.[109] The normalized integration difference of the *j*-coupled doublet ^{15}N peak indicates the absolute polarization level of the ^{13}C nuclei (Figure I-8). In the data shown in the Figure I-8, 33% of the ^{13}C polarization is achieved.

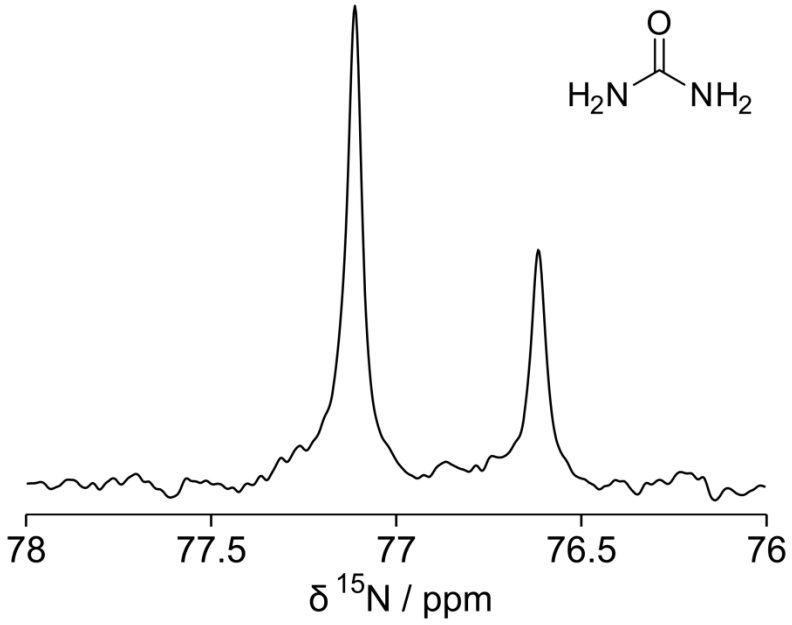

Figure I-8 : Hyperpolarized ^{15}N spectrum of the ^{13}C-labeled urea. The absolute polarization level of ^{13}C is determined from the normalized integration difference of the doublet peak. 20 μL of 1.5 M Urea-^{13}C and 15 mM OX63 radical were mixed in glassing solvent (60% ethylene and 40 % water).

Because of the temperature factor, dissolution DNP shows a higher total enhancement than other DNP methods. Accordingly, the signal gain from the D-DNP processes

extends the scope of the applications in high resolution NMR spectroscopy and magnetic resonance imaging (MRI).

The application of dissolution DNP was initially proposed by Golman and coworkers with the purpose of *in vivo* ^{13}C metabolic imaging.[111-116] Because of the wide chemical shift dispersion of ^{13}C spins and signal gain by the DNP process, hyperpolarized ^{13}C imaging provides not only sufficient spectral resolutions, but also a high signal-to-noise ratio. Typically, hyperpolarized pyruvate is used as a metabolic reporter in metabolic imaging studies.[112-115, 117-119] In the work of Golman and coworkers,[115] after the ^{13}C hyperpolarized pyruvate was injected in rats containing cancer cells, concentrations of transformation products of the pyruvate (lactate and alanine) were compared between normal tissues and the tumors. The high glycolysis rate of cancer cells gave rise to an abnormally high lactate concentration in the cancer tumors. In addition, an MRI based measurement of pH using hyperpolarized ^{13}C-labelled bicarbonate has been proposed as an alternative diagnostic method for cancer and inflammation detection. As the pH value of tumor tissue is significantly lower than the value of normal tissue, changes in tissue pH calculated from the concentration ratio between the hyperpolarized bicarbonate and carbon dioxide are used for detecting the diseases.[116]

In addition to the hyperpolarized imaging study, there have been many pilot studies dealing with the hyperpolarized biomolecules, such as amino acids, lipid membranes, and proteins.[120-124] Several different pulse sequences were implemented for the dissolution DNP applications. For example, the Eykyn and Denisov groups

demonstrated a ^{15}N hyperpolarization method of a long-lived metabolite choline molecule, a precursor of cellular phospholipid metabolism.[125-126] In the choline DNP study, polarization transfer from the hyperpolarized ^{15}N to methylene protons by a reversed INEPT pulse was employed to provide a resolution that can distinguish the choline metabolites. As the metabolites play significant roles in biologically important processes, hyperpolarization of the molecules may open a new way to study *in vivo* metabolic measurements. Lerche and coworkers illustrated the hyperpolarized ^{13}C NMR experiments for studies of molecular interaction of ligand-protein binding.[127] Binders for the target protein, human serum albumin, were recognized through changing NMR parameters (peak height, line broadening, and chemical shift change) upon binding.

Because of shortcomings of the dissolution DNP, specifically, non-renewable hyperpolarization and limited life-time of the hyperpolarization state, the multiple scans to acquire multi-dimensional NMR spectra are very limited in the dissolution DNP experiments. To overcome the restrictions, several research groups have developed pulse schemes that measure 2D spectra within few seconds.[128-132] For example, the Frydman group initially offered a gradient-encoded single-scan two dimensional spectroscopy (ultrafast two-dimensional NMR) of 2D ^{15}N-^{1}H HSQC NMR spectra collected from ^{15}N-enriched urea solutions.[128-129]

One of the benefits of the dissolution DNP is the capability of utilizing optimal hyperpolarization generated at low temperature in solid state and of measuring real-time NMR spectrum in liquid state. Allowing for several orders of magnitude in signal enhancement, dissolution DNP makes it possible to monitor chemical and biological

reactions in real-time while the reactions proceed. The Hilty group presented a time-resolved DNP-enhanced ^{13}C NMR spectroscopy which examined the hydrolysis of N_{α}-benzoyl-$_{L}$-arginine ethyl ester (BAEE) by the serine protease trypsin.[133] By using a small flip angle pulse scheme, the progress of the enzyme catalyzed reaction was monitored by observing the consumption of reactant and formation of products over the course of three seconds. In the pulse scheme, only a small portion of the hyperpolarized signals is utilized for each scan, while the remaining signals are used for following scans. The signal intensity of the substrate from the time-resolved NMR spectra was fitted with a linear function. From the linear fit, the rate of catalysis (k_{cat}) was calculated with known substrate and enzyme concentrations. Additionally, the reaction intermediate (acetyl-adenylate) of the multi-step enzyme catalyzed reaction of acetyl-CoA synthetase was clearly detected by the hyperpolarized ^{13}C NMR spectroscopy by Lerche and coworkers.[134] The Hilty group has proposed temporal correlations to examine reaction mechanisms for fast organic reactions such as the Grignard addition and Diels-Alder reaction.[135-136] As hyperpolarized NMR signals flow from the reactant to the product while the reaction proceed, treatment of a selective inversion on a point of interest in the reactant provides direct correlation information among the reactant, intermediates, and product.

In most of the previous D-DNP applications, nuclear spins showing long longitudinal relaxation times (carbonyl carbon, quaternary carbon, and tertiary nitrogen) are used to avoid severe signal losses during sample injection. However, it is often required to analyze chemical structures or reactions for a majority of chemical

compounds with nuclear spins ^{1}H and ^{19}F, showing relatively fast relaxation times. For this purpose, the Hilty group developed a rapid sample injection system that can be adapted to the D-DNP system.[133, 137] The total transfer time of the polarized sample is on the order of a second, permitting a study of the spins exhibiting longitudinal relaxation times less than 1 s. Figure I-9 represents a high resolution DNP-enhanced NMR spectrum of a mixture of common organic solvents analyzed with the rapid injection system. Due to the benefit of the sample injection, all of the signals including methyl groups are clearly observed.

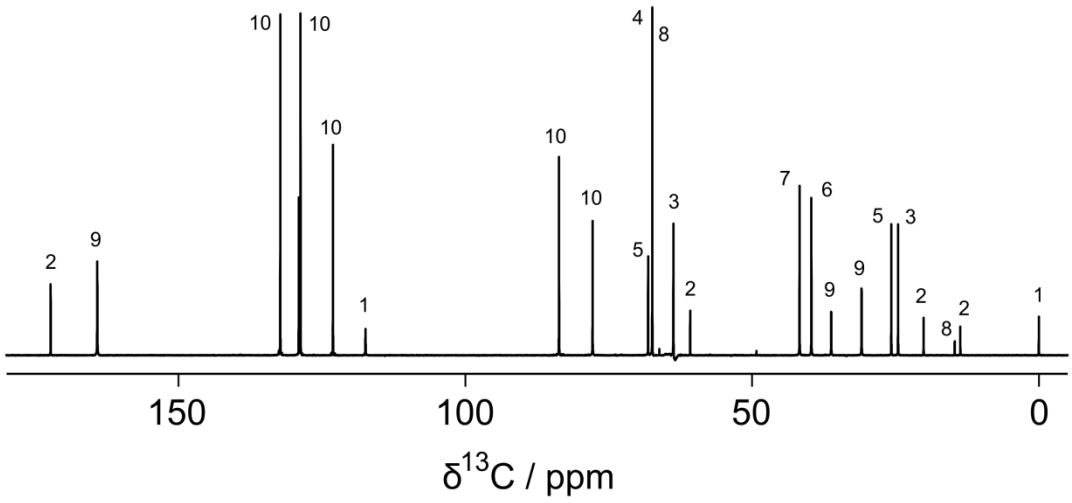

Figure I-9 : High resolution NMR spectrum of hyperpolarized common organic solvents ((1) acetonitrile, (2) ethyl acetate, (3) isopropyl alcohol, (4) 1,4-dioxane, (5) THF, (6) DMSO, (7) dimethyl sulfone, (8) diethyl ether, (9) *N*,*N*-dimethlyformamide, (10) phenylacetylene). All of the signals are clearly resolved with narrow line widths (2 ~ 3 Hz).

This dissertation aims to extend the use of dissolution DNP into new fields of research involving large molecules. The first approach is to characterize properties of proteins through the observations of small molecules that interact with proteins. Studies of the characterization of protein-ligand interactions and determination of competitive

ligand binding in combination with rapid sample dissolution are extensively examined with hyperpolarized ^{19}F and ^{1}H.[138-139] For the study of protein-ligand interactions with hyperpolarized ^{19}F, identification and quantification of ligand binding over a wide range of dissociation constant values with different binding kinetics have been explored. Besides the simple binding experiments, protein-mediated magnetization transfers between two competitive ligands were investigated for structural information on the binding epitope. The second approach is to investigate properties of polymers through the direct observation of the macromolecules. Real-time hyperpolarized ^{13}C NMR spectroscopy was investigated for the study of the reaction mechanism and kinetics.

CHAPTER II

NUCLEAR MAGNETIC RESONANCE OF HYPERPOLARIZED FLUORINE FOR CHARACTERIZATION OF PROTEIN-LIGAND INTERACTIONS*

Introduction

High-resolution Nuclear Magnetic Resonance (NMR) spectroscopy is an important technique in drug discovery.[11, 14, 140] In an industrial setting, NMR spectroscopy is mainly used to study interactions between ligands and the target protein, either through protein observation, ligand observation or indirect detection via a reporter ligand. Chemical shift perturbation spectroscopy of proteins in the presence of ligand can be used to demonstrate specific binding and to map the binding site, providing a high level of detail. In the context of screening large compound libraries[141] where the primary interest lies in high throughput determination of ligand binding, ligand based observation is preferred. A strength of NMR spectroscopy lies in its ability to detect even weak binding, with dissociation constants of up to 1 mM,[140, 142] which makes it the method of choice for the screening of fragment libraries.

Apart from work with carefully composed fragment libraries during the initial phase of a drug discovery campaign, multiple challenges remain for general applicability of ligand-observed NMR in drug discovery. Foremost, the obtainable signal-to-noise ratio is relatively low. In order to acquire workable ^{1}H spectra within 5–15 minutes, ligand

* This chapter is reproduced with permission from Y. Lee, H. Zeng, S. Ruedisser, A. Gossert, and C. Hilty. "Nuclear Magnetic Resonance of Hyperpolarized Fluorine for Characterization of Protein-Ligand Interactions." *Journal of the American Chemical Society* **2012**, 134, 17448-17451. Copyright 2012 the American Chemical Society.

concentrations of 100–200 μM are used in standard screening setups. This requirement excludes many ligands from analysis due to their often low solubility in water. Further, detection of binding by ligand-observed experiments is generally limited to ligands in fast exchange, excluding the most potent, tightly binding ligands from the analysis. Most lead compounds with drug-like properties fall into one of these categories (low solubility, slow exchange) and can therefore only be studied by expensive protein-observed NMR experiments[143] or, if a suitable reporter molecule is available, by reporter screening.[144-145]

Hyperpolarization of nuclear spins represents a significant opportunity to identify new leads due to a signal gain of several orders of magnitude. Dissolution dynamic nuclear polarization (DNP)[65] is well suited for application to this problem, since most small molecules can be brought to a spin-polarized state, and delivered in dilute form for use in an NMR experiment.[109] This technique has in the past most commonly been applied to ^{13}C nuclei,[123, 131, 134] which often exhibit slow spin relaxation that reduces the loss of polarization prior to the NMR experiment, among many applications also allowing the detection of ligand binding.[127] In this work, ^{19}F DNP is exploited. Experimentally, NMR of hyperpolarized fluorine is enabled by rapid sample injection of the polarized aliquot, which counteracts the relatively short relaxation time and reduces loss of the hyperpolarized signal prior to the NMR experiment.[131, 137]

Experimental Section

Sample Preparation

For binding experiments, 3.6 µL of 10 mM TFBC (Maybridge, UK), 10 mM synthesized TFMCPP,[146] 10 mM FMBC (Maybridge, UK), and 10 mM trifluoroacetic acid (TFA) in water were mixed with 0.4 µL of 150 mM 4-hydroxy-2,2,6,6-tetramethylpiperidine 1-oxyl (TEMPOL; Sigma Aldrich, St. Louis, MO) in a glass forming solvent (80% d_6-DMSO and 20% D_2O v/v). For the experiments at near limit of detection, 1mM TFBC, 5 mM TFMCPP, 3 mM FMBC, and 1 mM TFA were mixed with 0.4 µL of the TEMPOL solution specified above. For titration experiments, 1.8 µL of TFBC (400, 200, 100, 50, 25 mM) / TFA (10 mM) and FMBC (160, 120, 60, 30, 15 mM) / TFA (10 mM) were mixed with 0.2 µL of the TEMPOL solution. For the DNP 1D CPMG experiments and the 1D experiment for direct observation of bound and free ligand, 1.8 µL of 74 mM FMCPP and 9 µL of 5.2 mM FMBC solution was mixed with 0.2 µL and 1 µL of TEMPOL solution, respectively.

DNP Polarization

The prepared solutions were polarized in a HyperSense DNP polarizer (Oxford Instruments, Tubney Woods, UK), by irradiating at 94.002 GHz microwave frequency and 100 mW power for 40 min at a temperature of 1.4 K. The polarized sample was dissolved by 4 mL pre-heated buffer solution (50 mM Tris, 100 mM NaCl, and 5 mM $CaCl_2$, pH 8.0), and transferred to a sample injector.[133, 137] The sample was then injected into a 5 mm NMR tube preinstalled in the NMR spectrometer and mixed with a 25 µL

buffer solution or trypsin solution, resulting in a total volume of 450 µL. Trypsin was obtained from EMD, Gibbstown, NJ and used without further purification. The dilution factor in the dissolution of the hyperpolarized sample can be estimated from the characteristics of the dissolution system,[137] but was here determined more precisely, by determining the ligand concentration of a dissolved sample of high concentration. This ligand concentration was determined by ^{19}F NMR and HPLC after acid denaturation of trypsin. Calibration curves established with samples of known concentration were used (Figure II-1).

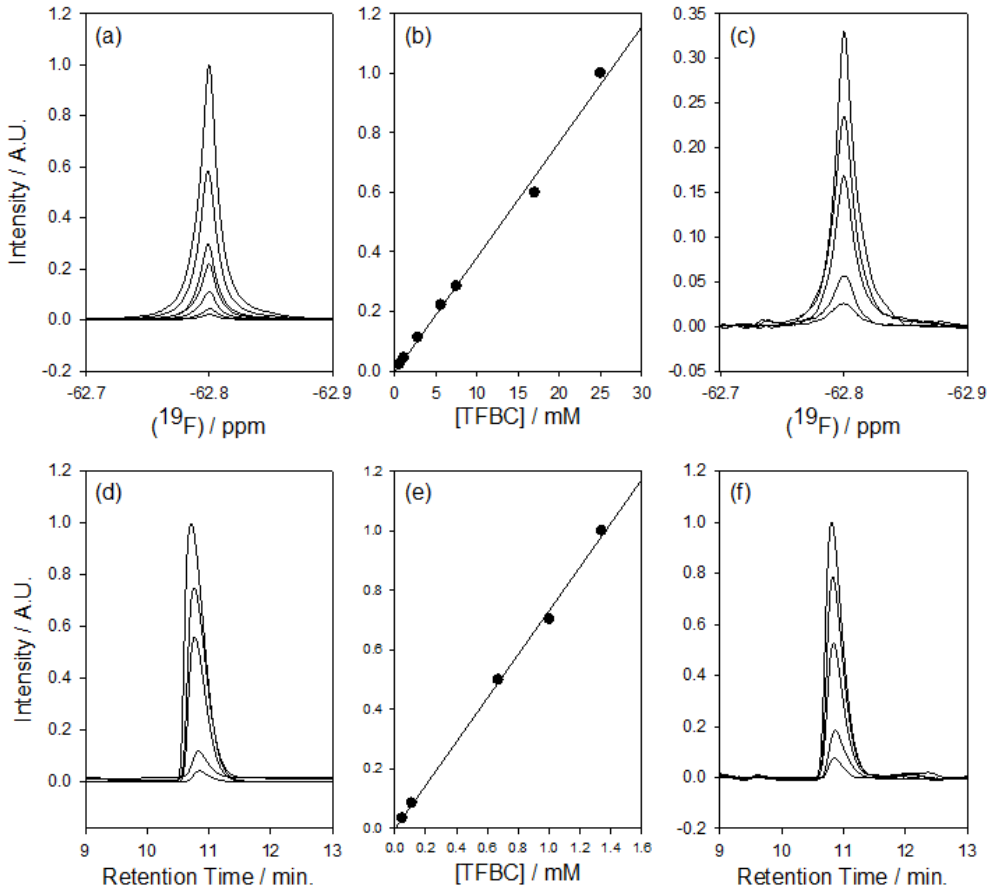

Figure II-1 : The final concentrations of TFBC in the DNP ligand titration were determined by NMR (c), and HPLC (f) with a standard calibration. Seven, and five standard TFBC samples were used for the NMR (a, b) and HPLC (c, d) standard calibrations, respectively.

NMR Spectroscopy

All the spectra were acquired by a 400 MHz NMR spectrometer (Bruker Biospin, Billerica, MA), equipped with a room temperature broadband observe (BBO) probe with extended ^{1}H tuning range to reach ^{19}F (Bruker Biospin, Billerica, MA), and modified with a poly ether ether ketone (PEEK) coil insert. NMR experiments were triggered after an injection time of 420 ms and a stabilization time of 800 ms set in the sample injection device. Sample temperature after the injection was ~30 ℃. For the detection of binding, a single scan spectrum with 32768 complex data points was acquired after a $\pi/2$ pulse excitation, the pulse strength was $\gamma B1 = 15.6$ kHz, the carrier frequency was set to -90 ppm and the spectral width was 100 ppm. The CPMG pulse sequence was applied for 100 ms after the $\pi/2$ pulse excitation, using $\gamma B1 = 15.6$ kHz and a delay between π pulses of 200 μs. The pulse strength was $\gamma B1 = 15.1$ kHz. The time between π pulses was 420 μs, during which 8192 digitized points were averaged to form one displayed data point. Background signals were subtracted, and data was normalized as indicated in the figure caption. All of the spectra in ligand titrations and direct observation were measured with $\pi/2$ excitation pulses as described above. For conventional NMR measurements, five different TFBC (588 μM ~ 2806 μM), trypsin (78 μM), TFA (3 mM) mixtures were prepared in buffer solution (50 mM Tris, 100 mM NaCl, and 5 mM $CaCl_2$, pH 8.0). ^{19}F NMR spectra for these samples were measured at 28 ℃ with 52 ~ 496 transients. The NMR data for all spectra was processed using the TOPSPIN 3.0 program (Bruker Biospin), and peaks were fitted using MatNMR.[147] The line width in response to ligand concentration in ligand titration was fitted to Equation (II-5) using

Matlab (MathWorks, Natick, MA). Chemical shift of ^{19}F was calibrated in reference to the ^{1}H spectrum of 1% TMS in $CDCl_3$ according to the IUPAC recommendations 2001.[148-149]

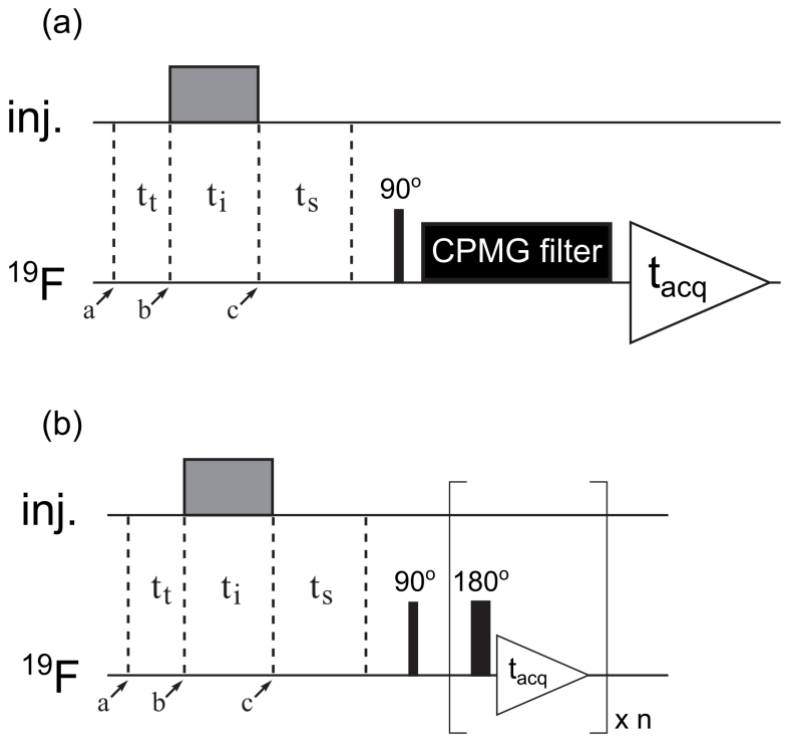

Figure II-2 : The protein-ligand interaction is monitored with two different pulse sequences. The polarized sample was transferred from the polarizer to the home-built sample injector for a transfer time (t_t). The sample was injected from the injection loop to a 5 mm NMR tube, which was preinstalled in a 400 MHz NMR spectrometer. NMR experiment was triggered after an injection time (t_i) of 445 ms and 800 ms stabilization time (t_s). a) $\pi/2$ pulse excitation scheme with CPMG filter for the detection of binding. b) Single scan CPMG pulse scheme. One averaged data point is measured for each time interval between π pulses in a CPMG experiment, and the delay between adjacent π pulses was 420 μs.

Simulations of Line Width and Chemical Shift Difference

The effects of exchange on the line width and chemical shifts were simulated by Matlab. The chemical equation for the protein (P) ligand (L) binding is

$$P + L \underset{k_{off}}{\overset{k_{on}}{\rightleftharpoons}} PL \qquad \text{(II-1)}$$

in which $k_{off} = k_{on} \times K_D$. Since we only observe the ligand, Equation (II-1) can be rewritten in exchange form as

$$L(1, free) \underset{k_{-1}}{\overset{k_1}{\rightleftharpoons}} L(2, bound) \qquad \text{(II-2)}$$

with $k_1 = k_{on}[P]$ and $k_{-1} = k_{off}$. Given the fraction of bound ligand $p_b = \frac{[PL]}{[L]+[PL]}$ and K_D, $[P]$ is calculated to be $[P] = \frac{K_D \cdot p_b}{1-p_b}$. The evolution of the magnetization was computed numerically from the Bloch equations, using the solutions given in Cavanagh et al. (pages 392-396).[150] Parameters chosen were the auto relaxation rates $\rho_1 = 0.5\, s^{-1}$, $\rho_2 = \rho_1 + \pi \cdot \Delta\Delta\nu_{1/2}$, and resonance frequencies $\Omega_1 = 0$, $\Omega_2 = \gamma \cdot B \cdot 10^{-6} \cdot \Delta\delta$, whereby the index 1 refers to the free ligand, and the index 2 to the bound ligand. The initial magnetization was set to $M_1(0) = 1 - p_b$ and $M_2(0) = p_b$. The simulated FID $M_1(t) + M_2(t)$ was then calculated numerically using the programs Matlab and Mathematica (Wolfram Research, Champaign, IL). The simulated spectrum was obtained from Fourier transform, and chemical shift and line width was directly calculated from the spectrum.

The parameters that were used for the simulations (Figure II-12 and Figure II-13) cover those determined for TFBC as well as FMBC binding to trypsin, and curves are plotted for several on-rates falling into the typical range near the diffusion limit.[151] It appears evident that, while in general the dependence of line width and chemical shift on the fraction of bound ligand is highly non-linear, a linear approximation as necessary for determination of according to Equation (II-5) from the manuscript is valid for small

values of p_b . Due to a large initial slope, the fit parameters $\Delta\Delta\nu_{1/2,\,max}$ and $\Delta\delta_{max}$ can be larger than the true line width of the bound ligand and chemical shift difference. However, this fact does not influence the quality of the K_D determination, as long as all measured points fall into the linear regime of the curves shown.

Results and Discussion

In In many respects, fluorine is an ideal target nucleus for the study of protein−ligand interactions by NMR spectroscopy. The use of fluorine is motivated by its importance in pharmaceuticals, where these atoms impart specific properties pertaining to electronic structure, hydrophobicity, or metabolic stability.[152-153] In addition, 20% of marketed drugs contain fluorine. For the purpose of NMR analysis, the high gyromagnetic ratio and 100% natural abundance of ^{19}F lead to a high signal intensity.[154] With state of the art equipment in conventional NMR spectroscopy, it is possible to screen libraries of compounds containing CF_3 and CF groups at concentrations of 18 and 35 μM, respectively.[155] The chemical shift of ^{19}F is sensitive to the local environment of the nucleus and to the change that occurs upon binding. This can lead to strong exchange broadening effects, aiding detection of weakly binding compounds.[141, 156] Additionally, the large chemical shift anisotropy of ^{19}F nuclei also leads to strong line broadening at slow molecular tumbling, as, for example, upon binding to a protein with a long rotational correlation time.[156] Finally, there is usually no background signal from protein or buffer components, and a pharmaceutical typically contains only one or a small number of fluorine atoms, reducing signal overlap. The

resulting simplicity of an ^{19}F NMR spectrum allows screening of mixtures of large numbers of compounds.

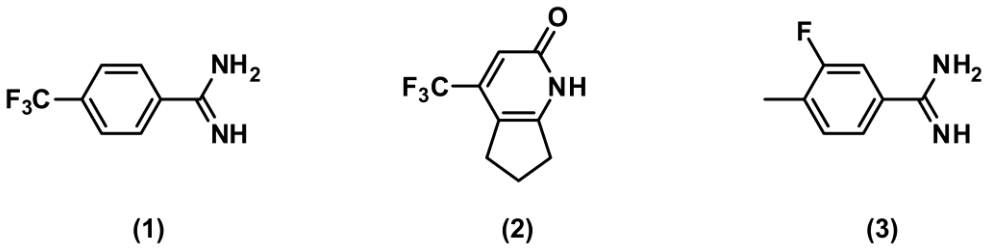

Figure II-3 : Structures of three fluorinated ligands binding to the serine protease bovine trypsin: (1) 4-(trifluoromethyl)benzenecarboximidamide hydrochloride (TFBC), (2) 4-(trifluoromethyl)-1,5,6,7-tetrahydro-2*H*-cyclopenta[*b*]pyridin-2-one (TFMCPP), and (3) 3-fluoro-4-methylbenzenecarboximidamide hydrochloride (FMBC)

Three representative fluorinated ligands for the serine protease trypsin are shown in Figure II-3. These ligands exhibit different binding kinetics in the slow and fast exchange regime and have binding constants covering nearly three orders of magnitude.[157] These ligands were originally discovered by different ^{19}F-based assays (FAXS: Fluorine chemical shift Anisotropy and eXchange for Screening) and their binding mode has been characterized with crystal structures. Figure II-4 shows hyperpolarized ^{19}F spectra of a mixture of the three fluorinated ligands together with sodium trifluoroacetate (TFA; used as an internal standard). Hyperpolarization increased the TFBC, TFMCPP, FMBC, and TFA signals by factors of 800, 450, 1500, and 3000 fold, respectively, compared to the signal of thermal polarization in the 400 MHz NMR spectrometer.

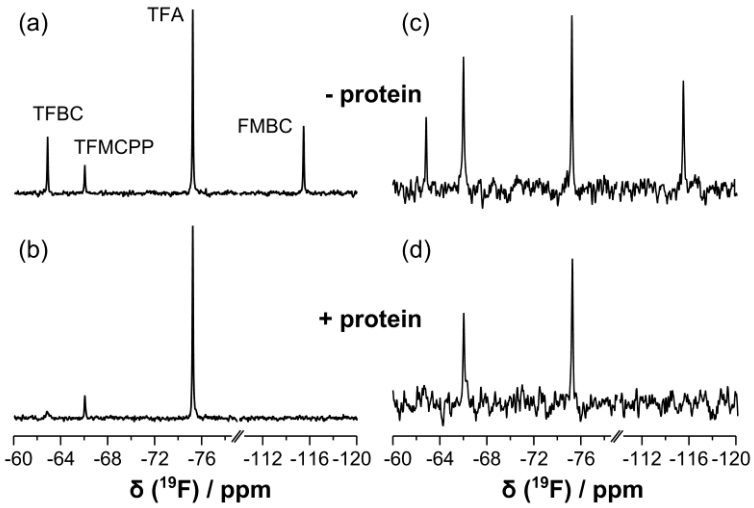

Figure II-4 : Hyperpolarized ^{19}F NMR spectra of TFBC (−62.8 ppm), TFMCPP (−66.0 ppm), FMBC (−115.4 ppm), and TFA (−75.2 ppm) acquired on a 400 MHz spectrometer equipped with a room temperature broad-band probe head tuned to fluorine. Shown are spectra of (a, b) 10 μM TFBC, 10 μM TFMCPP, 10 μM TFA, and 30 μM FMBC in the (a) absence and (b) presence of 50 μM trypsin and (c, d) 1 μM TFBC, 5 μM TFMCPP, 1 μM TFA, and 3 μM FMBC in the (c) absence and (d) presence of 50 μM trypsin. Spectra (a) and (b) were acquired using a single π/2 excitation pulse followed by a 100 ms CPMG filter. Spectra (c) and (d) were acquired after a single π/2 excitation pulse.

From a comparison of the spectra recorded in the absence (Figure II-4a) and presence of protein (Figure II-4b), binding can readily be observed for the three ligands from several NMR parameters, including reduction in peak height, increase in line broadening and chemical shift change. To increase the effects of spin-spin relaxation of the ligand in bound form, a Carr-Purcell-Meibom-Gill (CPMG)[158-159] filter was applied. In the presence of trypsin, a significant signal loss was observed for the strong binder FMBC, a line broadening for intermediate binder TFBC, and only a small signal loss for the weak binder TFMCPP. The difference in peak height for this molecule can be further accentuated by increasing the CPMG time (Figure II-5).

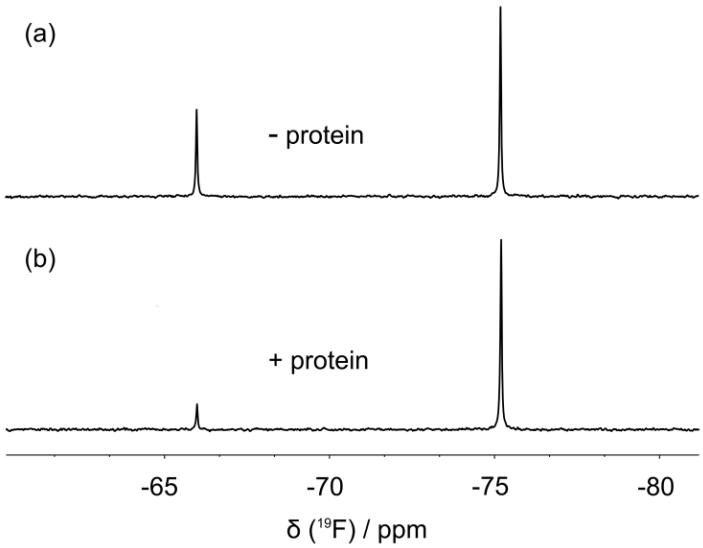

Figure II-5 : Spectra of TFMCPP (-66.0 ppm), and TFA (-75.2 ppm) hyperpolarized on ^{19}F. 20 µM TFMCPP, and 10 µM TFA, a) in the absence of protein, and b) in the presence of 133 µM protein. Spectra were recorded at 400 MHz, using CPMG filter experiments with 500 ms delay.

The signal intensity and chemical shift of the control molecule, TFA, is used as a reference since there is no interaction with the protein. Traces c) and d) in Figure II-4 are experiments carried out near detection limits of the instrumentation used, with 1 µM TFBC, 5 µM TFMCPP, and 3 µM FMBC. It would be straightforward to further reduce the detection limit by using a cryogenically cooled NMR probe or higher NMR field strength.

Binding of the strong binder FMBC, which exhibits binding kinetics in the slow exchange regime can clearly be detected through total signal loss, which occurs because of an excess of protein in the DNP experiment. In contrast, conventional ligand based NMR experiments often use a 10- to 20- fold excess of ligand. For ligands in the slow exchange regime, conventional experiments give rise to only a small reduction in the overall signal, resulting in unreliable detection of binding.[160]

Furthermore, multiple ligands are often tested simultaneously in one sample for drug screening. If more than one ligand binds to the protein competitively in conventional NMR experiments, the weaker binder may not be detected because the stronger binders occupy most of the binding sites of the protein. This problem is also eliminated by using ligand concentrations smaller than protein concentration in DNP experiments with multiple ligands.

As an alternative to 1D spectroscopy, weakly binding ligands are readily identified by measuring the transverse relaxation rate (R_2). Single scan CPMG experiments are applicable to DNP polarized samples; under the condition that only one ^{19}F signal is present. Signal decays from such experiments, of 174 μM ligand TFMCPP in the presence and absence of 88 μM trypsin are shown in Figure II-6. A fit of each trace to a single exponential indicated relaxation rates of 2.2 s^{-1} and 0.59 s^{-1} for the samples with and without protein, respectively. These rates are in agreement with values obtained from conventional CPMG experiments (2.0 s^{-1} and 0.54 s^{-1}; Figure II-7). The difference in R_2 values clearly indicates that TFMCPP interacts with the protein. In contrast, R_2 values of the control molecule TFA, which were measured from separate samples, did not show a significant change in the presence (0.53 s^{-1}) and absence (0.50 s^{-1}) of the same concentration of trypsin (Figure II-8).

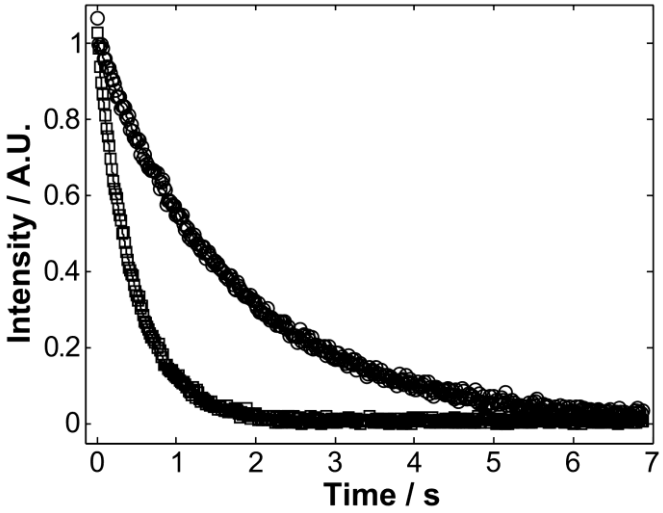

Figure II-6 : Magnitudes of the time-domain signals of 174 μM DNP polarized TFMCPP in the presence (□) and absence (○) of 88.0 μM trypsin. One averaged data point is shown for each time interval between π pulses in a CPMG experiment, and the delay between adjacent π pulses was 420 μs. Background signals from the NMR probe were removed by subtracting the signal acquired using the same pulse sequence without a sample in the magnet. Data were independently normalized to unit intensity at $t = 0$.

In addition to simple determination of binding, it can be of interest to quantify the strength of the protein-ligand interaction, expressed in the form of the dissociation constant K_D. The fraction of bound ligand, p_b, is given by

$$p_b = \frac{c_P + c_L + K_D - \sqrt{(c_P + c_L + K_D)^2 - 4c_P c_L}}{2c_L} \qquad \text{(II-3)}$$

where c_P and c_L are the total protein and ligand concentrations, respectively.[151] In traditional NMR experiments for the determination of K_D, fast exchange between the bound and free form of the ligand is often assumed. In this case, two readily observable spectral parameters, the line-width at half maximum $v_{1/2}$, as well as the change in chemical shift Δδ, are proportional to p_b.[155] A fit of one of these experimentally determined quantities to Equation II-3. can then be used to estimate the dissociation

constant. In the hyperpolarized experiments used here, the same approach is in principle viable. Since this method relies on the comparison of spectra obtained from different stopped-flow sample injections,[137] the precision of the measurement can however be greatly improved by comparing the chemical shift or line width of the ligand under study to a non-binding reference, in order to remove the effect of variations between experiments.

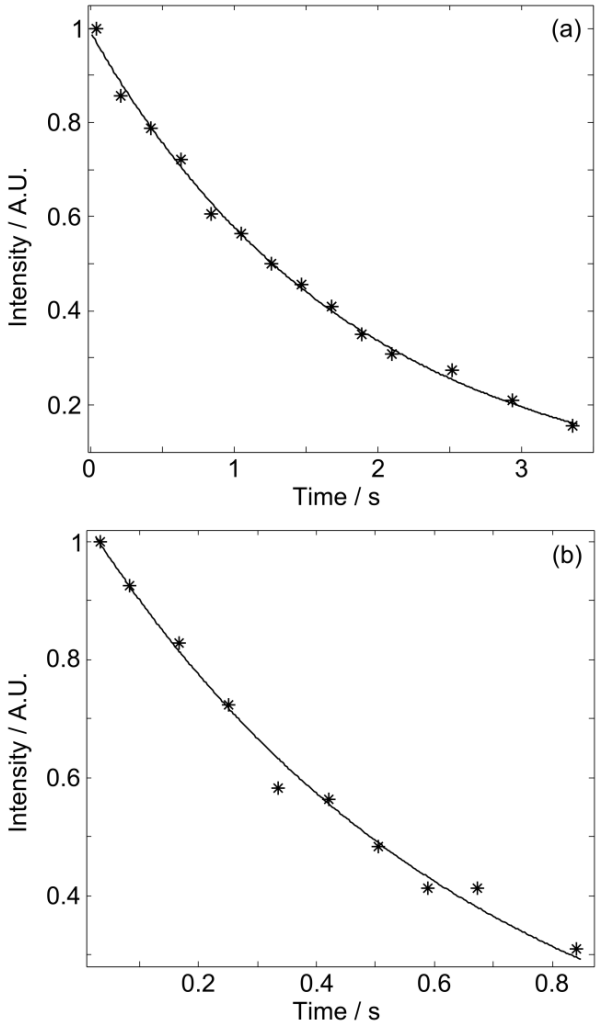

Figure II-7 : Conventional (non-hyperpolarized) CPMG experiment of 174 µM TFMCPP a) in the absence of 88.0 µM trypsin and b) in the presence of trypsin. Relaxation rates obtained from fit to a single exponential are 0.54 s^{-1} and 2.0 s^{-1}, respectively.

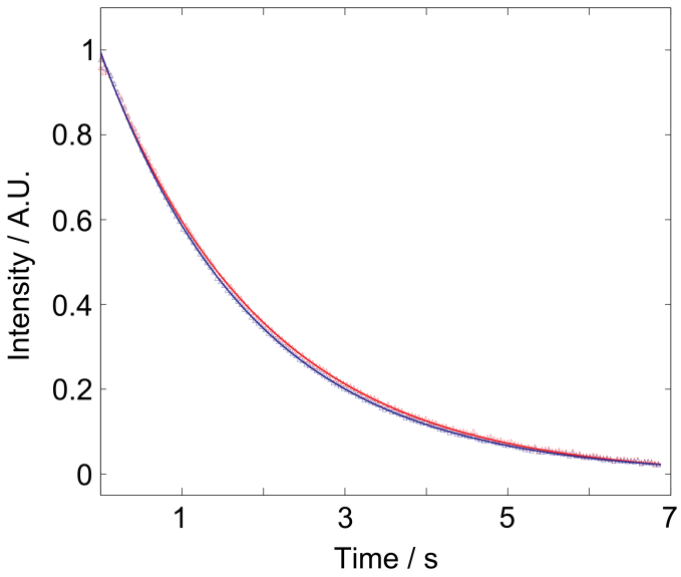

Figure II-8 : Magnitude of time-domain signals of 174 µM DNP polarized TFA without (red) and with 88.0 µM trypsin (blue) obtained from a CPMG experiment. Experimental parameters were identical to those in Figure 3. Relaxation rates obtained from fit to a single exponential are 0.50 s^{-1} and 0.53 s^{-1} for the samples in the absence and presence of trypsin, respectively. The relaxation rates measured by conventional CPMG experiments are both 0.50 s^{-1} for samples in the absence and presence of trypsin.

Practically, we prefer the measurement of the line width, which is easier to determine than the chemical shift of the typically broad lines. The parameter of interest derived from the hyperpolarized experiment is then the change in line width in function of ligand concentration,

$$\begin{aligned}\Delta\Delta\nu_{1/2}(c_P,c_L) &= \left[\nu_{1/2}^{(\text{Ligand})}(c_P,c_L)-\nu_{1/2}^{(\text{Reference})}(c_P,c_L)\right] \\ &-\left[\nu_{1/2}^{(\text{Ligand})}(0,c_L)-\nu_{1/2}^{(\text{Reference})}(0,c_L)\right]\end{aligned} \tag{II-4}$$

Carrying out a titration of protein or ligand concentration requires a new hyperpolarized sample for each data point, hence the number of data points should be chosen judiciously. Titrations using 5 points are shown in Figure II-9. The change in line width can then readily be fit to the proportionality relation,

$$\Delta\Delta\nu_{1/2}(c_P,c_L) = p_b \cdot \Delta\Delta\nu_{1/2,\max} \tag{II-5}$$

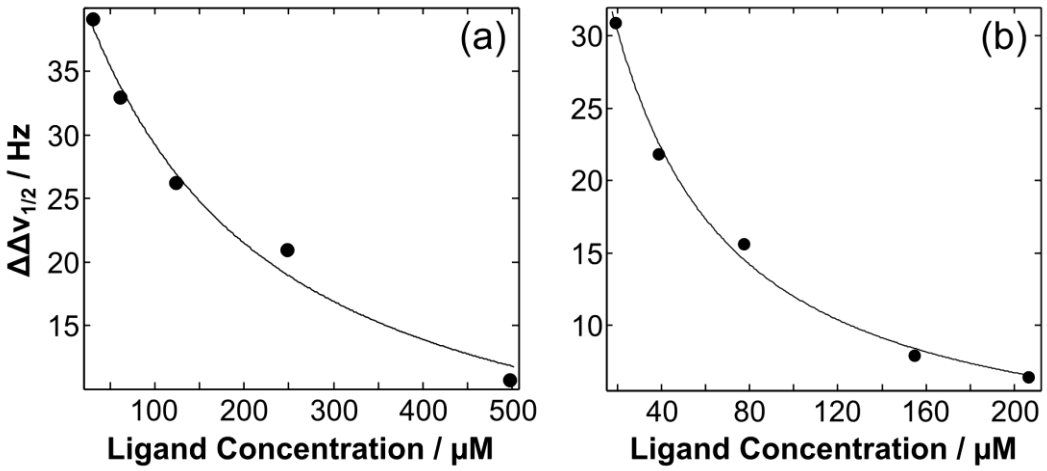

Figure II-9 : Titration of trypsin with the DNP-polarized ligands (a) TFBC and (b) FMBC. Each data point represents $\Delta\Delta\nu_{1/2}$ calculated according to equation 2 using TFA as the reference. The fits to equation 3 are indicated by the solid lines. K_D values of 148 (66−230) and 24 (12−36) µM were obtained for TFBC and FMBC, respectively (the 95% confidence ranges obtained from the individual fits are indicated in parentheses). The resulting $\Delta\Delta\nu_{1/2,max}$ values were 299 (191−407) and 167 (130−230) Hz, respectively. The titrations used (a) 26 and (b) 9 µM trypsin.

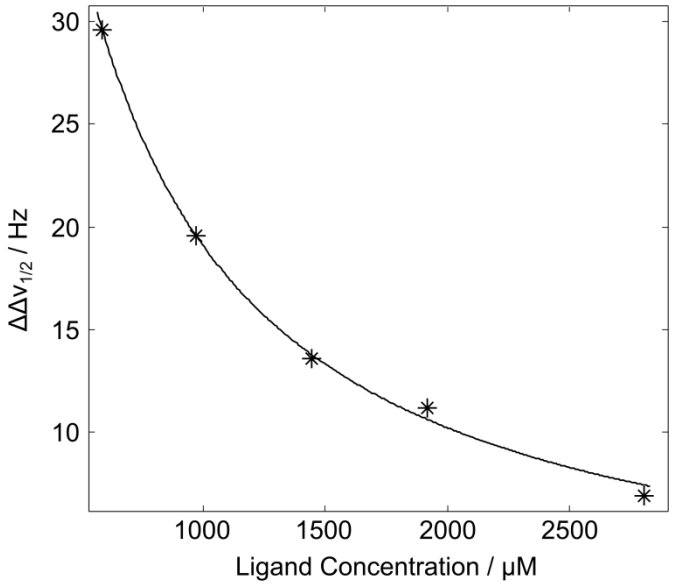

Figure II-10 : Determination of the dissociation constant of TFBC with trypsin by conventional NMR. Ligand titration carried out with a fixed trypsin concentration (78 µM). Determined KD and $\Delta\Delta\nu_{1/2,\ max}$ were 133 µM and 280 Hz, respectively.

The fit determines two independent parameters, the dissociation constant K_D, and the apparent maximum change in line width $\Delta\Delta\nu_{1/2,max}$. For comparison, titrations using conventional NMR (Figure II-10) and a K_D determination by isothermal titration calorimetry (ITC) are determined. The results obtained from the various experimental measurements are summarized in Table II-1.

Equation (II-5) is true only in the case of fast exchange; other-wise significant nonlinearities can be introduced due to exchange broadening. The consideration of the exchange contribution is not specific to the hyperpolarized experiment. However, in the hyperpolarized experiment, due to the enhanced sensitivity, a larger range of values for p_b becomes accessible, and the exchange effects can become more important. The spin system evolution under the influence of chemical exchange was examined based on the Bloch equations (Figure II-12 and Figure II-13).[150, 161] From the simulations, it becomes evident that under the experimental conditions examined the line broadening depends linearly on p_b for small values of p_b ($p_b < 0.2$), even if there is a significant exchange broadening. In this case, the parameter $\Delta\Delta\nu_{1/2,max}$ obtained from Equation (II-5) loses its significance. However, the accuracy of the K_D values obtained is not affected.

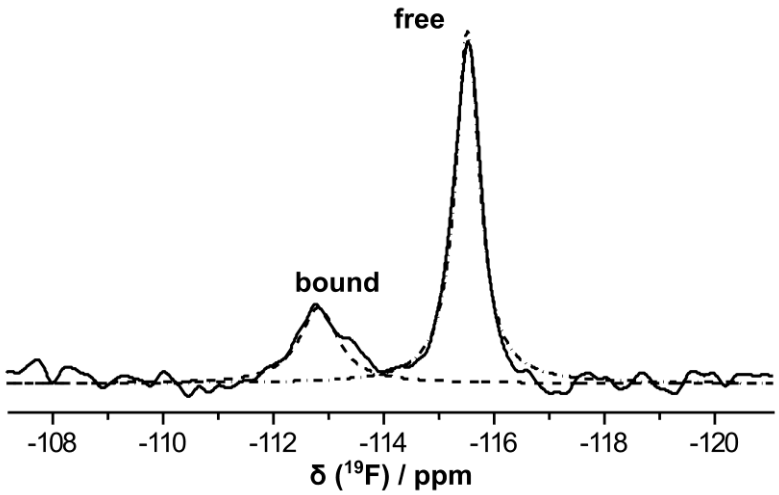

Figure II-11 : Hyperpolarized ^{19}F spectrum of 50 µM FMBC in the presence of 32 µM trypsin. The fraction of bound ligand, p_b, was directly determined from the ratio of the integrals obtained by peak fitting for the free (dot-dashed trace) and bound (dashed trace) forms, yielding a K_D value of 34.3 µM.

For the strongly binding ligand FMBC, the signals for the free and the bound form can be detected separately, since the ligand is in slow exchange. In this case, K_D can also be calculated from a single one-dimensional spectrum (Figure II-11 and Equation II-3). The obtained K_D values (Table II-1) are of the same order as the value from ligand titration, and from previous research, where a value of < 20 µM was determined.[157] Since the determination of the dissociation constant in this way relies on the observation of broad signals, which concomitantly lowers the signal-to-noise ratio, the use of hyperpolarization is particularly beneficial for high affinity ligands with nanomolar to low micromolar K_D.

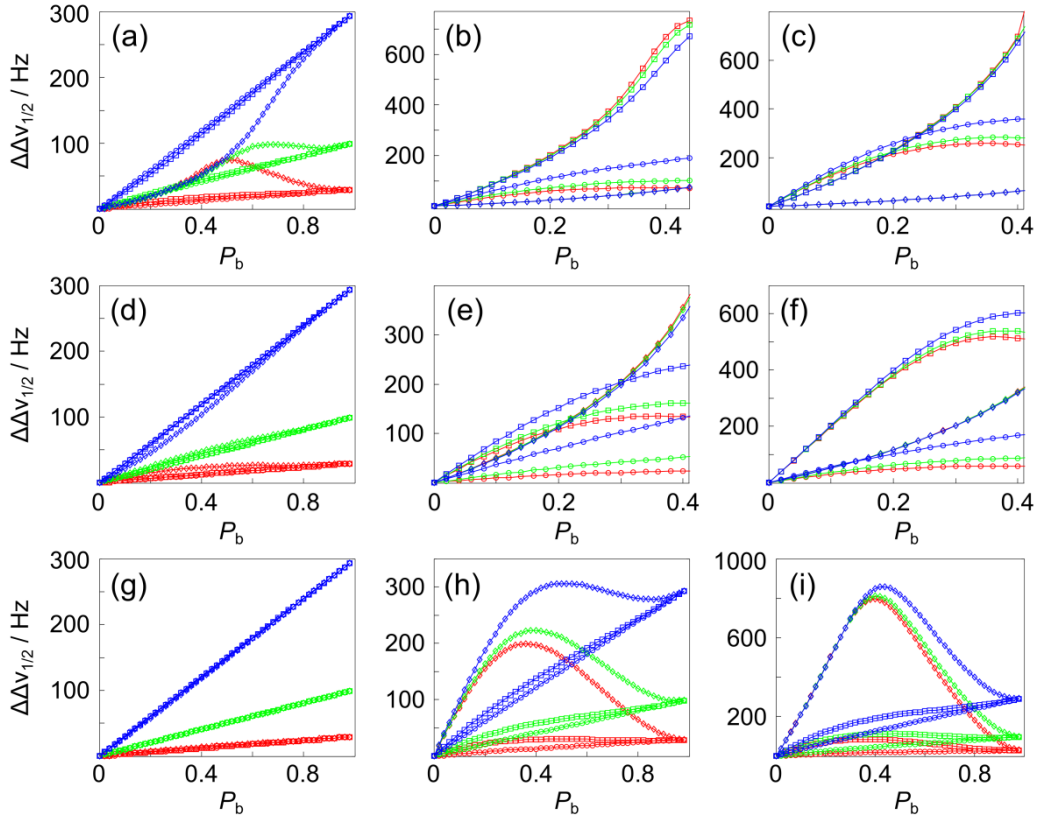

Figure II-12 : Expected change in line width, calculated for three different K_D values (K_D = 30 μM (a~c), K_D = 150 μM (d~f), K_D = 1000 μM (g~i)). Three different on-rates (k_{on}) in the range of the diffusion limit (k_{on} =10^9 (red), 10^8 (green), 10^7 (blue) $M^{-1}s^{-1}$), $\Delta\Delta\nu_{1/2,max}$ (30 Hz (—○—), 100 Hz(—□—), 300 Hz(—◊—)), and Δδ (100 Hz (a,d,g), 1000 Hz (b,e,h), and 2000 Hz (c,f,i)) were used.

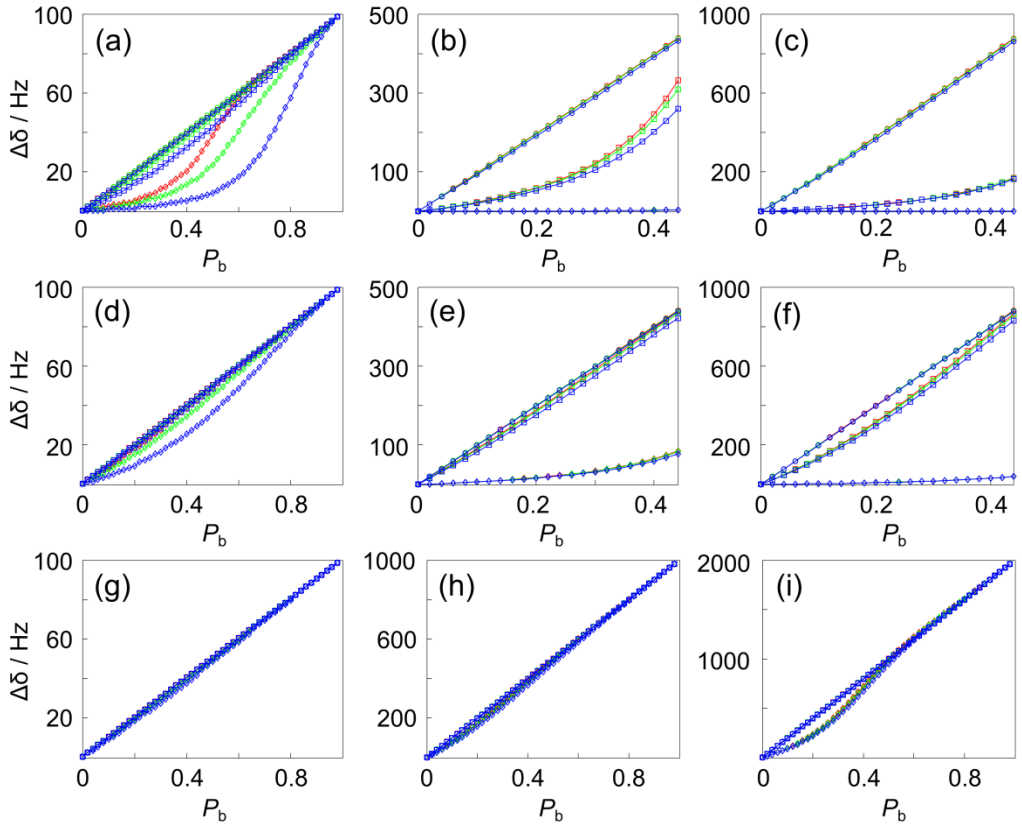

Figure II-13 : Expected change in chemical shift, calculated for the same parameters as in Figure II-12, namely three different K_D values (K_D = 30 µM (a~c), K_D = 150 µM (d~f), K_D = 1000 µM (g~i)). Three different on-rates (kon) in the range of the diffusion limit (k_{on}=10^9 (red), 10^8 (green), 10^7 (blue) $M^{-1}s^{-1}$.), $\Delta\Delta\nu_{1/2,max}$ (30 Hz (—○—), 100 Hz(—□—), 300 Hz(—◊—)), and Δδ (100 Hz (a,d,g), 1000 Hz (b,e,h), and 2000 Hz (c,f,i)) were used.

Table II-1 : Summary of K_D determination. †standard deviation of values obtained from >2 experiments are indicated, otherwise individual values are given. 95% confidence intervals obtained from each individual fit are larger than the spread of values; for typical ranges, see Figure II-9.

Ligand	Method	K_D † (μM)	$\Delta\Delta\nu_{1/2,max}$ (Hz)	# exp.
TFBC	DNP-NMR titration	142 ± 6	284 ± 13	5
	Thermal-NMR titration	122, 133	301, 280	2
	ITC titration	86	N/A	1
FMBC	DNP-NMR titration	15, 24	167, 217	2
	Thermal-NMR titration	35 ± 18	N/A	10

Conclusions

In summary, experiments based on hyperpolarized fluorine were shown that permit the identification and quantification of ligand binding over a wide range of K_D values and with different binding kinetics. Hyperpolarization allows accessing a wide range of protein to ligand ratios spanning up to 6 orders of magnitude without the need for very long measurement times. Not only the concentration of the ligand can be varied over a larger range (typically 1–200 μM) than in conventional NMR, but also the concentration of the protein (0.1–100 μM). The ability to record spectra at low ligand concentration with relatively high signal-to-noise ratio is an important advantage. (i) It enables direct detection of binding, especially for stronger binders in the slow exchange regime; (ii) It allows the study of ligands with low solubility in aqueous buffer; (iii) It represents an

advantage for K_D determination experiments, since a ratio of ligand : protein < 1 : 1 can be reached even when using typically low protein concentration. Using equal or smaller ligand concentrations than protein permits the robust detection of binding, including of strong binders with slow off-rates, which are easily missed in conventional ligand observation experiments. Furthermore, the single scan CPMG experiments would offer a way for robust, automated T_2 determination. An obvious limitation of the above experiments is that they require fluorine containing compounds. Using a well-characterized fluorinated ligand as a reporter molecule could however expand the applicability to other types of ligands.[144-145] On this basis, hyperpolarized ^{19}F NMR may be a viable alternative for inclusion in current workflows for validating protein-ligand interaction.

CHAPTER III

HYPERPOLARIZED BINDING POCKET NOE FOR DETERMINATION OF COMPETITIVE LIGAND BINDING*

Introduction

Changes in spectra measured by nuclear magnetic resonance (NMR) have long been used to identify the binding of ligands to biological macromolecules for drug discovery or other applications.[14, 140] NMR parameters such as chemical shift, spin relaxation or line width, and diffusion coefficients are sensitive indicators of binding.[162] Additionally, transfer of magnetization between protein and ligand can be used to determine binding sites and binding modes. In the saturation transfer difference (STD) experiment, radio-frequency irradiation is applied to a resonance on the protein, and spreads by spin diffusion through the protein. The saturation transfers to a ligand that binds to the protein, where a change in its NMR signal can be detected. In the case of competitively binding ligands, more specific information on the binding pocket can be obtained by observing protein mediated magnetization transfer between the two ligands. This experiment, termed "interligand NOEs for pharmacophore mapping" (INPHARMA) has recently been introduced by several of the authors of this work, and is especially useful when proteins are large or cannot be expressed with isotope labels (Figure III-1).[163-167] It relies on measuring a NOESY experiment in the presence of the target protein as well as

* This chapter is reproduced with permission from Y. Lee, H. Zeng, A. Mazur, M. Wegstroth, T. Carlomagno, M. Reese, D. Lee, S. Becker, C. Griesinger and C. Hilty. "Hyperpolarized Binding Pocket Nuclear Overhauser Effect for Determination of Competitive Ligand Binding." *Angewandte Chemie International Edition* **2012**, 51, 5179-5182. Copyright 2012 Wiley.

the two ligands. In the NOESY experiment, non-Boltzmann polarization is produced for the spins of each ligand, and it can also be traced back to the individual spins in the other ligand by frequency labeling in the t1 domain.[168] Due to the use of an NOE transfer relayed through the protein, the leading term for the interligand NOE is quadratic in the transfer efficiency. Given that direct NOEs rarely exceed 10% of the diagonal peak intensity, the product of two transfers yields low sensitivity of the experiment.[165]

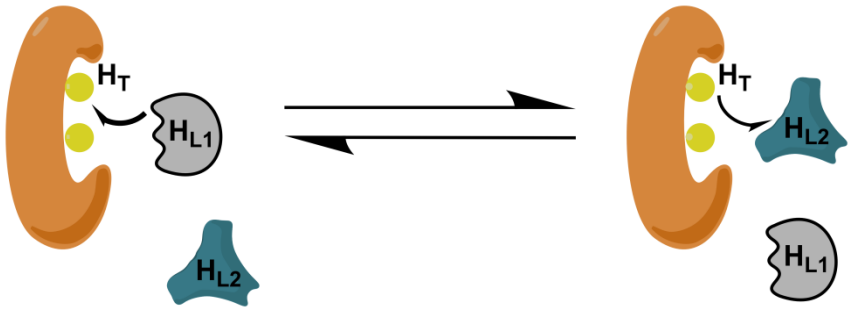

Figure III-1 : Scheme illustrating the transfer of magnetization from protons of ligand 1 (H_{L1}) to ligand 2 (H_{L2}) via protein (H_P) by means of competitive binding.

Recent developments in hyperpolarization techniques enable the generation of non-Boltzmann polarization of small molecules that is enhanced by several orders of magnitude compared to the simple population inversion achievable in a conventional NOESY experiment. Here, we present an experiment, where we use dynamic nuclear polarization (DNP)[65, 109] to polarize the ^{1}H spins[136, 169] of one of two ligands that competitively bind to a protein, and detect the transfer of a fraction of this large polarization via the protons in the binding pocket to the second ligand. The transfer between hyperpolarized ligand and binding pocket, termed here "hyperpolarized binding pocket NOE" (HYPER-BIPO-NOE) is related to the Spin Polarization-Induced NOE (SPINOE)[46] that has been described for hyperpolarized xenon. However in SPINOE

experiments the polarization of the protein is enhanced and Xe normally does not bind as selectively as the ligands that we use in these experiments do.[48] In the HYPER-BIPO-NOE, the magnetization transferred to the second ligand can be observed directly by recording a 1D spectrum. Alternatively, the buildup of signal as a function of time can be measured from a single hyperpolarized sample using small flip angle excitations, which gives additional information on the epitope of binding of the receiving ligand similarly to STD. However, in contrast to STD where the protein protons and therefore also the protons of the binding pocket are saturated, here the protons are enhanced beyond Boltzmann magnetization.

Experimental Section

Sample Preparation

Stock solutions were prepared as follows: Ligand 1, 2.9 mg of 5-benzyl-1,3-thiazol-2-amine in 32 µL d_6-DMSO and 8 µL D_2O (380 mM); ligand 2, 2.7 mg of 3-methyl-1H-indazole in 37 µL d_6-DMSO and 9 µL D_2O (370 mM); protein: 350 µM protein kinase A (PKA)[170] in D_2O PBS (phosphate buffered saline) buffer, additional 150 mM NaCl, 2 mM TCEP (tris(2-carboxyethyl)phosphine), and 2 mM sodium azide.

DNP Polarization

For DNP polarization, 0.9 µL of ligand 1 solution with 0.1 µL of 150 mM 4-Hydroxy-2,2,6,6-tetramethylpiperidine 1-oxyl (TEMPOL) free radical solution were mixed to yield a 1 µL aliquot of 342 mM benzyl-1,3-thiazol-2-amine and 15mM TEMPOL. The sample was polarized in a HyperSense system (Oxford Instruments,

Tubney Woods, UK) by irradiating 100 mW microwave power at 94.005 GHz frequency for 30 min, at a temperature of 1.4K. The polarized sample was dissolved by 4 mL pre-heated D_2O, and transferred to a sample injector. The sample was then injected into a 5 mm NMR tube, which was preinstalled in a 400 MHz NMR spectrometer (Bruker Biospin, Billerica, MA). For control experiments, 24.6 μL of D_2O buffer or PKA solution with 0.4 μL of ligand 2 stock solution was preloaded in the NMR tube before mixing with the hyperpolarized ligand 1. For the HYPER-BIPO-NOE experiments, 24.6 μL of PKA solution with 0.4 μL ligand 2 stock solution was preloaded. Estimated final concentrations after dissolution were 448 μM, 329 μM, and 19 μM for ligand 1, ligand 2 and protein, respectively. After injection and sample mixing, a waiting time of 2 s in single scan experiments, and 400 ms in small flip angle excitation experiments allowed for sample stabilization (τ_s) and NOE transfer.

NMR Spectroscopy

All of the spectra were measured at a temperature of 25 ℃ using the pulse sequence (trigger – presaturation – G_y – τ_s – [water suppression]$_4$ – $\pi/2$ – acquire) for the single scan experiment, and (trigger – presaturation – G_y – [water suppression]$_3$ – [G_y – water suppression – α_x – acquire]$_{16}$) for the small flip angle excitation experiment, in which [water suppression] is [shaped $\pi/2$ – G_x – shaped $\pi/2$ – G_y – shaped $\pi/2$ – G_z] (see Figure III-2). The carrier frequency was set to the resonance frequency of water. The presaturation was applied for 400 ms at the resonance frequency of residual DMSO at 2.68 ppm. The water resonance was selectively excited by EBURP2 shaped $\pi/2$ pulses of 20 ms duration, and dephased by randomized pulsed field gradients G_x, G_y or G_z (25..35

G/cm, 1 ms). This solvent suppression scheme was sufficiently selective, since the resonance frequency difference between water and the nearest protons of interest was 250 Hz. After a hard π/2 pulse or 20.7° (α_x) pulse, 4096 data points were collected over 320 ms. The NMR data was processed using the TOPSPIN 3.0 program (Bruker Biospin).

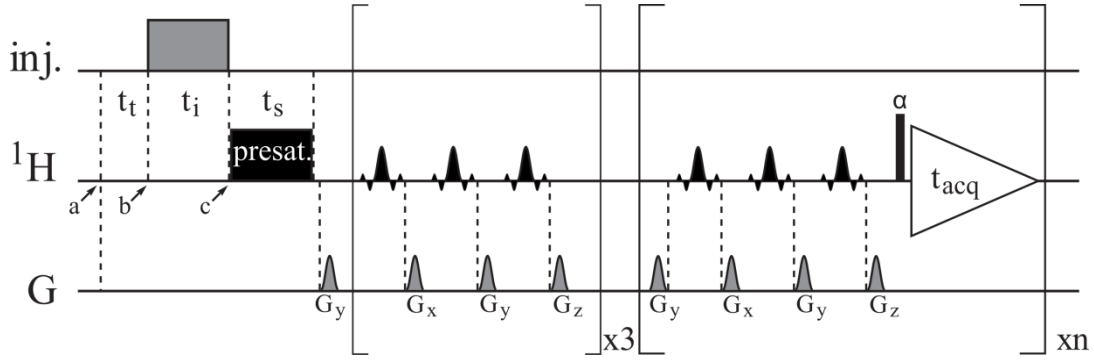

Figure III-2 : The INPHARMA buildup curve was measured by small flip angle pulses. The polarized sample was transferred from the polarizer to the home-built sample injector for a transfer time (t_t). The sample was injected from the injection loop to a 5 mm NMR tube, which was preinstalled in a 400 MHz NMR spectrometer. NMR experiment was triggered after an injection time (t_i) of 445 ms. During the 400 ms stabilization time (t_s), presaturation was applied at the frequency of residual ^{1}H resonance of d_6-DMSO. The water resonance was selectively excited by EBURP2 shaped π/2 pulses for 20 ms durations, and then dephased by randomized pulsed field gradients G_x, G_y or G_z (25..35 G/cm, 1 ms). After applying a 20.7° (α) pulse, 4096 data points were collected for 320 ms. Time interval between acquisitions was 0.4 s.

Results and Discussion

In the present experiments, the HYPER-BIPO-NOE effect is observed for the ligands 5-benzyl-1,3-thiazol-2-amine (ligand 1; Figure III-3a) and 3-methyl-1H-indazole (ligand 2; Figure III-3b), which bind competitively to protein kinase A (PKA). The non-hyperpolarized spectrum for a mixture of these ligands is shown in Figure III-3c.

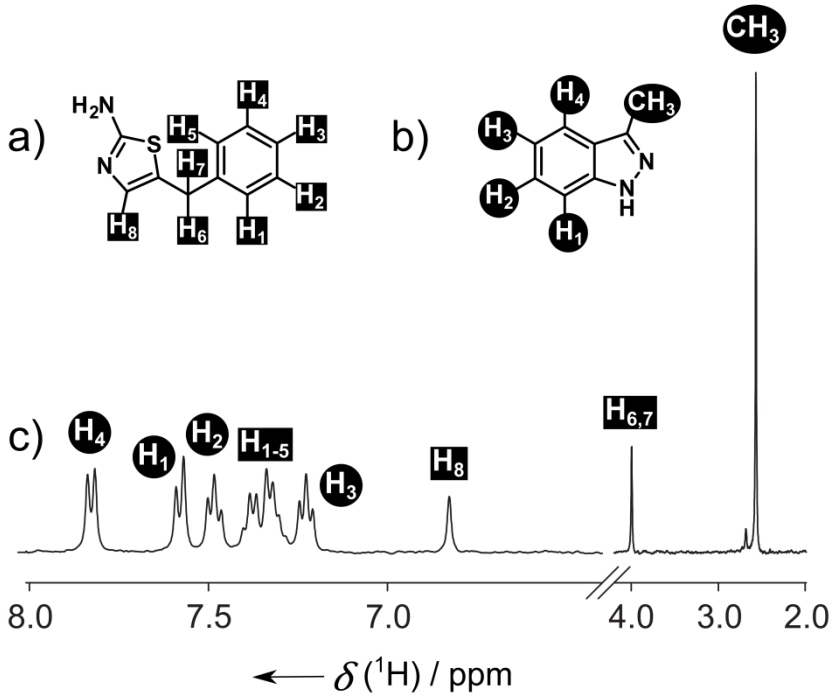

Figure III-3 : a) Structure of ligand 1 (5-benzyl-1,3-thiazol-2-amine). b) Structure of ligand 2 (3-methyl-1H-indazole). c) ^{1}H NMR spectrum (not hyperpolarized) of a mixture of ligand 1 and 2. Chemical shift assignments are indicated.

In the subsequent experiment, an aliquot of ligand 1 was hyperpolarized by DNP in the solid state, and dissolved in a stream of heated solvent. Preserving its polarization, it was rapidly injected into the NMR spectrometer, where it was mixed with the other sample components, including ligand 2 and protein. Due to an enhancement > 620 when compared to thermal polarization in the 400 MHz NMR spectrometer, the resulting spectra predominantly show the signals from ligand 1 (Figure III-4a). It can further be seen that, despite crowding in the spectral region for aromatic protons at ~ 7.5 ppm, the DNP-NMR spectra are of sufficient quality to distinguish the various resonances, which is a prerequisite for observing the interligand NOE (Figure III-4b). The transfer of signal to the second ligand can be observed in the top trace of Figure III-4b, which shows an

expanded representation of the spectra from Figure III-4a. The peaks for H_4, H_1, and CH_3 groups of ligand 2 are indirectly enhanced compared to their thermal polarization signal (bottom trace). This enhancement is sufficiently large to observe the interligand NOE transfer in a single scan, one-dimensional spectrum. The signal intensities of ligand 2 were also enhanced in hyperpolarized control experiments in the absence of protein (Control 1, second trace in Figure III-4b) and in the absence of polarized ligand 1 (Control 2, third trace in Figure III-4b) compared to the spectrum of thermally polarized ligand 2. By comparing the signal intensity of ligand 2 in the HYPER-BIPO-NOE experiment to the hyperpolarized control experiments, it can further be estimated that specific enhancement of the HYPER-BIPO-NOE over non-specific enhancement is a factor of 4.7, 3.4, and 5.7 for the H_4, H_1, and CH_3 groups, respectively. The kinetics of the HYPER-BIPO-NOE transfer and potential information about the binding modes of the two ligands can be obtained from measuring the build-up of signal on ligand 2 as a function of time. This measurement can be accomplished from a single hyperpolarized sample, by converting a fraction of polarization into observable coherence with small flip angle excitations at given time intervals (Figure III-5a).

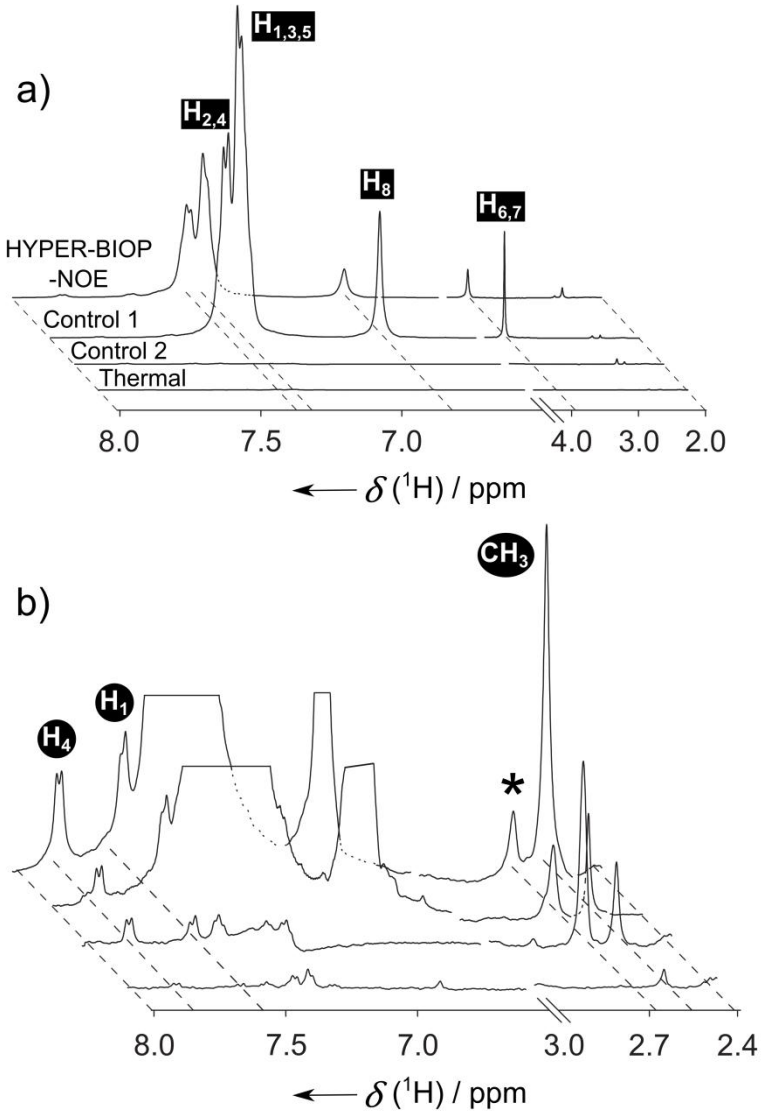

Figure III-4 : 1D HYPER-BIPO-NOE spectra, in full scale a), and expanded to show transferred signals b). Stacked spectra are, from top to bottom: Hyperpolarized ligand 1, with ligand 2 and protein (HYPER-BIPO-NOE); Hyperpolarized ligand 1, with ligand 2, but without protein (Control 1); Hyperpolarized d_6-DMSO / D_2O, with only ligand 2 and protein (Control 2); Thermal spectrum of the HYPER-BIPO-NOE sample (Thermal). (*) designates the resonance from residual DMSO, which was suppressed using presaturation prior to the acquisition of the spectra.

Integrated signal intensities of the resolvable protons of the hyperpolarized ligand 1, as well as of the non-polarized ligand 2 are shown in Figure III-5b and c, respectively. The buildup of signal intensities of the resonances from ligand 2 due to the HYPER-BIPO-

NOE effect can be seen in Figure III-5c. The course of signal intensity in function of time t can be modeled by evolution matrix (relaxation and kinetic terms).[164, 171] Under the assumption of fast kinetics, the evolution matrix $M = R + K$ can be approximated with a 3 × 3 matrix that correspond to the signal intensities observed from L_1, P and L_2.[171] In the HYPER-BIPO-NOE experiment, the signal from ligand L_1 is hyperpolarized, whereas the polarization of the protein P and ligand L_2 are from Boltzmann magnetization. Additionally, comparing Figure III-5b and c, it can be seen that the transferred magnetization for the entire buildup time is smaller than the initial magnetization. In this case, the back-transfer of magnetization can be ignored, and equations become considerably simplified. Under the assumption that $r_P \gg r_1, r_2$ and $r_1 \approx r_2$, the solutions are approximated by[171]

$$s_{\mathrm{L2,rel}} = \frac{\sigma_1^{*} \cdot \sigma_2^{**} \cdot t}{r_{\mathrm{P}}} = \frac{pb_1 \cdot p_2 \cdot \sigma_1 \cdot \sigma_2 t}{p\rho_{\mathrm{P}} + p_1\rho_{\mathrm{PL1}} + p_2\rho_{\mathrm{PL2}}} \qquad \text{(III-1)}$$

Equation (III-1) illustrates that the transferred signal is proportional to the product of both cross relaxation rates. Since the cross relaxation rates depend on the distances of the proton in a ligand to the protons in the protein, a more efficient transfer indicates a closer contact. For Equation (III-1), it should be noted that, since r_1 and r_2 are averages of bound and free relaxation rates, the condition $r_1 \approx r_2$ would be fulfilled if the fraction of bound state is similar for ligand 1 and ligand 2.

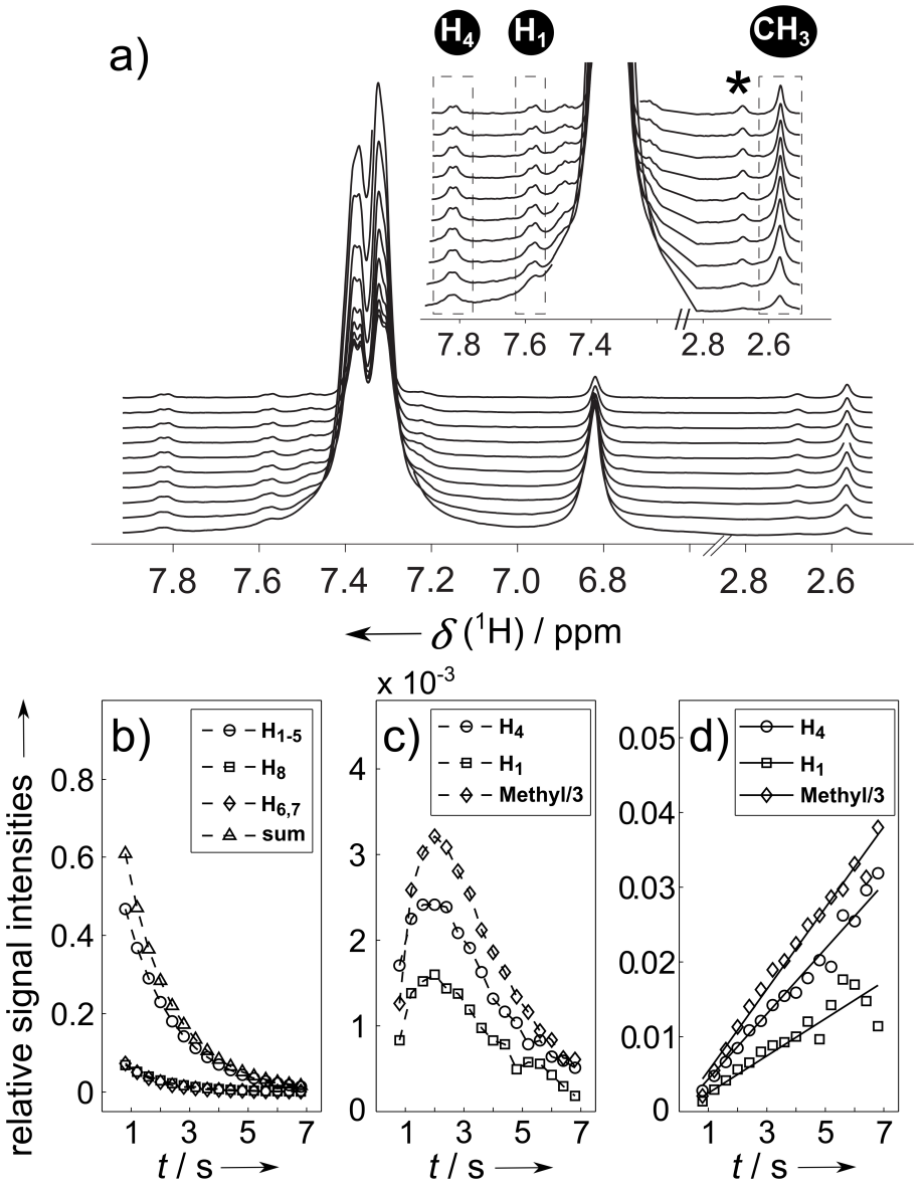

Figure III-5 : Buildup of HYPER-BIPO-NOE signal as a function of time. a) Series of spectra recorded from a single sample of hyperpolarized ligand 1 mixed with ligand 2 and protein. Spectra were recorded with 20.7° flip angle α, at intervals of 0.4 s. b) Integrals of ligand 1 taken from spectra in a). c) integrals of ligand 2 taken from spectra in a). The intensity of the methyl resonance is divided by 3. d) Integrals of peaks of ligand 2 divided by the sum of the integrals of ligand 1 and fitted with a linear function. (*) is a solvent resonance that was suppressed prior to the experiment using presaturation.

This is approximately true for the ligands used here, but would not always be expected to be the case. In the experimental data, in Figure III-5d, the integrals of resonances from

ligand 2 were divided by the sum of integrals of ligand 1. This treatment is reasonable under the assumption that magnetization transferred from ligand 1 to the protein is equally distributed through spin diffusion. Individual differences in polarization and cross-relaxation rates of protons in ligand 1 are then assumed to be averaged. The relative intensities that are obtained can be compared to Equation (III-1), and primarily contain information on the mode of binding of ligand 2. The data from Figure III-5d indicates that the methyl group of ligand 2 has the most efficient magnetization exchange with ligand 1, followed by protons H_4 and then H_1. This methyl group should therefore also have a close contact to the protein, which is mediating the magnetization exchange, and should be buried deep in the binding pocket while proton H_1 should be more distant from or less surrounded by protons of the protein. This finding for the methyl group and also for the protons H_1 and H_4 is in agreement with the previously determined structures of protein kinase A with the ligand 3-pyridin-4-yl-1*H*-indazole (ligand A).[165] The ligand A features a piperidyl instead of the methyl of ligand 2. In the crystal structure and according to INPHARMA data in the research,[165] this piperidyl group is buried in the protein comprising an equivalent binding epitope as suggested here for ligand 2. Additionally, full relaxation matrix calculations were performed with 10^6 pairwise combinations of the structures of the PKA in complex with the ligands using our home written program.[138] The peak integrals determined from the calculation and DNP experiment were well agreed together. The coincidence of this result shows that the analytical solution is in an excellent agreement with the presented numerical result.

Conclusions

Using a new experiment termed HYPER-BIPO-NMR, protein mediated interligand NOEs between two competitively binding ligands were observed. DNP hyperpolarization of one of the ligands provided a sensitivity contrast sufficiently large to avoid the need of using spin-state selective or two-dimensional NMR experiments for observing the transferred magnetization. In screening experiments for ligand binding, the observation of the transferred magnetization can be used to rapidly identify that both ligands bind to the same protein. Additionally, the buildup of transferred signal intensity from ligand 1 to ligand 2 as a function of time can be obtained from a single hyperpolarized experiment. The magnitude of the buildup rate is a function of the contact between individual spins on the receiving ligand and the protein, and as such provides limited structural information on the binding epitope. The information obtained from the HYPER-BIPO-NOE experiment may be contrasted to that available from the related STD and INPHARMA experiments. The characterization of the binding mode of ligand 2 in the present experiments is similar to what may be obtained with STD, which could also be applied with hyperpolarization. However, unlike STD, the HYPER-BIPO-NOE based experiment uses ligand 1 for a selective enhancement of the binding pocket. Therefore, we expect this experiment to exhibit selectivity towards a pair of ligands binding in the same pocket. On the other hand, since the present experiment does not distinguish between different spins on ligand 1, the correlation between spins on the two ligands that are in equivalent positions when binding to the protein, as in INPHARMA, is not observed. Such information could potentially be recovered by applying selective

inversion[128, 135] or 2D gradient encoding techniques. Even though the present report focuses on the observation of competitive binding of two ligands to a protein, the HYPER-BIPO-NMR experiment is not limited to this application. Rather, it presents a more general way to selectively enhance the magnetization of the binding pocket in a protein. In other experiments, the enhanced signal could for example also be used to selectively assign and observe those resonances, and with ^{13}C or ^{15}N labeled proteins could also be used with heteronuclear NMR experiments. Especially for larger proteins, where full assignments cannot easily be obtained, the selective enhancement may greatly facilitate the study of an active site.

CHAPTER IV

DETECTION OF LIVING ANIONIC SPECIES IN POLYMERIZATION REACTION USING HYPERPOLARIZED NMR*

Introduction

NMR has long played a pivotal role in studying reaction mechanisms in the field of polymer chemistry, since the technique reveals molecular structures and interactions with atomic resolution.[172-174] In the overwhelming majority of uses, NMR is applied as a steady-state method for analyzing products after completion of a reaction. It is then often necessary to use sophisticated synthetic strategies such as the selective incorporation of stable isotopes, to infer information about the reaction mechanism.[175-176] A more direct and potentially more powerful approach to characterizing a reaction is the monitoring of species that arise as the reaction occurs. Using dissolution dynamic nuclear polarization,[109] a hyperpolarization technique that can enhance NMR signal by several orders of magnitude, it is possible to study chemical reactions in real time.[133]

Dissolution DNP is a two-step process, where a frozen aliquot of the analyte is hyperpolarized, and then injected into an NMR spectrometer for analysis. DNP provides sufficient sensitivity to enable ^{13}C NMR spectroscopy at natural isotope abundance even at millimolar to sub-millimolar analyte concentration. The use of ^{13}C with its large chemical shift range further facilitates resolution of the resonances of interest. Most

* This chapter is reproduced with permission from Y. Lee, G.S. Heo, H. Zeng, K.L. Wooley, and C. Hilty. "Detection of Living Anionic Species in Polymerization Reaction using Hyperpolarized NMR." *Journal of the American Chemical Society* **2013**, In Press. Copyright 2013 the American Chemical Society.

typically, dissolution DNP has been applied to small molecules containing nuclei with spin-lattice relaxation times of at least several seconds to avoid prohibitive relaxation losses during sample injection. Under certain conditions, it is possible to obtain hyperpolarized spectra of macromolecules, for example proteins that are biosynthetically labeled with ^{2}H to counteract spin relaxation.[177] However, if attempting to hyperpolarize a previously synthesized polymer of large molecular weight without specific isotope enrichment, it can be expected that most of the observable signal would decay before initiation of the NMR measurement. Hyperpolarized signals from polymers can nevertheless be observed, if a polymerization reaction is carried out in-situ in the NMR instrument starting from hyperpolarized monomers.[178] Since polarization is continuously incorporated at the site of monomer addition, the active site of the growing polymer chain can be selectively enhanced. Here, we use this unique feature of a hyperpolarized polymerization reaction to enable the detection of intermediate species as they arise during the synthesis of polystyrene by anionic polymerization of hyperpolarized styrene monomer.

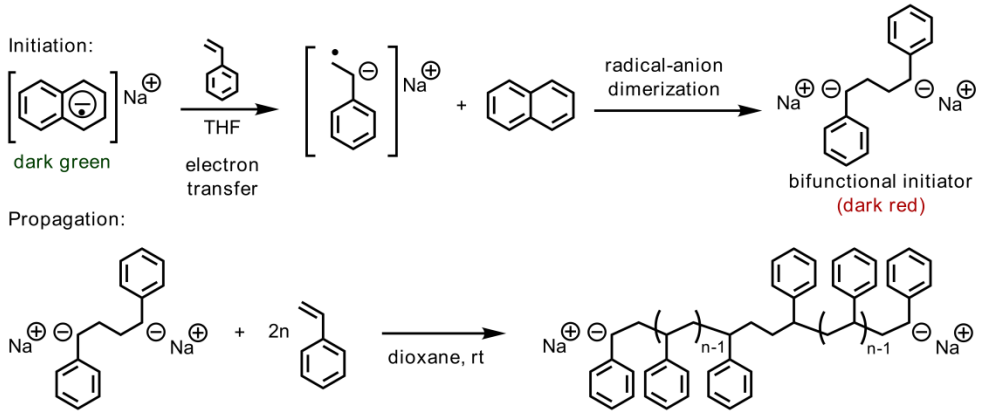

Figure IV-1 : Proposed mechanism of living anionic polymerization of styrene using sodium naphthalenide as an initiator.

Polystyrene can be synthesized by several different routes, including radical, anionic, cationic, and metallocene, or Ziegler-Natta catalyzed polymerizations.[179] Among these methods, the anionic mechanism is preferred if a polymer with a ultra-narrow molecular weight distribution is desired.[180-181] Since there are no termination steps and side reactions in an ideal situation, the synthetic technique is also applicable for synthesizing block copolymers.[182] Scheme 1 represents a mechanism for the living anionic polymerization of styrene, which was first demonstrated in 1956 by Szwarc and co-workers.[183-184] Styrene was polymerized in dioxane, with sodium naphthalenide as an initiator.[185] The generation of a bifunctional initiator takes place via single electron transfer from the sodium naphthalenide to a styrene monomer, followed by a dimerization between two of the resulting styryl radical anions. Initiation and propagation of styrene monomers then proceeds bidirectionally to generate telechelic polymer species, and growth continues until the monomer supply is exhausted.

Experimental Section

Sample Preparation

400 µL of styrene was mixed 15 mM free radical a,g-bisdiphenylene-b-phenylallyl (BDPA; Sigma Aldrich, St. Louis, MO) for DNP experiments, since styrene is self-glassing, and hence directly DNP polarizable. The reaction initiator was prepared by dissolving 2 g of pre-dried naphthalene and 500 mg of sodium film in 10 mL of tetrahydrofuran (THF). Subsequently, the initiator solution was sonicated for 5 minutes at a temperature of 298 K.

DNP Polarization

40 µL of styrene / BDPA mixture was hyperpolarized in a HyperSense instrument (Oxford Instruments, Tubney Woods, UK) for 3 h at a temperature of 1.4 K. During the polarization time, the sample was irradiated with microwaves (60 mW, 93.965 GHz) corresponding to $\omega_e - \omega_N$. Subsequently, the polarized sample was dissolved and injected into the NMR spectrometer. In preparation of dissolution, a 5 mm NMR tube was installed in the NMR instrument, and connected to the injection system. For experiments involving the polymerization reaction, 25 µL of initiator solution, sodium naphthalenide in THF, was preloaded in the NMR tube. The transfer lines in the DNP polarizer and injection system were purged with nitrogen gas to minimize sample contamination with room air. The sample was then dissolved in 4 mL pre-heated 1,4-dioxane, and transferred to a sample injector.[137] Injection into the NMR instrument used nitrogen gas pressures of 262 psi (forward pressure) and 150 psi (back pressure). Samples were mixed with initiator solution directly in the NMR tube, yielding a total sample volume of 500 µL.

NMR Spectroscopy and NMR Data Analysis

A series of ^{13}C spectra was acquired on a Bruker 400 MHz NMR spectrometer equipped with a broadband probe containing three pulsed field gradients (Bruker Biospin, Billerica, MA) at a temperature of 31 °C. NMR experiments were triggered after an injection time of 430 ms and a stabilization time of 400 ms. For the experiments without selective inversion, the pulse sequence (trigger – $[G_{x,y,z} - \alpha_x - \text{acquire}]_{\times 32}$) was

used. A total of 32 transients were acquired for 12.8 s, and the time between each transient was 0.4 s. For the each scan, a randomized pulsed field gradient $G_{x,y,z}$ (35..50 G/cm, 1 ms) was applied to ensure that no unwanted coherences remained from the previous scan. The small flip angle α of the excitation pulse was 16.7°, and the pulse strength γB1 was 29.1 kHz. In each scan, 16384 data points were acquired for an acquisition time of 340 ms. For the experiments with selective inversion, an IBURP2 shaped pulse of flip angle π and 20 ms duration at the resonance frequency of # C1 ~ # C5 in styrene and a randomized pulsed field gradient $G_{x,y,z}$ were added before the small flip angle pulse (trigger – shaped π – $G_{x,y,z}$ – [$G_{x,y,z}$ – α_x – acquire]$_{\times 32}$). During acquisition, WALTZ-16 ^{1}H decoupling was applied with a field strength γB_1 = 2.3 kHz. The living polymerization reaction was lasted for 10 min under the nitrogen gas pressure until that all monomers were consumed. At a subsequent time, the living end groups were protonated by adding 1 mL of methanol into the NMR tube. Chemical shifts of ^{13}C were calibrated against ^{1}H spectrum of 1 % of tetramethylsilane (TMS) in $CDCl_3$ according to the IUPAC recommendations.[149]

The raw NMR data were zero filling to 65,536 complex data points, and an exponential window function with a 2 Hz line broadening was applied before Fourier transform using the TOPSPIN 3.0 program (Bruker Biospin, Billerica, MA). Peak intensities of the reactant and intermediate were also determined by the TOPSPIN 3.0. Equation IV-16 in the text was used to fit the peak intensities of the reactant to provide two fit parameters ($S_M(0)$ and k') by MATLAB (The Math Works, Natick, MA). The peak intensities of the intermediate were fitted with Equation (IV-13) numerically by

MATLAB. The fit parameter r_P was optimized by minimizing the root mean square difference between the experimental peak intensities and simulated peak intensities.

MALDI-TOF Mass Spectroscopy

For mass spectrometry, the synthesized polystyrene from the DNP experiments, silver trifluoroacetate (AgTFA), and dithranol were dissolved in THF at concentrations of 1, 10 and 10 mg/mL, respectively. About 0.5 L of this mixture was deposited on a stainless steel sample holder. After air drying, the sample was analyzed by matrix assisted laser desorption ionization (MALDI) on a Voyager DE-STR mass spectrometer (Applied Biosystems, Foster City, CA) under optimized conditions in positive linear mode. The positive ions were generated by 100 pulsed nitrogen laser shots at 337 nm and accelerated through 25 kV. The AgTFA and dithranol served as cationization reagent and matrix, respectively. The mass spectrometry data is shown in

Quantitative Modeling of NMR Signal

The reaction mechanism for the polymerization of styrene consists of initiation (single electron transfer from the sodium naphthalenide to a styrene monomer), dimerization between two styryl radical anions to form a di-anion (complex), and propagation of polymerization from the di-anion until the monomer supply is exhausted. Under present experimental conditions, we assume that the steps of initiation and dimerization are instantaneous, such that it suffices to kinetically model the propagation step.[186] We further assume that there are no premature chain terminations, *i.e.* the concentration of living anionic polymer ends C_{P^-} does not change during the course of

the reaction, and is equal to the initially added initiator concentration I_0 . The propagation step is a second order reaction, therefore the rate of change of monomer concentration C_M is

$$\frac{dC_M}{dt} = -k_P \cdot C_{P_n} \cdot C_M = -k_P \cdot I_0 \cdot C_M = -k' \cdot C_M \qquad \text{(IV-1)}$$

The propagation rate constant k_P is assumed to be independent of the length of polymer chains, and

$$k' = I_0 \cdot k_P \qquad \text{(IV-2)}$$

is the pseudo first order reaction rate constant.

The solution for Equation (IV-1) is

$$C_M(t) = C_0 \cdot e^{-k' \cdot t} \qquad \text{(IV-3)}$$

where C_0 is the initial concentration of the styrene.

In the following, we consider the NMR signal arising from the active anionic chain ends, which is proportional to the spin polarization of the same site at the time of measurement. The chemical shift of anionic end sites is different from chemical shifts of corresponding atoms in the interior of a polymer molecule. Therefore, the change in spin polarization of the end sites is due to addition of hyperpolarization from freshly added monomers, due to the loss of previously present polarization when an end group transitions to the interior of the polymer due to addition of a monomer, and due to spin-lattice relaxation of the end group. It is noted that the contributions from the first two processes do not cancel because of the spin relaxation that reduces the polarization of the end group before the addition of a new monomer.

A convenient way of calculating the time evolution of spin polarization is to separately consider the concentrations of atoms in the spin-up (here designated as $\oplus$) and spin-down ($\ominus$) states. For example for the monomer, $C_M = C_M^{\oplus} + C_M^{\ominus}$. The longitudinal magnetization, which translates to the observable NMR signal is

$$S_M \propto C_M^{\oplus} - C_M^{\ominus} \tag{IV-4}$$

The time evolution of the spin-up and spin-down concentrations is given by

$$\frac{dC_M^{\oplus}}{dt} = \frac{r_M}{2} \cdot (C_M^{\ominus} - C_M^{\oplus}) - k' \cdot C_M^{\oplus} \tag{IV-5}$$

and

$$\frac{dC_M^{\ominus}}{dt} = \frac{r_M}{2} \cdot (C_M^{\oplus} - C_M^{\ominus}) - k' \cdot C_M^{\ominus} \tag{IV-6}$$

Where r_M represents the spin-lattice relaxation rate of the monomer. Combining Equations (IV-5) and (IV-6) yields

$$\frac{d}{dt}(C_M^{\oplus} - C_M^{\ominus}) = -r_M \cdot (C_M^{\oplus} - C_M^{\ominus}) - k' \cdot (C_M^{\oplus} - C_M^{\ominus}) \tag{IV-7}$$

Together with Equation (IV-4),

$$\frac{d}{dt} S_M(t) = -r_M \cdot S_M(t) - k' \cdot S_M(t), \tag{IV-8}$$

giving the solution

$$S_M(t) = S_{M_0} \cdot e^{-(k'+r_M)\cdot t} \tag{IV-9}$$

The equations for the anionic site P^- can be written in a similar way except that there are two kinetics terms, for the addition of signal from monomers and for the loss of signal to interior sites:

$$\frac{dC_{P^-}^{\oplus}}{dt} = \frac{r_{P^-}}{2} \cdot (C_{P^-}^{\ominus} - C_{P^-}^{\oplus}) + k_P \cdot C_M^{\oplus} \cdot (C_{P^-}^{\oplus} + C_{P^-}^{\ominus}) - k_P \cdot (C_M^{\oplus} + C_M^{\ominus}) \cdot C_{P^-}^{\oplus} \qquad \text{(IV-10)}$$

$$\frac{dC_{P^-}^{\ominus}}{dt} = \frac{r_{P^-}}{2} \cdot (C_{P^-}^{\oplus} - C_{P^-}^{\ominus}) + k_P \cdot C_M^{\ominus} \cdot (C_{P^-}^{\oplus} + C_{P^-}^{\ominus}) - k_P \cdot (C_M^{\oplus} + C_M^{\ominus}) \cdot C_{P^-}^{\ominus} \qquad \text{(IV-11)}$$

The concentration difference between the two spin states (Equation (IV-10) - (IV-11)) is

$$\begin{aligned} \frac{d}{dt}(C_{P^-}^{\oplus} - C_{P^-}^{\ominus}) = -r_{P^-} \cdot (C_{P^-}^{\oplus} - C_{P^-}^{\ominus}) + k_P \cdot (C_M^{\oplus} - C_M^{\ominus}) \cdot (C_{P^-}^{\oplus} + C_{P^-}^{\ominus}) \\ - k_P \cdot (C_M^{\oplus} + C_M^{\ominus}) \cdot (C_{P^-}^{\oplus} - C_{P^-}^{\ominus}) \end{aligned} \qquad \text{(IV-12)}$$

Using Equations (IV-2), (IV-3) and (IV-9), the equation for the longitudinal magnetization of the polymer end sites P^- becomes

$$\begin{aligned} \frac{d}{dt} S_{P^-}(t) &= -r_{P^-} \cdot S_{P^-}(t) + k_P \cdot S_M(t) \cdot I_0 - k_P \cdot C_M(t) \cdot S_{P^-}(t) \\ &= -r_{P^-} \cdot S_{P^-}(t) + k' \cdot S_M(0) \cdot e^{-(k' + r_M) \cdot t} - \frac{k' \cdot C_0 \cdot e^{-k' \cdot t}}{I_0} \cdot S_{P^-}(t) \end{aligned} \qquad \text{(IV-13)}$$

Based on this discussion, the experimentally determined monomer signal can be used for fitting Equation (IV-9). In order to account for the signal lost due to each small-flip angle pulse, the model curve for signal intensities is scales with $e^{(-\lambda \cdot (t - t_0))}$ where $\lambda = -\ln(\cos(\alpha)) / \Delta t$ (α; a flip angle, Δt; the time interval between NMR acquisitions, t_0; a time delay between the start of the chemical reaction and the start of the NMR acquisition).[187] Further, r_M was obtained from a dataset without reaction (Table IV-3). The fit, which was performed using MATLAB (The MathWorks, Natick, MA) then yielded the pseudo-first order rate constant k' and the initial monomer signal S_{M_0}.

For the signal intensities from product, which is described by the differential Equation (IV-13), numerical solutions can readily be found if all of the parameters are known. At this point in the data analysis, the parameters k' and S_{M_0} have already been determined from the fit of the monomer. The initial monomer concentration C_0 was determined from ^{1}H NMR spectra (see above).

From the monomer concentration, it would in principle be possible to calculate the sample dilution factor that is due to the dissolution process, and therefore estimate the initiator concentration I_0. However, we expected that a portion of the initiator would be deactivated before the NMR measurement. As an alternative, this concentration was determined from the polymer chain length distribution in the final reaction product. Under the conditions stated above, and under the assumption that all monomers were used up during the reaction time, the chain lengths follow a Poisson distribution[188-189]

$$p(n) = \frac{\lambda^{(n-1)} \cdot e^{-\lambda}}{(n-1)!} \qquad \text{(IV-14)}$$

where n is the chain length, and λ represents the average degree of polymerization. λ was determined by fitting the distribution $a \cdot p(i)$ to intensities corresponding to each chain length obtained from MALDI mass spectra. The initiator concentration, I_0 was then determined using[190-191]

$$\lambda = \frac{4 \cdot (C_0 - I_0)}{I_0} \qquad \text{(IV-15)}$$

The only remaining unknown in Equation (IV-13) is then the relaxation rate of the anionic chain ends, r_P. Since this is a differential equation, it is further necessary to

select initial conditions for the solution. Here, we assumed that $S_{P^-}(0) = 0$. The relaxation rate r_P was then determined by fitting to the experimental peak intensities, which had previously been scaled as described above to account for the small-flip angle excitation. Fitting was carried out in MATLAB, by minimizing the root mean square difference between the experimental peak intensities and the numerical solution to Equation (IV-13).

The assumption that initial polymer chain end signal is zero appears reasonable in light of the fact that the initial dimer is formed by association of two radical anions, which would be subject to rapid spin relaxation. However, if the lifetime of the radical ionic monomers is sufficiently short, it would be possible that a certain amount of initial polarization remains, which would reduce the goodness of the fit obtained.

Results and Discussion

For the DNP experiment, an aliquot of styrene monomers was hyperpolarized in the solid state at 1.4 K, then rapidly dissolved in dioxane heated at 200 ℃ under pressure and mixed with a solution of sodium naphthalenide in thtrahydrofuran, with in the NMR spectrometer.[137] The progress of the polymerization reaction was monitored for a duration of 13 s through a series of small flip angle excitations (Figure IV-2a). Due to a signal enhancement of more than 4000-fold compared to a conventional single scan NMR spectrum, predominantly the resonances of styrene were observed. In addition, however, the spectra contain several smaller signals, which were not detected in reference ^{13}C NMR spectra of the final reaction product polystyrene (Figure IV-2c) or

the reactant styrene (Figure IV-2d). These peaks, highlighted in green in Figure IV-2a, therefore apparently belong to reaction intermediates that are present only during the reaction progress. Here, based on characteristic chemical shifts, we may directly postulate that these resonances stem from the di-anionic polystyryl intermediate. The identity of each individual peak would in general, however, be difficult to determine simply based on observation in a 1D ^{13}C spectrum.

In order to determine the identity of such intermediates, peak splittings in an undecoupled ^{13}C spectrum can be useful, since these can be directly obtained from a sequence of one-dimensional spectra acquired from a hyperpolarized sample. In Figure IV-3b and c as well as Figure IV-4, individual peaks from a proton decoupled and a proton coupled (*i.e.* undecoupled) ^{13}C spectrum are illustrated. Despite the on-going reaction, the resolution in the spectra obtained is sufficient to resolve the expected peak splittings. For example, groups of doublet signals are observed in the range between 90 and 140 ppm. These signals arise from the ^{13}C nuclei in the phenyl ring (#3–5), which are each bonded to a single proton. A group of singlet signals is observed near 150 ppm, which, due to the absence of a directly bonded proton, can be assigned to the quaternary aromatic carbon #1.

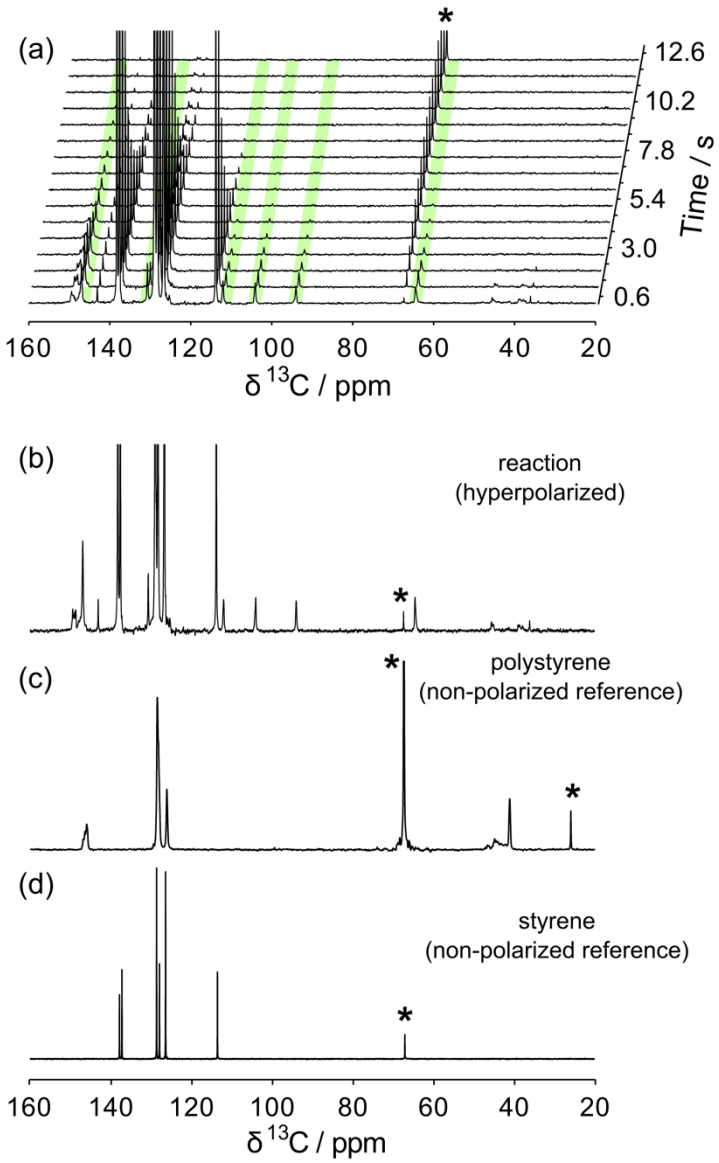

Figure IV-2 : a) Series of ^{13}C NMR spectra recorded from a single sample of hyperpolarized styrene mixed with sodium naphthalenide. b) Hyperpolarized ^{13}C NMR spectrum for the reaction between styrene and sodium naphthalenide. c) Non-hyperpolarized ^{13}C NMR spectrum of synthesized polystyrene. d) Non-hyperpolarized ^{13}C NMR spectrum of styrene monomer. (*) designates the resonances from 1,4-dioxane, and THF. The resonance from 1,4-dioxane in the polystyrene spectrum was suppressed using a selective 90° pulse and randomized pulsed field gradients.

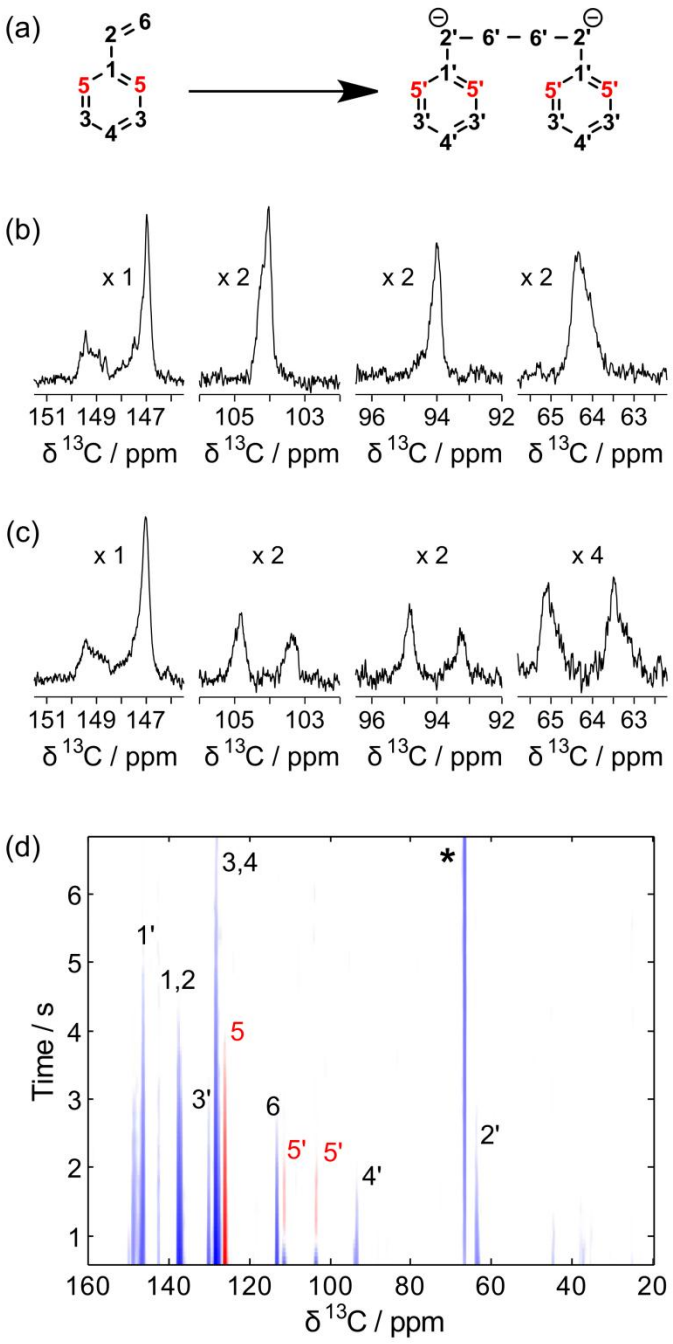

Figure IV-3 : a) Scheme for the living anionic polymerization of styrene. Two living ends are represented in a dimer molecule. b) Expanded views of ^{1}H decoupled ^{13}C spectrum of the reaction of hyperpolarized styrene. c) As in (b), except without ^{1}H decoupling. d) Hyperpolarized correlation experiment with a selective inversion on resonance #5 at the beginning of the reaction. Positive and negative signals are represented in blue and red, respectively. Scaling factors were indicated in each section in b), and c). (*) designates the resonances from 1,4-dioxane, and THF.

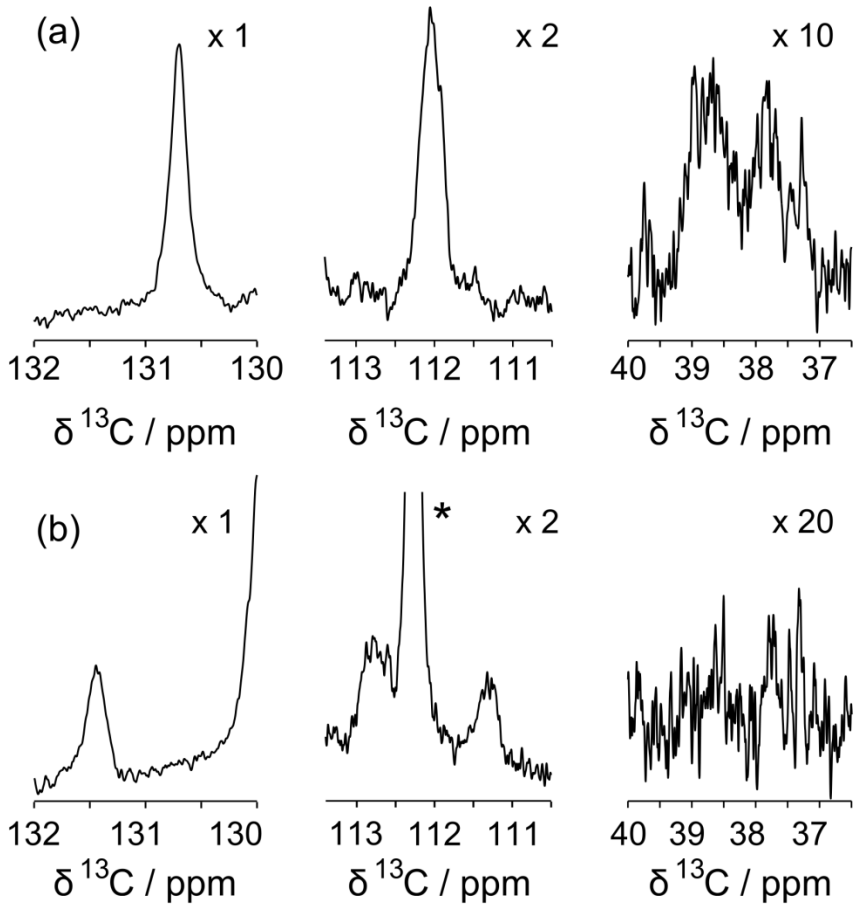

Figure IV-4 : a) Expanded views of peaks in ^{13}C spectra of the reaction of hyperpolarized styrene, with ^{1}H decoupling. b) As in (a), but without ^{1}H decoupling. Scaling factors used for plotting are indicated in each section. (*) designates the resonance from the #2 carbon of hyperpolarized styrene monomer; all other resonances are from polymer.

Although important information can be extracted from chemical shifts and coupling constants, this approach usually requires a certain amount of prior knowledge about the molecules under study. An inherent limitation of one-dimensional spectroscopy is the absence of direct correlations between different atoms, which in conventional NMR would be most readily solved by acquiring multi-dimensional spectra. Here, using hyperpolarized NMR of the dynamic system, we exploit a different type of correlation

that acts over time. The Zeeman population difference giving rise to the signals in a entire time series of spectra is generated by DNP at the beginning of the experiment. Therefore, a correlation between two chemical species that are transformed into each other can be established by selective manipulation of the spin state of one of those species, which then transfers to the other.[135-136] In Figure IV-3, a selective inversion was applied to the resonance of the *ortho* carbon (#5) in styrene. In the subsequent reaction, negative (red) signals were observed for the peaks at 112 ppm and 104 ppm, which can therefore be unambiguously assigned to #5′ in the polystyryl anion. All of the other, non-inverted spins on the reactant and intermediate yielded positive signals (blue). The two peaks observed for #5′ are due to the partial double bond character between #2 and #1, which hinders free rotation of the phenyl ring.[192] The resulting partial sp^2 hybridization character of the alpha carbon (#2) also manifests itself in the scalar coupling constant of J_{CH} = 152 Hz.[193] Close inspection of Figure IV-3d reveals that the peaks #5′ also show positive signals for a short time at the beginning of the reaction. Inevitably, the polymerization reaction started during sample injection, before the selective inversion pulse could be applied. The initial positive intensity in the product signal was generated from non-inverted monomers. In this reaction, the initiation step is much faster than the propagation step.[186] The signal change from positive to negative therefore confirms that the observed product signals during the course of the reaction were due to fresh additions of inverted monomers to the living intermediate, and not simply due to the initial dimer.

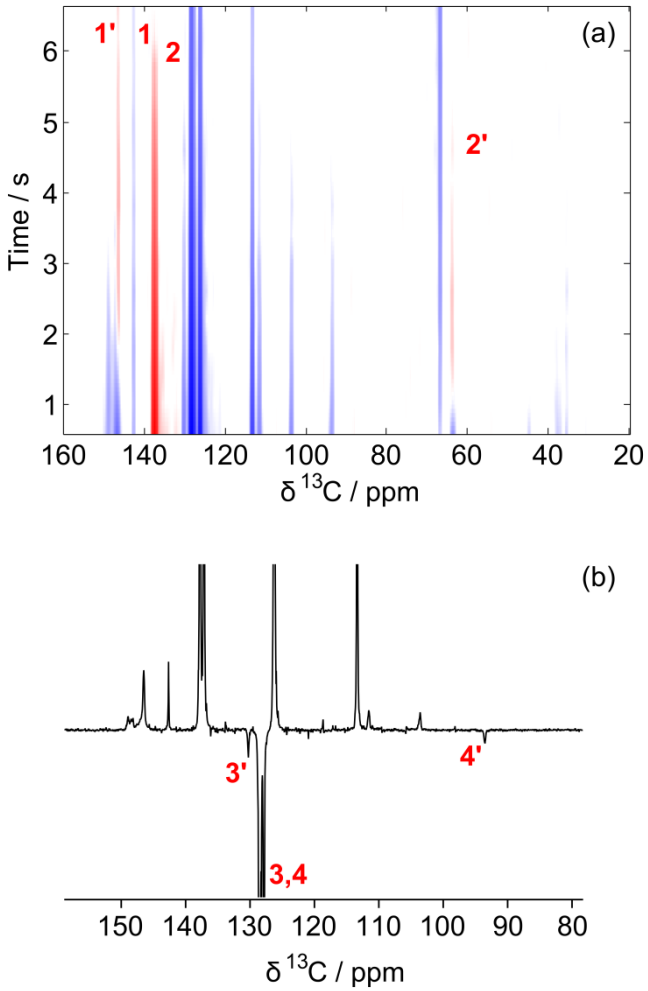

Figure IV-5 : a) Hyperpolarized correlation experiment with a selective inversion on resonance #1 (137.7 ppm), and #2 (137.0 ppm). Positive and negative signals are represented with red and blue, respectively. Only the target signal on peak #1, and #2 in the reactant and its corresponding signals (peak #1 (146.4 ppm) and #2 (63.9 ppm)) in the product represented with negative signal intensities (blue), while non-inverted spins on the reactant and product still represented with positive signal intensities (red). b) Hyperpolarized correlation experiment with a selective inversion on resonance #3 (128.5 ppm), and #4 (127.8 ppm).

In order to provide direct verification for the origin of the other peaks in the intermediate, the hyperpolarized ^{13}C correlation NMR experiments were repeated by changing the selective inversion to different spins of styrene (Figure IV-6). Inverted peaks were detected at 146.9 ppm, 64.5 ppm, 130.7 ppm and 94.0 ppm for carbons #1′ –

#4′. Selective inversion of #6 did not yield an observable inverted signal, likely due to increased spin relaxation in the polystyrene backbone. Based on a set of such inversion experiments, it is possible to quite generally and unambiguously assign the observed peaks from the reaction intermediate. Here, the determined chemical shifts of the active site in the growing polystyryl chain are in good agreement with the values of a mono-anionic polystyryl molecule determined by conventional NMR under equilibrium conditions.[192] A difference of 5.2 ppm was observed at the alpha carbon (peak #2′), which is likely due to the effect of the counter cation (δ (Na) > δ (Li)).[192]

Apart from the resonances discussed above, the spectra in Figure IV-2 and Figure IV-3 contain peaks from minor species. These peaks are not the focus of the present study, but could be analyzed to gain more information about the reaction conditions and possible side reactions. A sharp singlet signal at 143 ppm is noted. This chemical shift, along with 128.7, 36.1 and 31.6 ppm was also determined for synthesized 1,4-diphenylbutane (Figure IV-6), and in the reaction could belong to styrene oligomer that has been quenched by residual water. Additional peaks are also observed near 150 ppm (Figure IV-7). Based on chemical shift, these peaks may appear to be related to #1, however, they do not show inversion in the experiment of Figure IV-6.

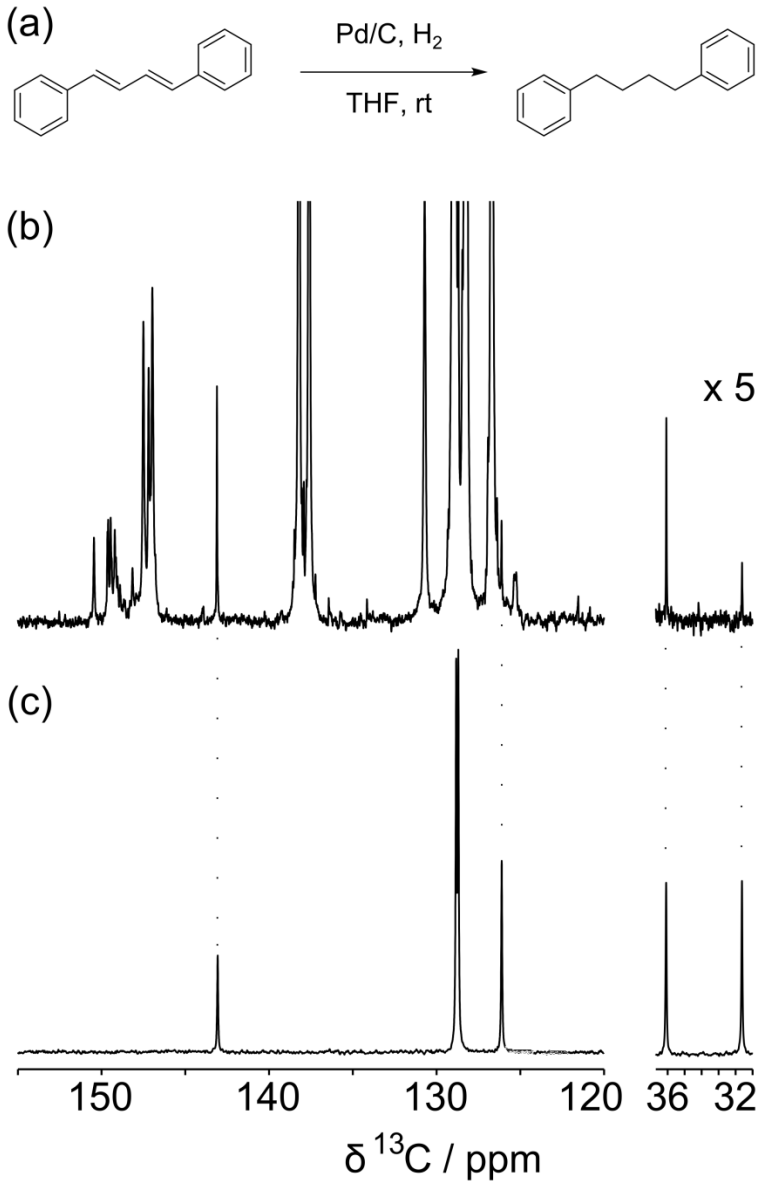

Figure IV-6 : a) Synthesis of 1,4-diphenylbutane. Pd/C (10 mg, 10 wt %) was added to a solution of 1,4-diphenyl-1,3-butadiene (100 mg) in THF. The round bottom flask containing the reaction mixture was evacuated from air and filled with H_2. Upon completion of the reaction as judged by thin layer chromatography (TLC) monitoring, Pd/C catalyst was filtered off on celite and carefully washed with THF. The combined filtrate was evaporated to give a 1,4-diphenylbutane in quantitative yield, b) hyperpolarized ^{13}C NMR spectrum for the reaction between styrene and sodium naphthalenide, c) thermal ^{13}C NMR spectrum for synthesized 1,4-diphenylbutane.

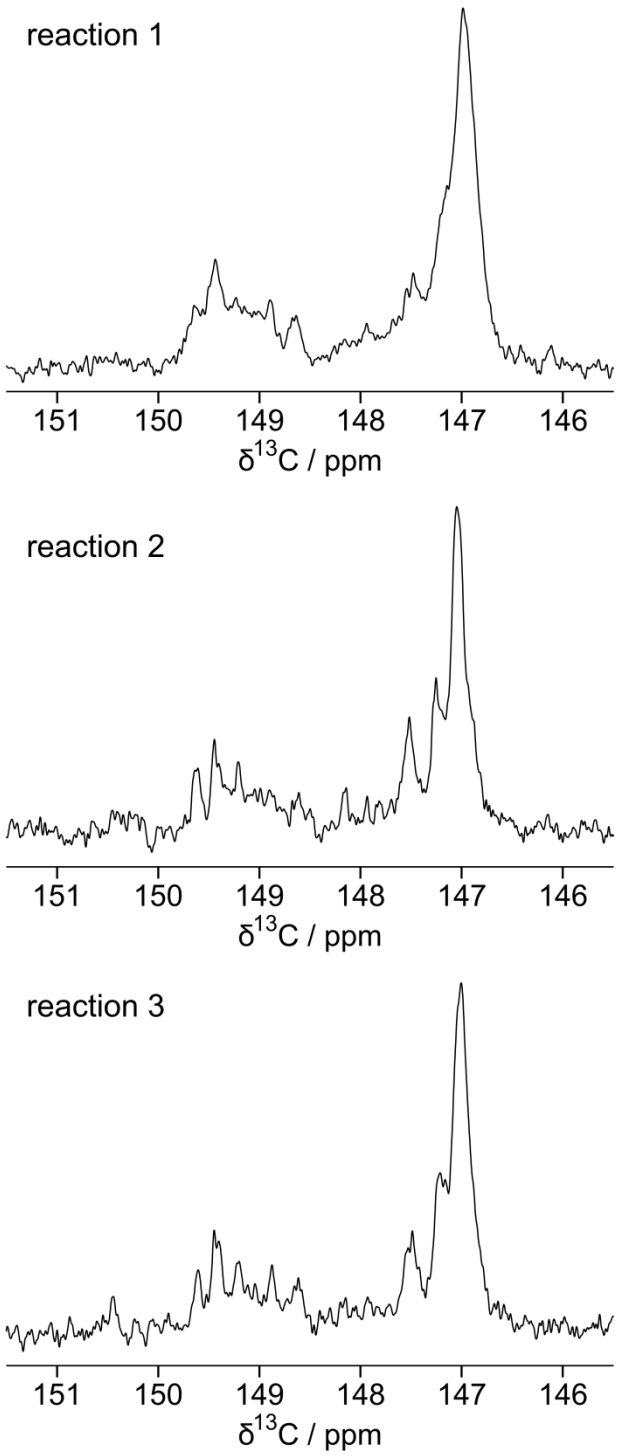

Figure IV-7 : Expanded views of the downfield region of ^{13}C spectra of the reaction of hyperpolarized styrene (with ^{1}H decoupling). The three panels show data from reactions 1–3.

In addition to the information pertaining to reaction mechanism, any real-time measurement also contains kinetic information. A benefit of the DNP-NMR technique is the capability to determine reaction mechanism and kinetics simultaneously from a single hyperpolarized sample. In order to extract kinetic information, it is, however, necessary to consider the process of spin-relaxation along with the reaction, since both give rise to changes in signal intensity. The DNP experiments start with large initial polarization, which decays towards the thermal equilibrium. The latter is negligible, therefore the only source of observable signals stems from the hyperpolarized styrene monomers. The living anionic polymerization discussed here is a second-order reaction, and its propagation rate is $v = k_P \cdot C_{P^-} \cdot C_M = k_P \cdot I_0 \cdot C_M$ where C_{P^-} and C_M represent the concentration of the propagating polystyryl anion and styrene monomer, respectively. We assumed that k_P is independent of the length of polymer chains. Since there is no termination step, C_{P^-} is constant, and equal to the concentration of the initiator I_0 . A pseudo first order reaction rate constant k' is defined as $k' = k_P \cdot I_0$. Taking the kinetics and spin relaxation r_M into account, the time evolution of signal intensities of styrene monomer S_M follows Equation (IV-9).

As the living polystyrene possesses negative charges at the chain ends, the anionic terminal carbon chemical environments are different from those of interior backbone structure, resulting in distinguishable chemical shifts. The signal intensities of the anionic chain end S_{P^-} can be calculated using a model where fresh polarization is added through addition of monomers, and polarization is lost both due to spin relaxation and

due to transitioning of a given moiety to the interior of the polymer. A differential equation for S_{P^-} is as follows in Equation (IV-13), where C_0 is an n initial concentration of styrene, and r_P is the spin relaxation rate of the anionic chain end, which is assumed to be independent of the length of polymer chains. In order to find a solution to this equation, it is further necessary to specify a boundary condition; here, $S_{P^-}(0) = 0$ is used based on the assumption that the signal of the dimer is negligible due to fast relaxation of its precursors, two radical anions.

The unknown reaction and relaxation rates can be obtained from fitting these models to time-resolved DNP-NMR data sets, such as shown in Figure IV-2a. In order to obtain these data, a series of fixed small flip angle pulses was applied to acquire NMR spectra at equal time intervals. To account for the depletion of polarization by small-flip angle pulses, Equation (IV-9), as well as the numerical solution of Equation (IV-13) was multiplied with factor of $e^{(-\lambda\cdot(t-t_0))}$ prior to calculating the root mean square difference. In the exponential, $\lambda = -\ln(\cos(\alpha))/\Delta t$ depends on the small flip angle α and the time interval between NMR acquisitions Δt.

The pseudo-first order reaction rate constants k' were obtained from fit of Equation (IV-9) to the thus normalized signal intensities of styrene monomer (Figure IV-8). This procedure requires knowledge of the relaxation rates of styrene monomer r_M, which were determined from a DNP experiment in the absence of a reaction (without addition of sodium naphthalenide). The propagation rate constant (k_P) was finally calculated with knowledge of the initiator concentration,[190-191] which was determined from the chain

length distribution obtained by matrix assisted laser desorption/ionization (MALDI) mass spectrometry of the reaction product (Figure IV-9).[188-189]

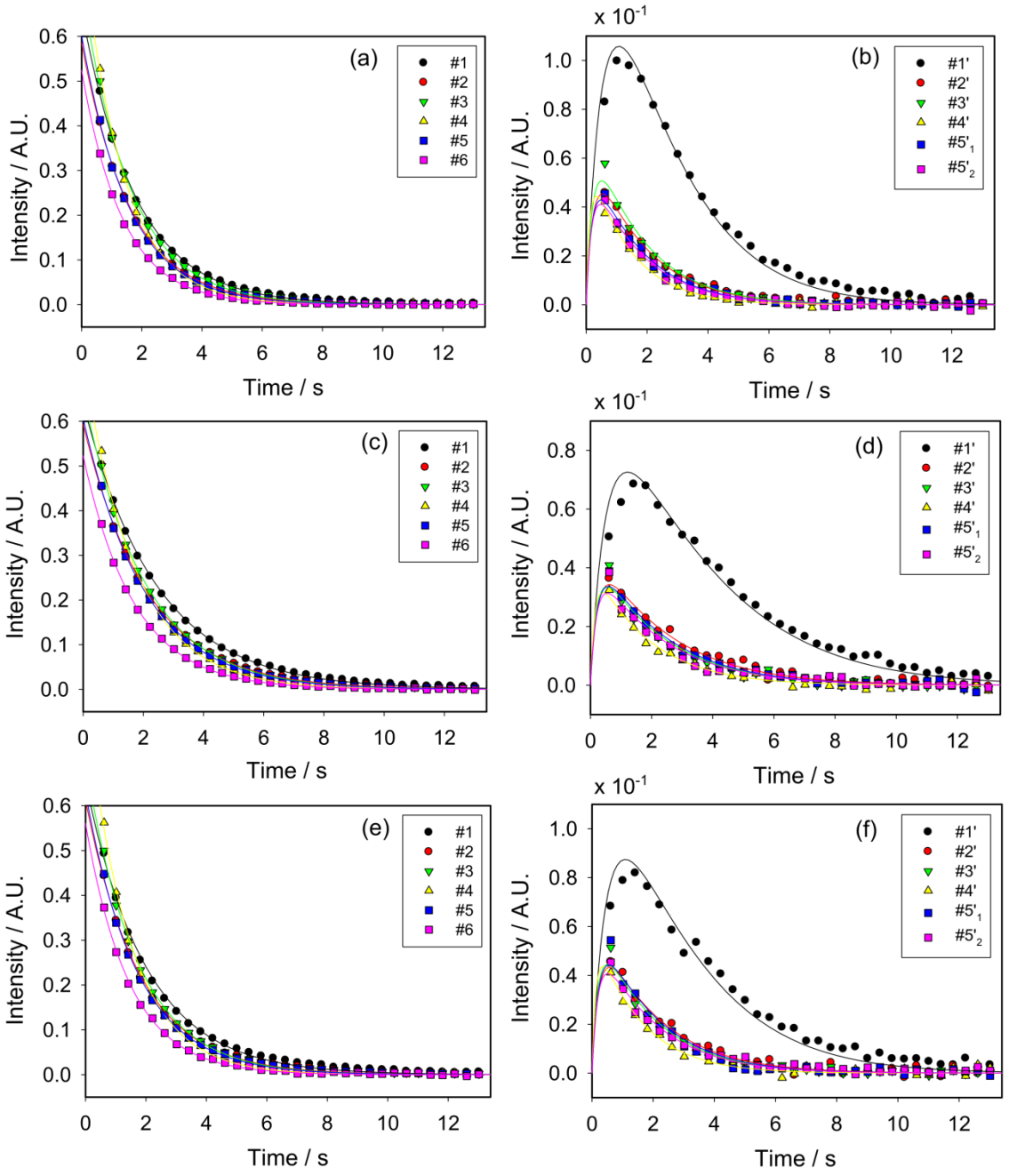

Figure IV-8 : Fits of the relative signal intensities of (a,c,e) styrene and (b,d,f) living ends of the intermediate for reaction 1 ~ 3 with Equation (IV-9) and Equation (IV-13).

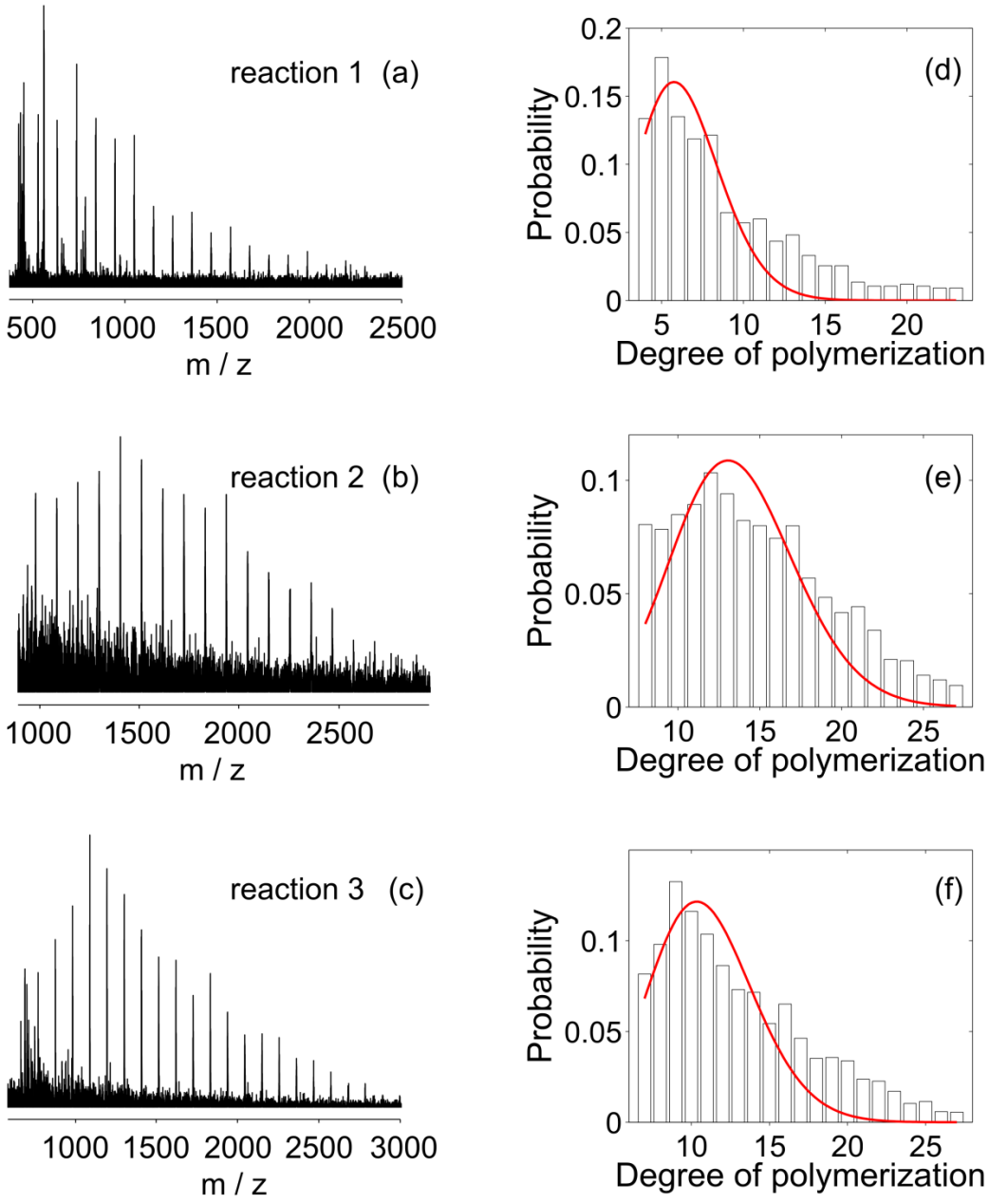

Figure IV-9 : MALDI-TOF Mass spectrum of the synthesized polystyrene from the DNP-NMR experiments (a ~ c) and their corresponding molecular distributions (d ~ f). Red lines represent fit lines with Poisson distribution function.

The average propagation rate constant based on three independent data sets was 5.6 ± 0.6 $M^{-1}s^{-1}$ (Table IV-1). This value is in excellent agreement with the literature (3.4 ~ 6.5 $M^{-1}s^{-1}$; measured under similar conditions, but without the additional 5% (v/v) of THF present in the DNP experiments).[194-196]

Table IV-1 : Determination of the propagation rate constant, k_P. [a] Calculated from Equation (IV-9) and reported as average value from six different carbon atoms of styrene. Individual values are reported in supporting Table IV-2. [b] Degree of polymerization; determined from the MALDI mass spectrum of reaction product. [C] Determined from comparison of the D.P. obtained from MALDI data with the known monomer concentration.

	k'[a] (s^{-1})	D.P.[b]	I_0[c] (mM)	k_P ($M^{-1}s^{-1}$)
Reaction 1	0.46	6.3	92	5.0
Reaction 2	0.32	13.6	54	5.9
Reaction 3	0.41	10.8	65	6.3

Although the reaction kinetics can unambiguously be determined from the monomer signals, we tested the proposed model for kinetics and spin relaxation in the styrene polymerization reaction by also fitting the signal intensities of the living end intermediate (Figure IV-8). This fit was calculated by adjusting a single unknown parameter, the relaxation rate r_P of the intermediate to minimize the root mean square difference between experimental data and the numerical solution of Equation (IV-13). The numerical solution was calculated in each iteration for r_P using a variable step Runge-Kutta method with given parameters (k', r_M, C_0). In addition, specification of initial conditions was required, which were taken as $S_{P^-}(0) = 0$ under the assumption

that signals from the initial dimer carries no signal due to rapid relaxation in its precursors, the styryl radicals.

Figure IV-8 shows signal intensities of the living intermediate with their corresponding numerical fit lines, and the obtained r_P values from the three independent data sets are summarized in Table IV-3. Despite the use of only one fit parameter, the curves agree remarkably well with the experimental data. Small differences, in particular at the beginning of the reaction, may be attributed to a certain amount of remaining signal on the initial styrene dimers, which, however, cannot be modeled reliably based on the available data. Additionally, the relaxation rates of all of the non-overlapping carbon atoms in the anionic chain ends r_P thus determined agree to within 12 % with reference rates obtained from a standard of polystyrene (Polymer Laboratories, Church Stretton, UK; average molecular weight M_n = 1360 g/mol), the measurement of which is, however, not selective for chain ends. Since the r_P value from the fit is obtained based on analysis of the kinetic parameters, the coincidence of the relaxation rates suggests overall validity of this method for analysis of the DNP data. Further, any errors introduced due to sample injection, mixing and turbulence[136, 169] appear to be minimal under the present conditions.

Table IV-2 : Determination of the pseudo first order reaction rate constant *k′*, using integrals from each peak of styrene monomer in the three reactions.

	#1 (s^{-1})	#2 (s^{-1})	#3 (s^{-1})	#4 (s^{-1})	#5 (s^{-1})	#6 (s^{-1})
Reaction 1	0.43	0.44	0.42	0.51	0.45	0.45
Reaction 2	0.29	0.29	0.30	0.34	0.30	0.30
Reaction 3	0.37	0.38	0.39	0.47	0.39	0.39

Table IV-3 : Apparent relaxation rates of the anionic living ends of polystyrene (r_P), of polystyrene, and of styrene monomer (r_M) [a] Both carbons #5 are equivalent in styrene monomer. [b] These values are overall relaxation rates for the standard polystyrene, not the rates for the specific living chain ends. Since signals of atoms #3 & #4 in polystyrene were overlapped, an average value is shown. Only one rate is shown for #5, since both protons in polystyrene are magnetically equivalent.

	Par. name	#1 (s^{-1})	#2 (s^{-1})	#3 (s^{-1})	#4 (s^{-1})	$\#5_1$ (s^{-1})	$\#5_2$ (s^{-1})	#6 (s^{-1})
Monomer (DNP polarized)[a]	r_M	0.027	0.077	0.10	0.14	0.098		0.19
Monomer(non-hyperpolarized)[a]		0.033	0.076	0.094	0.13	0.093		0.16
Polymer (non-hyperpolarized)[b]		1.0	4.2	3.3		3.8		5.0
Reaction 1	r_P	1.1	3.7	4.0	7.1	4.2	4.5	N/A
Reaction 2	r_P	0.85	3.1	3.9	5.7	3.4	3.8	N/A
Reaction 3	r_P	0.96	3.3	3.9	6.3	3.4	3.8	N/A

Conclusions

We showed an application of solid-to liquid state DNP-NMR method to examine the living anionic polymerization of styrene. Experiments based on hyperpolarized ^{13}C NMR spectroscopy allow study of the reaction mechanism and kinetics, simultaneously, while the reaction progresses. Continuous propagation of hyperpolarized monomers *via*

the reaction intermediate generates a selective hyperpolarization of the active living site, providing a sufficient sensitivity to capture the living species without signal averaging or stable isotope labeling. In addition to monitoring the polymerization reaction in real-time, the correlation experiment with a selective inversion on the spin of interest offers unambiguous identification of the chemical shifts from the reaction intermediate. The living anionic polymerization reaction studied here is sensitive to water and air. Nevertheless, the DNP-NMR technique in combination with a closed rapid sample injection system could provide a sufficiently inert environment for the successful study of the reaction. Systematic modifications, which allow for loading the active initiator and dried solvents while excluding air contact, may further improve the experimental results. On this premise, the method presented here represents an attractive means for fundamental studies of polymerization reactions, where alternative techniques would involve cumbersome isotope labeling and synthesis strategies. Having demonstrated the overall DNP-NMR approach for the study of reactants and highly reactive polymerization intermediates during the living anionic polymerizations of styrene, this technique shows promise for applicability to lesser studied polymerization systems.

CHAPTER V

DISSOLUTION DNP STUDY OF LIVING RING-OPENING POLYMERIZATION OF L-LACTIDE

Introduction

Since Szwarc's first demonstration of living polymerization in 1956, a variety of studies on living polymerization reactions have been conducted.[183] The unique characteristics of the synthetic methodology, basically no terminations and side reactions, a fast initiation step, and constant chain growth rate, enable researchers to synthesize polymers with a predictable molar mass and low polydispersity index (PDI). Several different types of polymers such as polystyrene, polypropylene, and polylactide have been created through the living polymerization technique.[184, 197-198]

Polylactide (PLA) is an aliphatic polyester, which can be degraded to low molecular weight oligomers by microorganisms. Because of this biodegradable property, the polymer can be a valuable substitute for petroleum-based products such as polyethylene and polystyrene.[199-200] Traditionally, aliphatic polyesters have been synthesized through a ring-opening polymerization (ROP) with metals.[201] However, this synthetic methodology is not an ideal approach for electronic or medical applications since the resulting polymers may contain residual metal ions. Therefore, a new synthetic method using organic catalysts has been investigated by several research groups. Catalytic properties of numerous organic catalysts including cyclic carbenes, thiourea amines, and bicyclic guanidine-based catalysts were examined for a solution-phase ROP of cyclic

esters.[202-205] Among them, triazabicyclodecene (TBD) exhibited higher catalytic activity with a narrow polydispersity index in the resulting polymer when compared to the other organic catalysts.[204]

After the discovery of this new class of catalysts, it is very important to understand the reaction mechanisms since this will allow researchers not only to further improve catalysts, but also find the best reaction conditions. From several mechanistic studies, two different reaction mechanisms (a nucleophilic catalytic mechanism and a hydrogen bonding mechanism) of the ROP of cyclic esters were proposed, however, none of them were experimentally proved by directly capturing reaction intermediates that arise as the reaction occurs. In computational and kinetic studies,[204, 206-207] the hydrogen bonding mechanism is preferred to the nucleophilic catalytic mechanism because of the lower energy barriers of reaction intermediates in the hydrogen bonding mechanism. Additionally, recent researches revealed that amidine bases can be used as nucleophiles for the ring-opening polymerization of L-lactide.[208]

One of the potential advantages of the hyperpolarization method described in previous chapters is the ability to observe ^{13}C signals in a single scan without isotope labeling.[109] A large chemical shift dispersion of ^{13}C spins enables clear observations of the reactant and product without severe signal overlap. Here, we demonstrate a general applicability of dissolution DNP to the field of polymer science. As the exemplary case for this application, lesser studied polymerization reaction, ring-opening polymerization of L-lactide catalyzed by TBD and benzyl alcohol, is presented.

Experimental Section

Sample Preparation

1.5 M of L-lactide and 15 mM of organic free radical α,γ-bisdiphenylene-β-phenylallyl (BDPA; Sigma Aldrich, St. Louis, MO) were mixed in a glass-forming solvent (80 % THF and 20% water (v/v)) for DNP experiments. The reaction initiator (benzyl alcohol) and catalyst (TBD) were premixed in CH_2Cl_2.

DNP Polarization

40 μL of L-lactide / BDPA mixture solution was hyperpolarized in a HyperSense instrument (Oxford Instruments, Tubney Woods, UK) for 2 h. During the polarization time, A 60 mW power of microwaves with a frequency of 93.965 GHz ($\omega_e - \omega_N$) was irradiated to the sample at a temperature of 1.4 K. (60 mW, 93.965 GHz). Afterwards, the sample was dissolved in 4 mL pre-heated toluene, and loaded into a 1 mL injection loop. The initial 475 μL of the sample solution in the injection loop, which represents the part of the stream of solvent containing the highest analyte concentration, was injected into a 5 mm NMR tube that was preinstalled in the NMR spectrometer. The injection took place by applying nitrogen gas pressures (260 psi and 150 psi for forward and backward pressures, respectively). The polarized L-lactide was mixed with a solution of initiator and catalyst directly in the NMR tube, yielding a total sample volume of 500 μL.

NMR Spectroscopy

A series of ^{13}C spectra was acquired on a Bruker 400 MHz NMR spectrometer equipped with a broadband probe containing three pulsed field gradients (Bruker Biospin, Billerica, MA) at a temperature of 31 ℃. NMR experiments were triggered after an injection time of 400 ms and a stabilization time of 400 ms. For the experiments without a selective inversion, the pulse sequence (trigger – [α_x – acquire – $G_{x,y,z}$]$_{\times 32}$) was used. A total of 16 transients were acquired for 6.6 s, and the time between each transient was 0.4 s. For the each scan, a randomized pulsed field gradient $G_{x,y,z}$ (35..50 G/cm, 1 ms) was applied to ensure that no unwanted coherences remained from the previous scan. The small flip angle α of the excitation pulse was 16.7°, and the pulse strength γB1 was 29.1 kHz. In each scan, 16384 data points were acquired for an acquisition time of 340 ms. For the experiments with a selective inversion (Figure V-1), an IBURP2 shaped pulse of flip angle π and 20 ms duration at the resonance frequency of the ester carbon in L-lactide and a randomized pulsed field gradient $G_{x,y,z}$ were added before the small flip angle pulse (trigger – shaped π – $G_{x,y,z}$ – [α_x – acquire – $G_{x,y,z}$]$_{\times 32}$).

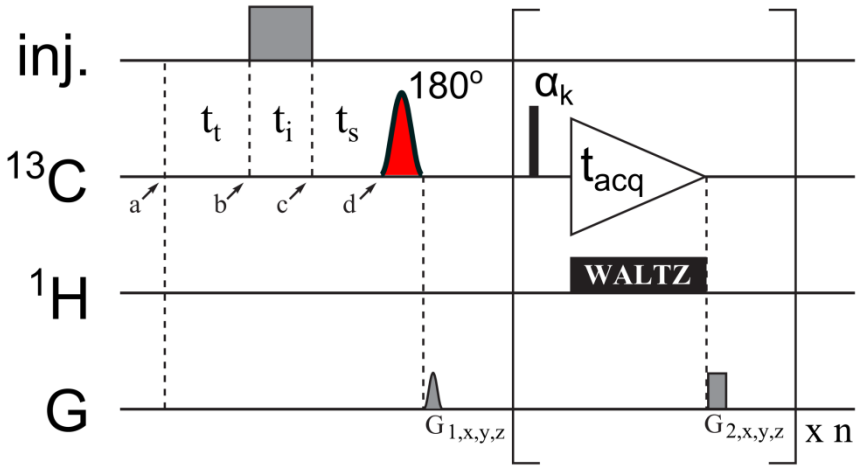

Figure V-1 : The ring-opening polymerization was monitored using small flip angle excitation. The polarized monomer was transferred from the polarizer to the home-built sample injector for a transfer time (t_t). The sample was injected from the injection loop to a 5 mm NMR tube, which was preinstalled in a 400 MHz NMR spectrometer. The NMR experiment was triggered after an injection time (t_i) of 400 ms and a stabilization time (t_s) of 400 ms. The resonance of carbonyl carbon in the monomer was selectively inverted by IBURP2 shaped π pulse applied for a duration of 20 ms, and a randomized pulsed field gradient $G_{x,y,z}$ was added before the small flip angle pulse.

Results and Discussion

As a starting point, ^{13}C spectra of L-lactide and synthesized polylactide were measured uisng non-hyperpolarized NMR spectroscopy (Figure V-2). Since the chemical shifts of ^{13}C nuclei are quite sensitive to local environments and molecular structures, the lactide monomer and polylactide from the reference spectra were clearly identified.

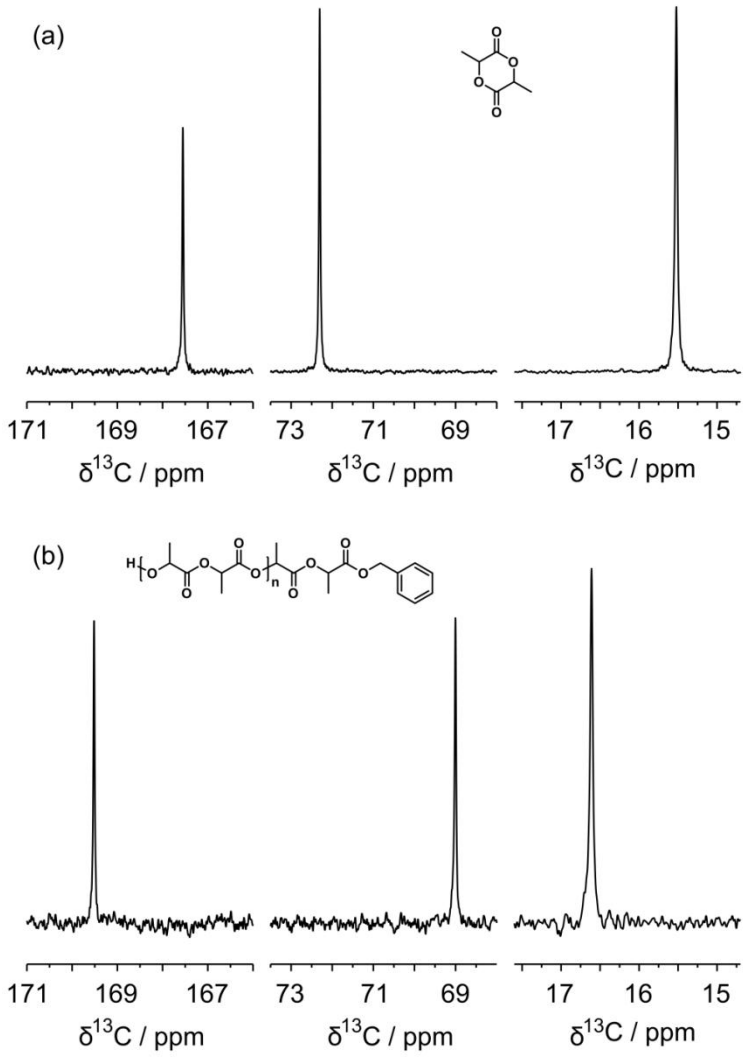

Figure V-2 : Non-hyperpolarized ^{13}C NMR spectrum of monomer L-lactide (a), and synthesized product polylactide (b).

For the DNP experiment, an aliquot of L-lactide was hyperpolarized in the solid state, dissolved in toluene, and rapidly mixed with the initiator and catalyst, benzyl alcohol and TBD, respectively. The progress of the polymerization reaction, a depletion of the reactant L-lactide and a formation of the product polylactide, was monitored by time-resolved ^{13}C NMR spectra through a series of small flip angle excitation (Figure V-3). Benefitting from the wide chemical shifts dispersion of ^{13}C spins, the reactant L-

lactide and the product polylactide were subsequently detected while the reaction proceeded. These resonances appear at 167.6 ppm and 169.5 ppm, respectively.

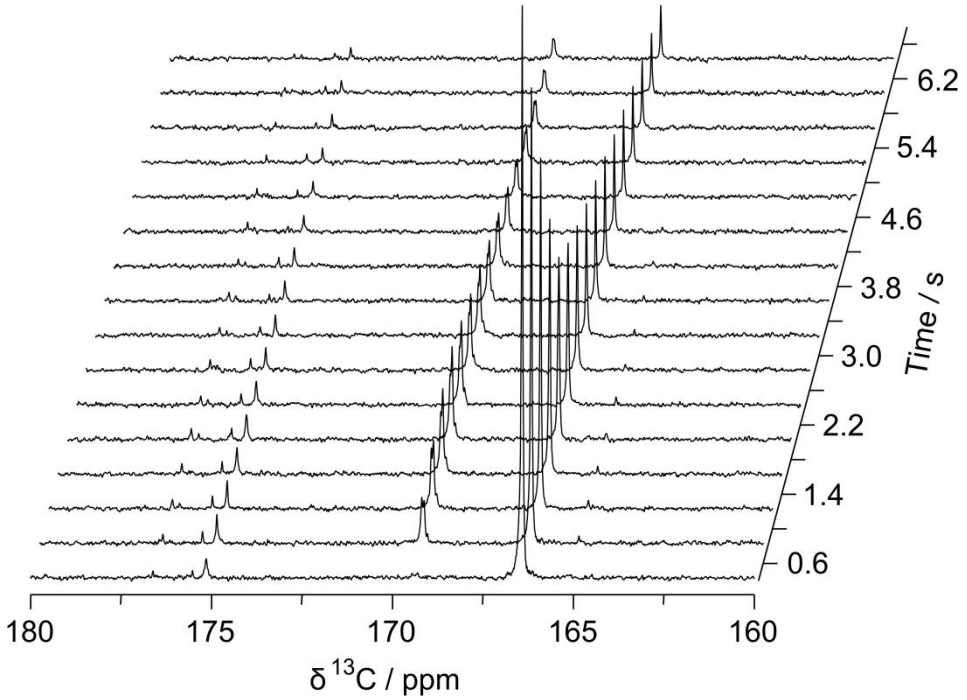

Figure V-3 : Stacked plot of ^{13}C NMR spectra during the progress of the polymerization reaction. Only the spectral region for the ester carbon is displayed. The spectra were acquired by a series of small flip angle pulses. Time resolution was 400 ms.

In addition to the signals corresponding to the reactant and the product, extra signals near 175 ppm were subsequently detected, which were not observed in reference spectra (Figure V-2) measured in equilibrium condition. To elucidate the origins of the additional signals, the temporal chemical shift correlation experiment was used.[135] As illustrated in the pulse sequence (Figure V-1), a shaped π pulse was applied to the ester carbon (167.6 ppm) of L-lactide at the beginning of the reaction. The implementation of the selective inversion on a specific spin system of L-lactide provides spin connectivity

between the reactant, intermediate, and product. The resulting spectra are shown in Figure V-4.

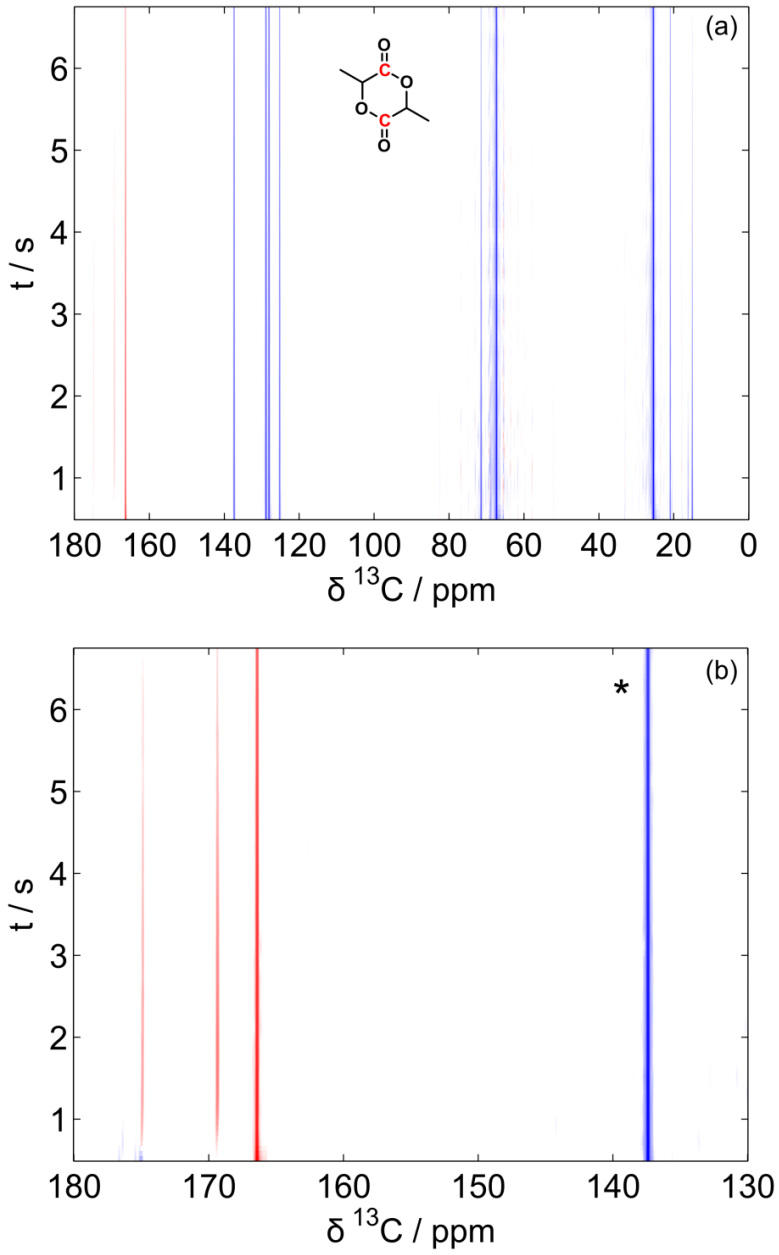

Figure V-4 : (a) Hyperpolarized correlation experiment with a selective inversion on a resonance from ester carbon in L-lactide at the beginning of the reaction. Hyperpolarized signals from the glassing solvent, a mixture of toluene and THF, were also displayed. (b) Expanded view of the correlation experiment. Positive and negative signals are represented in blue and red, respectively. (*) designates the resonance from Toluene.

Since the ester carbon initially translates as a negative signal due to influence of the inversion pulse, the targeted spin in monomer at 167.6 ppm and its corresponding spin in polymer at 169.5 ppm showed negative signal intensities (red color), while non-inverted spins of the reactant and product yielded positive signal intensities (blue color) (Figure V-4). As the chemical shift of the inverted signal at 169.5 ppm matched the value in the reference product spectrum, the correlation experiment offers an unambiguous identification of the reaction product while the reaction processes.

Additionally, the extra signals near 175.2 ppm also showed a negative temporal spin correlation with L-lactide monomer. Based on the spin connectivity, the extra signal may belong to the potential reaction intermediate that is proposed in the previous studies.[206, 208] However, the correlation experiment alone cannot provide direct evidence that the negative signal at 175.2 ppm belongs to the reaction intermediates, even though the chemical shift agree well with a feature of the amide functional group which is proposed in the nucleophilic mechanism.[206, 208] The extra signal may alternatively correspond to side products or a chain end of the polylactide which is a complex between ring-opened lactide and benzyl alcohol. Additional studies, for example using selective saturation, could potentially be used to support the correlation information between these species. Moreover, kinetic studies and ^{15}N isotope labeling on the TBD catalyst can further develop the present result.

Conclusions

After the first DNP study with styrene in the previous chapter, this study showed a general applicability of dissolution DNP-NMR technique in polymer chemistry. Here we demonstrated the real-time DNP-NMR measurements for the study of the reaction mechanism of living ring-opening polymerization of L-lactide catalyzed by TBD and benzyl alcohol. In particular, the presented dissolution DNP-enhanced NMR spectroscopy is not only limited to this polymerization. The dissolution DNP technique can be potentially used as a powerful method to reveal unknown mechanisms and kinetic information in a wide variety of chemical processes.

CHAPTER VI

EXTENSION OF OBSERVABLE REACTION TIME THROUGH DEUTERIUM ISOTOPE LABELING

Introduction

NMR of hyperpolarized nuclear spins affords a signal enhancement of several orders of magnitude when compared to conventional NMR. Hyperpolarization techniques, in particular Dynamic Nuclear Polarization (DNP)[66, 109] are thus pointing the way towards the application of NMR spectroscopy for the measurement of non-equilibrium processes. This technique appears especially well suited for the study of enzyme reactions because of the ability to distinguish different reaction pathways in addition to the kinetics of the reaction. Despite the strong points of DNP, the study of reactions is more favorable for carbon spins with long relaxation time, such as carbonyl and quaternary carbons due to the longer preservation of the hyperpolarized state. As described previously,[133] the signal intensity of a carbon atom bonded to protons, the methyl carbon of N_{α}-benzoyl-$_{L}$-arginine ethyl ester (BAEE) in this case, showed a fast signal decay due to strong intramolecular dipole-dipole interactions, reducing the observable reaction time. However, the life-time of the hyperpolarization can be substantially extended by reducing the spin-lattice relaxation with deuteration of molecules. Deuteration of molecules is very common method in protein NMR spectroscopy, since the isotope labeling can dramatically reduce spin relaxations of the macromolecules, resulting in better sensitivity. Here, we demonstrate the effect of

deuteration for real-time study of reaction kinetics. As a model reaction, the hydrolysis of N_α-benzoyl-$_L$-arginine methyl-d_3 ester (BAME-d_3) by trypsin, was chosen.

Experimental Section

Synthesis of N_α-benzoyl-$_L$-arginine methyl-d_3 ester

0.4 mmol of N_α-benzoyl-$_L$-arginine ("BA"; Alfa Aesar, Ward Hill, MA) and two equivalents of trimethylchlorosilane (TMSCl) were mixed in 3 mL of methanol-d_4 (Cambridge Isotope Laboratories, Andover, MA), and the mixture was gently stirred for 24 h at a room temperature. Subsequently, residual methanol-d_4 and TMSCl were evaporated in a concentrator (Savant Instruments, Holbrook, NY).[209] The reaction product was characterized by ^{1}H and ^{13}C NMR, as well as by reverse-phase high performance liquid chromatography (HPLC; Shimadzu, Columbia, MD).

DNP Polarization

For DNP polarization, 20 µL of 0.5 M BAME-d_3 or BAEE, 1 mM Gadolinium (III) diethyltriaminepentaacetic acid (Gd(DTPA); Sigma Aldrich, St. Louis, MO), and 15 mM Tris (8-carboxyl-2,2,6,6-tetra[2-(1-hydroxymethyl)]-benzo(1,2-d:4,5-d')bis(1,3)dithiole-4-yl) methyl sodium salt ("OX63"; Oxford Instruments, Tubney Woods, UK) were mixed in a glass-forming solvent (60% ethylene glycol (Mallinckrodt Baker, Phillipsburg, NJ) and 40% water (vol/vol)). Hyperpolarization took place in a HyperSense system (Oxford Instruments, Tubney Woods, UK), by irradiating a 60 mW power of 93.974 GHz (ω_e - ω_N) microwave frequency at a temperature of 1.4 K. After polarizing for 3 h, the sample was dissolved in 4 mL pre-heated buffer solution (100mM

potassium phosphate, pH 7.0), and automatically loaded into a 1 mL injection loop. The initial 325 μL of the sample solution in the injection loop, which represents the part of the stream of solvent containing the highest analyte concentration, was injected into a 5 mm NMR tube for 430 ms (injection time) that was preinstalled in the NMR spectrometer.[133, 137] The injection took place by applying nitrogen gas pressures (262 psi and 150 psi for forward and backward pressures, respectively). For the experiments of the enzyme catalyzed reaction, 25 μL of 1.5 mM trypsin (EMD, Gibbstown, NJ) solution (50 mM potassium phosphate, pH 3.0) was preloaded in the NMR tube before mixing with the polarized BAME-d_3 solution. Finally, the NMR measurement was triggered after a 335 ms stabilization time. The total required time delivering the sample from the polarizer to the NMR tube was 1.8 s. Final concentrations of the reaction product, BA, and trypsin after the reaction were determined by reverse-phase HPLC at wavelengths of 253 nm and 280 nm, respectively.

NMR Spectroscopy and Data Processing

A series of ^{13}C spectra was acquired on a Bruker 400 MHz NMR spectrometer equipped with a broadband probe containing three pulsed field gradients (Bruker Biospin, Billerica, MA) at a temperature of 27 ℃. The spectra were acquired using the pulse sequence like, (trigger – [shaped 90 – $G_{x,y,z}]_3$ – [G_z – α_x – acquire FID]$_{16}$). To suppress the strong signal of the glass-forming agent (ethylene glycol, 62.7 ppm), three EBURP2[210] shaped 90° pulse with 10 ms duration and pulsed field gradients ($G_{x,1}$ = 35 G/cm, $G_{y,2}$ = 35 G/cm, $G_{z,3}$ = 35 G/cm; 1 ms) were applied. Total 32 transients were acquired for 6 s, and the time delay between each transient was 0.4 s. For each scan, a

randomized pulsed field gradient $G_{z,4}$ (35..50 G/cm, 1 ms) was applied to remove unwanted coherences remained from the previous scan. The small flip angle α of the excitation pulse was 18.2°, and the pulse strength was 25 kHz. For each scan, 16,384 data points were acquired for an acquisition time of 340 ms. ^{1}H and ^{2}H decoupling were applied for the acquisition time with WALTZ-16 where the field strength are 2.3 kHz and 0.83 kHz, respectively. The raw data were zero filling to 65,536 complex data points, and an exponential window function with a 3 Hz line broadening was applied before Fourier transform using the TOPSPIN 2.1 program (Bruker Biospin, Billerica, MA). Peak integration and curve fitting were performed by MATLAB (The MathWorks, Natick, MA). Analytical solutions of the differential equations described in the text were found by Mathematica (Wolfram Research, Champaign, IL).

Reaction Mechanism and Kinetics

As a typical serine protease, the enzyme trypsin (*E*) hydrolyzes proteins or peptide chains at a carboxyl side of an arginine, or lysine amino acids.[211-212] In this model study, N_{α}-benzoyl-$_{L}$-arginine methyl-d_3 ester (BAME-d_3; S) was synthesized for the trypsin catalyzed reaction. This reaction is in three steps: (1) formation of an enzyme-substrate complex (*ES*); (2) acylation of the active site, serine-195, (EP_2) and release of CD_3OH (P_1); (3) hydrolysis of the acylenzyme intermediate and production of benzoyl-$_{L}$-arginine (P_2).[212]

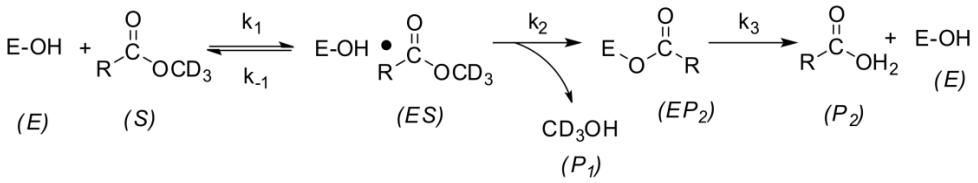

Figure VI-1 : Reaction mechanism for trypsin catalyzed hydrolysis of BAME-d_3

Two spins showing slow spin-lattice relaxation (ester carbonyl carbon and deuterated methyl carbon), due to lack of nearby protons or deuteration, were chosen to monitor the time course of signal intensities of the reactant *S* and products P_1, P_2. The effect of deuteration on the spin-lattice relaxation time was examined by hyperpolarized T_1 measurements of two substrates, BAME-d_3 and BAEE (Figure VI-2). Except deuteration on methyl group in BAME-d_3, chemical structures and physical properties of these substrates are similar. The relaxation time of the carbonyl carbons in both substrates were comparatively similar. However, the deuterated methyl carbon in BAME-d_3 showed six times longer lifetime than the corresponding carbon in BAEE. The isotope labeling enables the extension of life-time of the hyperpolarized state, providing better sensitivity for spins of interest.

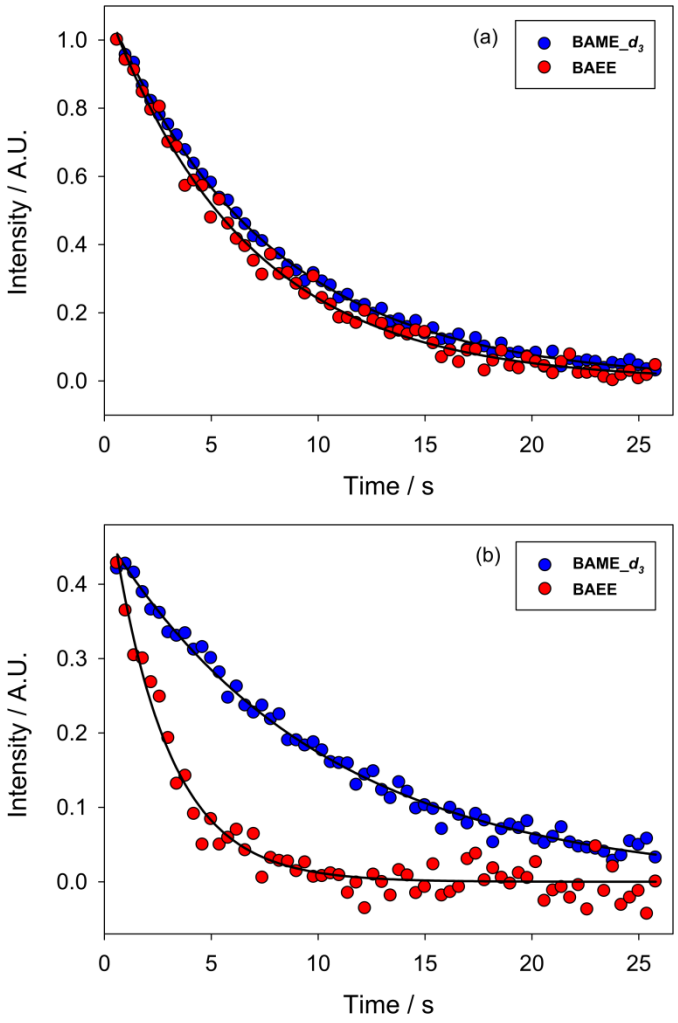

Figure VI-2 : Hyperpolarized T_1 measurements of BAME-d_3 and BAEE ((a) carbonyl carbon, (b) methyl carbon). Fits of the two traces to single exponentials indicated spin-lattice relaxation times of (a) 11 s and 9 s, (b) 18 s and 3 s for BAME-d_3 and BAEE, respectively.

^{13}C hyperpolarized BAME-d_3 (*S*) was reacted with trypsin, then the consumption of reactant and formation of products were subsequently monitored by a series of small flip angle pulses one-dimensional NMR spectra. During the experimental time, the reaction carries over the polarization from the reactant *S* to the products P_1, P_2. As a result, the peak intensities of the reactant decrease, while the peak intensities of product increase, as shown in Figure VI-3. Besides the effect of the reaction kinetics, all of the signals

decay because of their individual spin relaxations and the application of successive small-flip angle pulses in the NMR experiment.

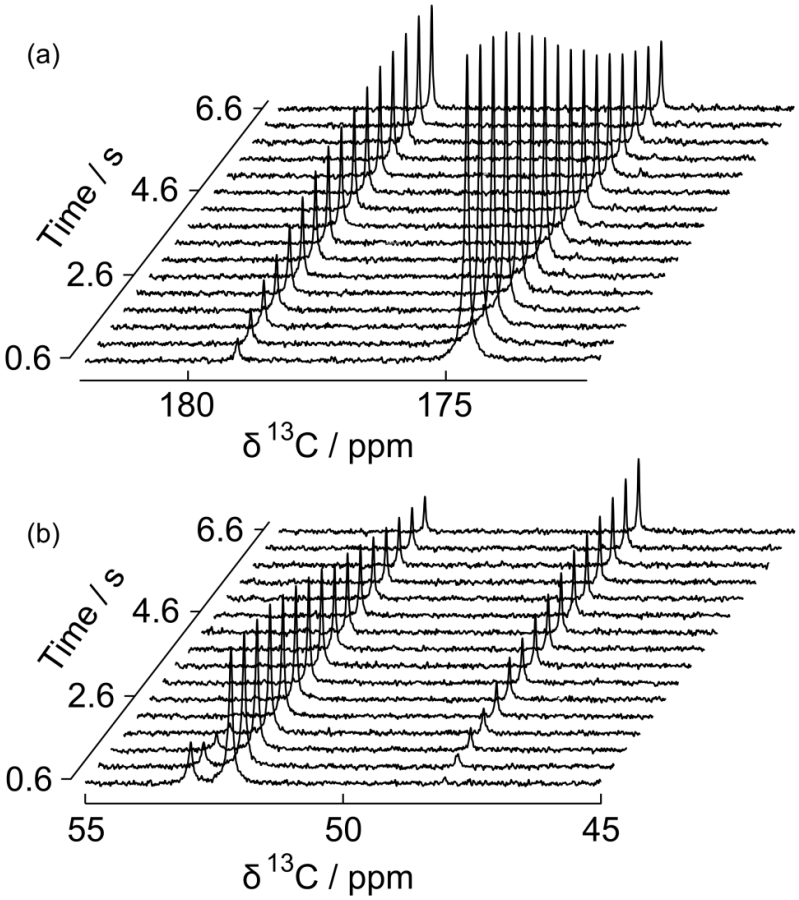

Figure VI-3 : Stacked plots of the successively acquired spectra during the progress of the reaction. (a) carbonyl carbon in BAME-d_3(*S*) and BA (P_2). (b) deuterated methyl carbon in BAME-d_3 (*S*) and CD_3OH (P_1).

In order to determine reaction kinetics, the effects of spin relaxation and reaction on the signal intensity of each species needs to be considered. The reaction kinetics can be described by three-step Michaelis-Menten equation,[212]

$$\nu_0 = \frac{\nu_{\max}[S]}{K_M + [S]} \qquad \text{(VI-1)}$$

$$K_M = \frac{k_{cat} + k_{-1}}{k_1} \tag{VI-2}$$

$$v_{\max} = k_{cat}[E]_{tot} \tag{VI-3}$$

$$k_{cat} = \frac{k_2 k_3}{k_2 + k_3} \tag{VI-4}$$

Under the reaction conditions used, the initial concentration of the substrate $[S]_0$ is much larger than K_M. With the steady state approximation, the reaction rate can therefore be assumed to be a constant, $v = v_{\max} = k_{cat} \cdot [E]_{tot}$. The time dependent concentration of reactant is $[S] = [S]_0 - vt$. The DNP experiments start with non-renewable initial hyperpolarization of *S*. By ignoring the thermal polarization, the initial hyperpolarization prior to the NMR experiment provides the only source for the observable signal in this system. The signal intensity *I* is proportional to the polarization level *p* and the concentration of each species. In the expressions for the signal intensity, the kinetics would alter the concentration of each species in this system, and the relaxation would decrease their polarization levels. For simplicity, the dependence of the signal on the relaxation of *S* can be removed by scaling the signal intensity with a factor of $e^{r_S \cdot t}$. Using the thus defined relative signal intensity, the relaxation rates of all species are reduced by the relaxation rate of *S*, r_S. Specifically, if all species exhibit the same relaxation rate, the effect of spin relaxation is completely removed from the equations. These relative signal intensities are then proportional to the concentrations. The differential equation for the relative signal intensity of the substrate would be

$$\frac{dI_{S,rel}}{dt} = -\frac{\nu \cdot I_0}{[S]_0} \qquad \text{(VI-5)}$$

Additionally, during the experiments, in each scan a hard pulse with fixed small flip angle α was used to convert $\sin(\alpha)$ of the total longitudinal magnetization to the observable transverse magnetization, while $\cos(\alpha)$ of the longitudinal magnetization is preserved for following scans. This fixed flip angle scheme introduces an envelope function of $e^{-\lambda \cdot t}$, with $\lambda = \frac{-\ln(\cos(\alpha))}{\Delta t}$, and Δt the time delay between scans to the observed signal intensities.[136, 138] To compensate the effect of the small flip angle excitation, the experimental signal intensities I then have to be scaled up by $e^{\lambda \cdot t}$. Solving the differential equation, the final relative signal intensity of the S is

$$I_{S,rel} = I_S \cdot e^{(r_S + \lambda) \cdot t} = I_0 \cdot (1 - \frac{\nu t}{[S]_0}) \qquad \text{(VI-6)}$$

Fit of Experimental Signal Intensities

Equation (VI-6) was used to fit the signal intensities of the substrates, BAME-d_3 and BAEE. The relative signal intensity of S, $I_{S,rel}$, is always a linear function with a slope of $\nu / [S]_0$. In Equation (VI-6), the relaxation rate of the substrate was determined from independent experiments in similar conditions for input parameters of the fits. The influence of small flip angle pulses λ was calculated from the NMR experimental parameters. Given these known parameters, the two unknown parameters, I_0 and $\nu / [S]_0$ can be obtained from the fits.

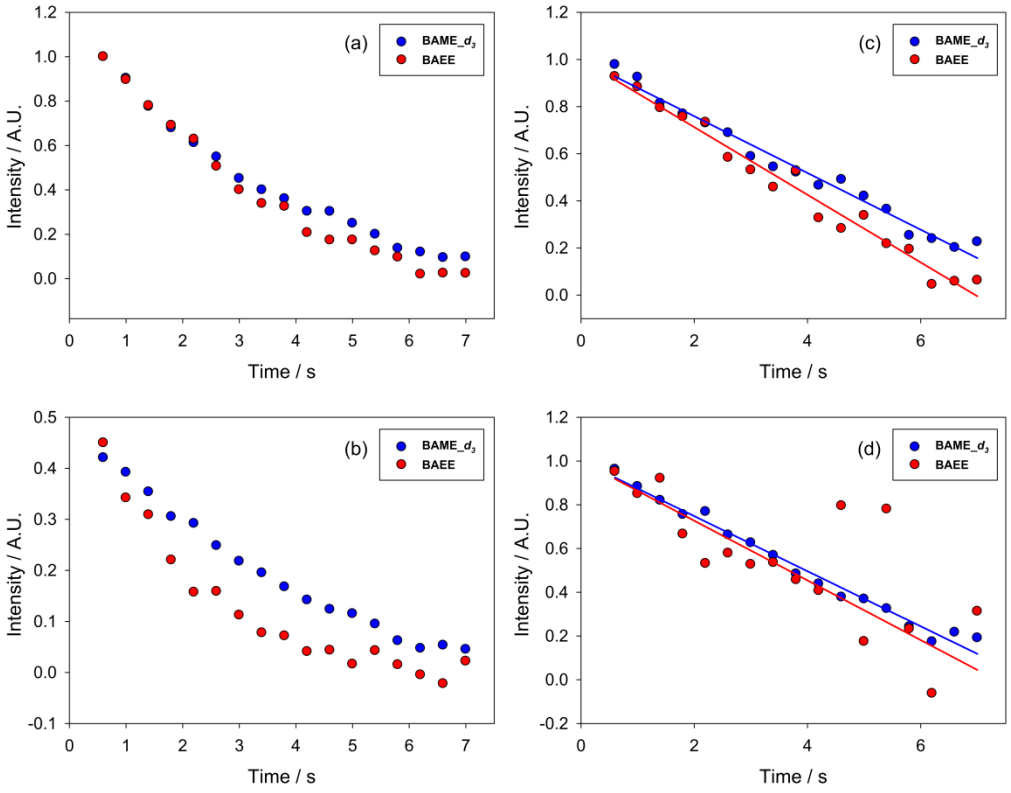

Figure VI-4 : Signal intensities of (a) carbonyl carbon and (b) methyl carbon in BAME-d_3 and BAEE during the progress of the reaction. Fit of the relative signal intensities of (c) carbonyl carbon and (d) methyl carbon in BAME-d_3 and BAEE with Equation (VI-6).

With the value of $\nu/[S]_0$ from the fits and known concentration of the reactant and enzyme determined after reaction, the reaction rate constant k_{cat} of BAME-d_3 can quantitatively be found to be 12.4 s^{-1} and 13.1 s^{-1} from the carbonyl and deuterated methyl carbons, respectively. The k_{cat} of BAEE determined from the carbonyl carbon (13.1 s^{-1}) is in excellent agreement with the literature (12.1 s^{-1}).[133] The short life-time of hyperpolarized state of the methyl carbon degrades quality of the linear fit, resulting in inaccurate quantitative analysis of reaction kinetics.

Since BAME-d_3 contains chromophores, these values can also be validated by UV-visible spectrophotometry where it shows 12.5 s^{-1}. Benefitting from the extension of

observable reaction time through deuteration on the spin of interest, the reaction rate from deuterated methyl carbon in BAME-d_3 could be quantitatively addressed.

Conclusions

DNP-enhanced NMR spectroscopy in combination with the proposed kinetic model makes possible to investigate non-equilibrium processes of the kinetics of multi-step enzyme catalyzed reaction in real-time. The enormous NMR signal intensity gained from the DNP process permits the acquiring of time-resolved ^{13}C NMR spectra near physiological conditions with natural abundance. Additionally, the effect of deuteration on real-time kinetics was addressed by comparing longitudinal relaxation rates between the two substrates. The synthetic strategy, trans-esterification, provides the deuteration of the substrate on the point of interest, resulting in substantial reduction of spin relaxation rate. The isotope labeling helps the extension of life-time of the hyperpolarized state of corresponding carbon to improve sensitivity. The long-lived hyperpolarization state would be further helpful to study slow chemical reactions as well as to improve quality of data for quantitative analysis.

CHAPTER VII

GENERAL CONCLUSIONS

Hyperpolarization techniques, in particular dissolution dynamic nuclear polarization (D-DNP) make a contribution to overcoming sensitivity limitation of NMR spectroscopy through signal enhancements in NMR measurement, leading to study new fields of researches in real time. The high level of nuclear polarization can be achieved through polarization transfers from free electron spins to nuclear spins by saturating the electron spin transitions with microwave irradiation at a cryogenic temperature. Despite the strong advantages of D-DNP, this method has often been limited to the study of molecules containing nuclear spins involving long longitudinal relaxation times because the hyperpolarization may be lost during a sample transfer time before the NMR measurement can be initiated. However, implementation of the rapid sample injection system resolved the current limitation of dissolution DNP technique. Through the rapid sample injection, it becomes possible to conduct experiments with nuclear spins exhibiting short relaxation times (such as ^{1}H and ^{19}F and ^{13}C). In this dissertation, several dissolution DNP methods have been demonstrated to characterize various reactions involving large molecules.

In a first project, ^{19}F DNP enhanced NMR spectroscopy is exploited for the characterization of protein-ligand interactions. An enhancement in the ^{19}F signal of several thousand fold by dynamic nuclear polarization allows for the detection of the binding events and binding affinities of fluorinated small molecules in the strong-, intermediate-, and weak-binding regimes. The capability recording NMR spectra at a

low ligand concentration permits the detection of ligands in slow exchanges that are not easily responsive to drug screening by traditional NMR methods. The relative speed and additional information gained may make the hyperpolarization-based approach an interesting alternative for use in drug discovery.

In a second project, ^{1}H DNP enhanced NMR spectroscopy is developed for the characterization of the binding epitope via protein mediated interligand NOEs between two competitively binding ligands (HYPER-BIPO-NMR). The sensitivity contrast is obtained from the hyperpolarization of one of the ligands, resulting in the prevention of the need of using stable isotope labeling or two-dimensional NMR experiments for observing the transferred signals. Limited structural information of the binding epitope is determined from the magnitude of the buildup rate between individual spins on the receiving ligand and the protein. Since the HYPER-BIPO-NMR spectroscopy utilizes the hyperpolarized ligand as a means of selective enhancement of the binding pocket, this method can be used to determine residues in the active site for ^{13}C or ^{15}N labeled proteins from heteronuclear NMR experiments.

In a third project, the DNP enhanced real-time NMR spectroscopy is demonstrated in the study of the non-equilibrium processes for the living anionic polymerization of styrene and living ring-opening polymerization of L-lactide. The hyperpolarization of monomers provides a sufficient signal-to-noise ratio to detect ^{13}C NMR signals in real time while the reaction progresses. In combination with the temporal correlation schemes, the spin of interest is unambiguously identified. In the study of the multi-step enzymatic reaction, partial deuteration on the substrate by the simple synthetic strategy

enables extension of observable time window that is accessible to the dissolution DNP experiments. The kinetic model in combination with intrinsic spin relaxations explains the time course of signal intensity of the reactant, resulting in provision of the catalytic information.

In summary, several dissolution DNP techniques have been demonstrated for studying chemical reactions and interactions involving large molecules. Utilizing the large signal enhancement initially produced on small molecules through DNP, it become possible to characterize properties of the macromolecules. These capabilities of the D-DNP led to advances in the investigation of protein-ligand interactions and chemical reactions, making dissolution DNP an attractive method for the study of a variety of chemical processes.

REFERENCES

1. Cavanagh, J.; Fairbrother, W. J.; Palmer, A. G.; Skelton, N. J., *Protein NMR Spectroscopy: Principles And Practice*. Academic Press, Inc. : San Diego, 1996; p 587.

2. Knight, W. D. *Phys. Rev.* **1949**, *76*, 1259-1260.

3. Proctor, W. G.; Yu, F. C. *Phys. Rev.* **1950**, *77*, 717-717.

4. Proctor, W. G.; Yu, F. C. *Phys. Rev.* **1951**, *81*, 20-30.

5. Gutowsky, H. S.; McCall, D. W. *Phys. Rev.* **1951**, *82*, 748-749.

6. Anderson, W. A.; Freeman, R. *J. Chem. Phys.* **1962**, *37*, 85-103.

7. Overhauser, A. W. *Phys. Rev.* **1953**, *92*, 411-415.

8. Carver, T. R.; Slichter, C. P. *Phys. Rev.* **1953**, *92*, 212-213.

9. Solomon, I. *Phys. Rev.* **1955**, *99*, 559-565.

10. Gardner, K. H.; Kay, L. E. *Annu. Rev. Bioph. Biom.* **1998**, *27*, 357-406.

11. Meyer, B.; Peters, T. *Angew. Chem. Int. Ed.* **2003**, *42*, 864-890.

12. Searle, M. S. *Prog. Nucl. Magn. Reson. Spectrosc.* **1993**, *25*, 403-480.

13. Otting, G. *Prog. Nucl. Magn. Reson. Spectrosc.* **1997**, *31*, 259-285.

14. Pellecchia, M.; Sem, D. S.; Wüthrich, K. *Nat. Rev. Drug Discovery* **2002**, *1*, 211-219.

15. Watts, A. *Nat. Rev. Drug Discovery* **2005**, *4*, 555-568.

16. Peng, J. W.; Moore, J.; Abdul-Manan, N. *Prog. Nucl. Magn. Reson. Spectrosc.* **2004**, *44*, 225-256.

17. Stockman, B. J.; Dalvit, C. *Prog. Nucl. Magn. Reson. Spectrosc.* **2002**, *41*, 187-231.

18. Shoolery, J. N. *Anal. Chem.* **1993**, *65*, 731A-741A.

19. Emsley, J. W.; Feeney, J. *Prog. Nucl. Magn. Reson. Spectrosc.* **2007**, *50*, 179-198.

20. Thurber, K. R.; Yau, W.-M.; Tycko, R. *J. Magn. Reson.* **2010**, *204*, 303-313.

21. Ernst, R. R.; Anderson, W. A. *Rev. Sci. Instrum.* **1966**, *37*, 93-102.

22. Morris, G. A.; Freeman, R. *J. Am. Chem. Soc.* **1979**, *101*, 760-762.

23. Bodenhausen, G.; Ruben, D. J. *Chem. Phys. Lett.* **1980**, *69*, 185-189.

24. Pervushin, K.; Riek, R.; Wider, G.; Wüthrich, K. *Proc. Natl. Acad. Sci. U. S. A.* **1997**, *94*, 12366-12371.

25. Styles, P.; Soffe, N. F.; Scott, C. A.; Cragg, D. A.; Row, F.; White, D. J.; White, P. C. J. *J. Magn. Reson.* **2011**, *213*, 347-354.

26. Günther, U. Springer Berlin Heidelberg, 2011, pp 1-47.

27. Maly, T.; Debelouchina, G. T.; Bajaj, V. S.; Hu, K. N.; Joo, C. G.; Mak-Jurkauskas, M. L.; Sirigiri, J. R.; van der Wel, P. C. A.; Herzfeld, J.; Temkin, R. J.; Griffin, R. G. *J.Chem. Phys.* **2008**, *128*.

28. Bowers, C. R.; Weitekamp, D. P. *Phys. Rev. Lett.* **1986**, *57*, 2645-2648.

29. Bowers, C. R.; Weitekamp, D. P. *J. Am. Chem. Soc.* **1987**, *109*, 5541-5542.

30. Natterer, J.; Bargon, J. *Prog. Nucl. Magn. Reson. Spectrosc.* **1997**, *31*, 293-315.

31. Duckett, S. B.; Newell, C. L.; Eisenberg, R. *J. Am. Chem. Soc.* **1994**, *116*, 10548-10556.

32. Kovtunov, K. V.; Beck, I. E.; Bukhtiyarov, V. I.; Koptyug, I. V. *Angew. Chem. Int. Ed.* **2008**, *47*, 1492-1495.

33. Blazina, D.; Duckett, S. B.; Dyson, P. J.; Lohman, J. A. B. *Chem.-Eur. J.* **2003**, *9*, 1045-1061.

34. Hübler, P.; Bargon, J. *Angew. Chem. Int. Ed.* **2000**, *39*, 3701-3703.

35. Ross, B. D.; Bhattacharya, P.; Wagner, S.; Tran, T.; Sailasuta, N. *Am. J. Neuroradiol.* **2010**, *31*, 24-33.

36. Duckett, S. B.; Mewis, R. E. *Acc. Chem. Res.* **2012**, *45*, 1247-1257.

37. Golman, K.; Axelsson, O.; Jóhannesson, H.; Månsson, S.; Olofsson, C.; Petersson, J. S. *Magn. Reson. Med.* **2001**, *46*, 1-5.

38. Zacharias, N. M.; Chan, H. R.; Sailasuta, N.; Ross, B. D.; Bhattacharya, P. *J. Am. Chem. Soc.* **2011**, *134*, 934-943.

39. Adams, R. W.; Aguilar, J. A.; Atkinson, K. D.; Cowley, M. J.; Elliott, P. I. P.; Duckett, S. B.; Green, G. G. R.; Khazal, I. G.; Lopez-Serrano, J.; Williamson, D. C. *Science* **2009**, *323*, 1708-1711.

40. Barton, A. S.; Newbury, N. R.; Cates, G. D.; Driehuys, B.; Middleton, H.; Saam, B. *Phys. Rev. A* **1994**, *49*, 2766-2770.

41. Albert, M. S.; Cates, G. D.; Driehuys, B.; Happer, W.; Saam, B.; Springer, C. S.; Wishnia, A. *Nature* **1994**, *370*, 199-201.

42. Moller, H. E.; Chen, X. J.; Saam, B.; Hagspiel, K. D.; Johnson, G. A.; Altes, T. A.; de Lange, E. E.; Kauczor, H. U. *Magn. Reson. Med.* **2002**, *47*, 1029-1051.

43. Sozzani, P.; Comotti, A.; Simonutti, R.; Meersmann, T.; Logan, J. W.; Pines, A. *Angew. Chem. Int. Ed.* **2000**, *39*, 2695-2698.

44. Room, T.; Appelt, S.; Seydoux, R.; Hahn, E. L.; Pines, A. *Phys. Rev. B* **1997**, *55*, 11604-11610.

45. Haake, M.; Pines, A.; Reimer, J. A.; Seydoux, R. *J. Am. Chem. Soc.* **1997**, *119*, 11711-11712.

46. Navon, G.; Song, Y. Q.; Room, T.; Appelt, S.; Taylor, R. E.; Pines, A. *Science* **1996**, *271*, 1848-1851.

47. Dubois, L.; Da Silva, P.; Landon, C.; Huber, J. G.; Ponchet, M.; Vovelle, F.; Berthault, P.; Desvaux, H. *J. Am. Chem. Soc.* **2004**, *126*, 15738-15746.

48. Landon, C.; Berthault, P.; Vovelle, F.; Desvaux, H. *Protein Sci.* **2001**, *10*, 762-770.

49. Xu, Y.; Tang, P. *Biochim. Biophys. Acta, Biomembr.* **1997**, *1323*, 154-162.

50. Lawler, R. G. *J. Am. Chem. Soc.* **1967**, *89*, 5519-5521.

51. Closs, G. L. *J. Am. Chem. Soc.* **1969**, *91*, 4552-4554.

52. Closs, G. L.; Trifunac, A. D. *J. Am. Chem. Soc.* **1970**, *92*, 2183-2184.

53. Kaptein, R.; Oosterhoff, J. L. *Chem. Phys. Lett.* **1969**, *4*, 195-197.

54. Kaptein, R.; Oosterhoff, L. J. *Chem. Phys. Lett.* **1969**, *4*, 214-216.

55. Sekhar, A.; Cavagnero, S. *J. Magn. Reson.* **2009**, *200*, 207-213.

56. Lee, J. H.; Sekhar, A.; Cavagnero, S. *J. Am. Chem. Soc.* **2011**, *133*, 8062-8065.

57. Maeda, K.; Lyon, C.; Lopez, J.; Cemazar, M.; Dobson, C.; Hore, P. J. *J. Biomol. NMR* **2000**, *16*, 235-244.

58. Berliner, L. J.; Kaptein, R. *J. Biol. Chem.* **1980**, *255*, 3261-3262.

59. Kaptein, R.; Dijkstra, K.; Nicolay, K. *Nature* **1978**, *274*, 293-294.

60. Berliner, L. J.; Kaptein, R. *Biochemistry* **1981**, *20*, 799-807.

61. Mok, K. H.; Hore, P. J. *Methods* **2004**, *34*, 75-87.

62. Mok, K. H.; Kuhn, L. T.; Goez, M.; Day, I. J.; Lin, J. C.; Andersen, N. H.; Hore, P. J. *Nature* **2007**, *447*, 106-109.

63. Garssen, G. J.; Kaptein, R.; Schoenmakers, J. G.; Hilbers, C. W. *Proc. Natl. Acad. Sci. U. S. A.* **1978**, *75*, 5281-5285.

64. Siebert, H.-C.; Kaptein, R.; Beintema, J.; Soedjanaatmadja, U.; Wright, C.; Rice, A.; Kleineidam, R.; Kruse, S.; Schauer, R.; Pouwels, P. W.; Kamerling, J.; Gabius, H.-J.; Vliegenthart, J. G. *Glycoconjugate J.* **1997**, *14*, 531-534.

65. Abragam, A., *The Principles of Nuclear Magnetism*. Clarendon Press, Oxford: 1961.

66. Abragam, A.; Goldman, M. *Rep. Prog. Phys.* **1978**, *41*, 395-467.

67. Carver, T. R.; Slichter, C. P. *Phys. Rev.* **1956**, *102*, 975-980.

68. Jeffries, C. D. *Annu. Rev. Nucl. Sci.* **1964**, *14*, 101-134.

69. Abragam, A. *Phys. Rev.* **1955**, *98*, 1729-1735.

70. Jeffries, C. D. *Phys. Rev.* **1957**, *106*, 164-165.

71. Pound, R. V. *Phys. Rev.* **1950**, *79*, 685-702.

72. Borghini, M. *Phys. Rev. Lett.* **1968**, *20*, 419-421.

73. Borghini, M.; Scheffler, K. *Phys. Rev. Lett.* **1971**, *26*, 1362-1365.

74. Hwang, C. F.; Hill, D. A. *Phys. Rev. Lett.* **1967**, *18*, 110-112.

75. Hwang, C. F.; Hill, D. A. *Phys. Rev. Lett.* **1967**, *19*, 1011-1014.

76. Byvik, C. E.; Wollan, D. S. *Phys. Rev. B* **1974**, *10*, 791-800.

77. Wollan, D. S. *Phys. Rev. B* **1976**, *13*, 3686-3696.

78. Müller-warmuth, W.; Meisegresch, K. *Adv. Magn. Reson.* **1983**, *11*, 1-45.

79. Song, C.; Hu, K. N.; Joo, C. G.; Swager, T. M.; Griffin, R. G. *J. Am. Chem. Soc.* **2006**, *128*, 11385-11390.

80. Lumata, L.; Jindal, A. K.; Merritt, M. E.; Malloy, C. R.; Sherry, A. D.; Kovacs, Z. *J. Am. Chem. Soc.* **2011**, *133*, 8673-8680.

81. Goldman, M., *Spin temperature and nuclear magnetic resonance in solids*. Clarendon Press Oxford: 1970.

82. Wind, R. A.; Ardenkjær-Larsen, J.-H. *J. Magn. Reson.* **1999**, *141*, 347-354.

83. Münnemann, K.; Bauer, C.; Schmiedeskamp, J.; Spiess, H. W.; Schreiber, W. G.; Hinderberger, D. *Appl. Magn. Reson.* **2008**, *34*, 321-330.

84. Armstrong, B. D.; Lingwood, M. D.; McCarney, E. R.; Brown, E. R.; Blümler, P.; Han, S. *J. Magn. Reson.* **2008**, *191*, 273-281.

85. McCarney, E. R.; Armstrong, B. D.; Lingwood, M. D.; Han, S. *Proc. Natl. Acad. Sci. U. S. A.* **2007**, *104*, 1754-1759.

86. Armstrong, B. D.; Han, S. *J. Am. Chem. Soc.* **2009**, *131*, 4641-4647.

87. Armstrong, B. D.; Choi, J.; López, C.; Wesener, D. A.; Hubbell, W.; Cavagnero, S.; Han, S. *J. Am. Chem. Soc.* **2011**, *133*, 5987-5995.

88. Cheng, C.-Y.; Goor, O. J. G. M.; Han, S. *Anal. Chem.* **2012**, *84*, 8936-8940.

89. Reese, M.; Turke, M. T.; Tkach, I.; Parigi, G.; Luchinat, C.; Marquardsen, T.; Tavernier, A.; Hofer, P.; Engelke, F.; Griesinger, C.; Bennati, M. *J. Am. Chem. Soc.* **2009**, *131*, 15086-15087.

90. Dorn, H. C.; Wang, J.; Allen, L.; Sweeney, D.; Glass, T. E. *J. Magn. Reson.* **1988**, *79*, 404-412.

91. Reese, M.; Lennartz, D.; Marquardsen, T.; Höfer, P.; Tavernier, A.; Carl, P.; Schippmann, T.; Bennati, M.; Carlomagno, T.; Engelke, F.; Griesinger, C. *Appl. Magn. Reson.* **2008**, *34*, 301-311.

92. Wind, R. A.; Duijvestijn, M. J.; Vanderlugt, C.; Manenschijn, A.; Vriend, J. *Prog. Nucl. Magn. Reson. Spectrosc.* **1985**, *17*, 33-67.

93. Wind, R. A.; Anthonio, F. E.; Duijvestijn, M. J.; Smidt, J.; Trommel, J.; de Vette, G. M. C. *J. Mag. Reson.* **1983**, *52*, 424-434.

94. Afeworki, M.; Mckay, R. A.; Schaefer, J. *Macromolecules* **1992**, *25*, 4084-4091.

95. Becerra, L. R.; Gerfen, G. J.; Temkin, R. J.; Singel, D. J.; Griffin, R. G. *Phys. Rev. Lett.* **1993**, *71*, 3561-3564.

96. Hall, D. A.; Maus, D. C.; Gerfen, G. J.; Inati, S. J.; Becerra, L. R.; Dahlquist, F. W.; Griffin, R. G. *Science* **1997**, *276*, 930-932.

97. Torrezan, A. C.; Han, S. T.; Mastovsky, I.; Shapiro, M. A.; Sirigiri, J. R.; Temkin, R. J.; Barnes, A. B.; Griffin, R. G. *IEEE Trans. Plasma Sci.* **2010**, *38*, 1150-1159.

98. Bajaj, V. S.; Farrar, C. T.; Hornstein, M. K.; Mastovsky, I.; Vieregg, J.; Bryant, J.; Elena, B.; Kreischer, K. E.; Temkin, R. J.; Griffin, R. G. *J. Magn. Reson.* **2003**, *160*, 85-90.

99. Jacso, T.; Franks, W. T.; Rose, H.; Fink, U.; Broecker, J.; Keller, S.; Oschkinat, H.; Reif, B. *Angew. Chem. Int. Ed.* **2012**, *51*, 432-435.

100. Salnikov, E.; Rosay, M.; Pawsey, S.; Ouari, O.; Tordo, P.; Bechinger, B. *J. Am. Chem. Soc.* **2010**, *132*, 5940-5941.

101. Linden, A. H.; Lange, S.; Franks, W. T.; Akbey, Ü .; Specker, E.; van Rossum, B.-J.; Oschkinat, H. *J. Am. Chem. Soc.* **2011**, *133*, 19266-19269.

102. Reggie, L.; Lopez, J. J.; Collinson, I.; Glaubitz, C.; Lorch, M. *J. Am. Chem. Soc.* **2011**, *133*, 19084-19086.

103. Bayro, M. J.; Debelouchina, G. T.; Eddy, M. T.; Birkett, N. R.; MacPhee, C. E.; Rosay, M.; Maas, W. E.; Dobson, C. M.; Griffin, R. G. *J. Am. Chem. Soc.* **2011**, *133*, 13967-13974.

104. Lelli, M.; Gajan, D.; Lesage, A.; Caporini, M. A.; Vitzthum, V.; Miéville, P.; Héroguel, F.; Rascón, F.; Roussey, A.; Thieuleux, C.; Boualleg, M.; Veyre, L.; Bodenhausen, G.; Coperet, C.; Emsley, L. *J. Am. Chem. Soc.* **2011**, *133*, 2104-2107.

105. Lesage, A.; Lelli, M.; Gajan, D.; Caporini, M. A.; Vitzthum, V.; Miéville, P.; Alauzun, J.; Roussey, A.; Thieuleux, C.; Mehdi, A.; Bodenhausen, G.; Coperet, C.; Emsley, L. *J. Am. Chem. Soc.* **2010**, *132*, 15459-15461.

106. Zagdoun, A.; Casano, G.; Ouari, O.; Lapadula, G.; Rossini, A. J.; Lelli, M.; Baffert, M.; Gajan, D.; Veyre, L.; Maas, W. E.; Rosay, M.; Weber, R. T.; Thieuleux, C.; Coperet, C.; Lesage, A.; Tordo, P.; Emsley, L. *J. Am. Chem. Soc.* **2011**, *134*, 2284-2291.

107. Rossini, A. J.; Zagdoun, A.; Lelli, M.; Canivet, J.; Aguado, S.; Ouari, O.; Tordo, P.; Rosay, M.; Maas, W. E.; Copéret, C.; Farrusseng, D.; Emsley, L.; Lesage, A. *Angew. Chem. Int. Ed.* **2012**, *51*, 123-127.

108. Rossini, A. J.; Zagdoun, A.; Hegner, F.; Schwarzwälder, M.; Gajan, D.; Copéret, C.; Lesage, A.; Emsley, L. *J. Am. Chem. Soc.* **2012**, *134*, 16899-16908.

109. Ardenkjaer-Larsen, J. H.; Fridlund, B.; Gram, A.; Hansson, G.; Hansson, L.; Lerche, M. H.; Servin, R.; Thaning, M.; Golman, K. *Proc. Natl. Acad. Sci. U. S. A.* **2003**, *100*, 10158-10163.

110. Wenckebach, W. T. *Appl. Magn. Reson.* **2008**, *34*, 227-235.

111. Golman, K.; Olsson, L. E.; Axelsson, O.; Mansson, S.; Karlsson, M.; Petersson, J. S. *British Journal of Radiology* **2003**, *76*, S118-S127.

112. Golman, K.; Ardenaer-Larsen, J. H.; Petersson, J. S.; Mansson, S.; Leunbach, I. *Proc. Natl. Acad. Sci. U. S. A.* **2003**, *100*, 10435-10439.

113. Day, S. E.; Kettunen, M. I.; Gallagher, F. A.; Hu, D. E.; Lerche, M.; Wolber, J.; Golman, K.; Ardenkjaer-Larsen, J. H.; Brindle, K. M. *Nat. Med.* **2007**, *13*, 1382-1387.

114. Golman, K.; in't Zandt, R.; Thaning, M. *Proc. Natl. Acad. Sci. U. S. A.* **2006**, *103*, 11270-11275.

115. Golman, K.; in't Zandt, R.; Lerche, M.; Pehrson, R.; Ardenkjaer-Larsen, J. H. *Cancer Res.* **2006**, *66*, 10855-10860.

116. Gallagher, F. A.; Kettunen, M. I.; Day, S. E.; Hu, D. E.; Ardenkjaer-Larsen, J. H.; in't Zandt, R.; Jensen, P. R.; Karlsson, M.; Golman, K.; Lerche, M. H.; Brindle, K. M. *Nature* **2008**, *453*, 940-943.

117. Hu, S.; Larson, P. E. Z.; VanCriekinge, M.; Leach, A. M.; Park, I.; Leon, C.; Zhou, J.; Shin, P. J.; Reed, G.; Keselman, P.; von Morze, C.; Yoshihara, H.; Bok, R. A.; Nelson, S. J.; Kurhanewicz, J.; Vigneron, D. B. *Magn. Reson. Imaging*.

118. Hu, S.; Yoshihara, H. A. I.; Bok, R.; Zhou, J.; Zhu, M.; Kurhanewicz, J.; Vigneron, D. B. *Magn. Reson. Imaging* **2012**, *30*, 1367-1372.

119. Reed, G. D.; Larson, P. E. Z.; Morze, C. v.; Bok, R.; Lustig, M.; Kerr, A. B.; Pauly, J. M.; Kurhanewicz, J.; Vigneron, D. B. *J. Magn. Reson.* **2012**, *217*, 41-47.

120. Lerche, M. H.; Meier, S.; Jensen, P. R.; Hustvedt, S.-O.; Karlsson, M.; Duus, J. Ø .; Ardenkjæ r-Larsen, J. H. *NMR Biomed.* **2011**, *24*, 96-103.

121. Wilson, D. M.; Hurd, R. E.; Keshari, K.; Van Criekinge, M.; Chen, A. P.; Nelson, S. J.; Vigneron, D. B.; Kurhanewicz, J. *Proc. Natl. Acad. Sci. U. S. A.* **2009**, *106*, 5503-5507.

122. Kurdzesau, F.; van den Brandt, B.; Comment, A.; Hautle, P.; Jannin, S.; van der Klink, J. J.; Konter, J. A. *J. Phys. D: Appl. Phys.* **2008**, *41*.

123. Bowen, S.; Sekar, G.; Hilty, C. *NMR Biomed.* **2011**, *24*, 1016-1022.

124. Day, I. J.; Mitchell, J. C.; Snowden, M. J.; Davis, A. L. *Appl. Magn. Reson.* **2008**, *34*, 453-460.

125. Gabellieri, C.; Reynolds, S.; Lavie, A.; Payne, G. S.; Leach, M. O.; Eykyn, T. R. *J. Am. Chem. Soc.* **2008**, *130*, 4598-4599.

126. Sarkar, R.; Comment, A.; Vasos, P. R.; Jannin, S.; Gruetter, R.; Bodenhausen, G.; Hall, H.; Kirik, D.; Denisov, V. P. *J. Am. Chem. Soc.* **2009**, *131*, 16014-16015.

127. Lerche, M. H.; Meier, S.; Jensen, P. R.; Baumann, H.; Petersen, B. O.; Karlsson, M.; Duus, J. O.; Ardenkjaer-Larsen, J. H. *J. Magn. Reson.* **2010**, *203*, 52-56.

128. Frydman, L.; Blazina, D. *Nat. Phys.* **2007**, *3*, 415-419.

129. Mishkovsky, M.; Frydman, L. *ChemPhysChem* **2008**, *9*, 2340-2348.

130. Panek, R.; Granwehr, J.; Leggett, J.; Kockenberger, W. *Phys. Chem. Chem. Phys.* **2010**, *12*, 5771-5778.

131. Bowen, S.; Zeng, H.; Hilty, C. *Anal. Chem.* **2008**, *80*, 5794-5798.

132. Zeng, H.; Bowen, S.; Hilty, C. *J. Magn. Reson.* **2009**, *199*, 159-165.

133. Bowen, S.; Hilty, C. *Angew. Chem. Int. Ed.* **2008**, *47*, 5235-5237.

134. Jensen, P. R.; Meier, S.; Ardenkjaer-Larsen, J. H.; Duus, J. O.; Karlsson, M.; Lerche, M. H. *Chem. Commun.* **2009**, 5168-5170.

135. Bowen, S.; Hilty, C. *Anal. Chem.* **2009**, *81*, 4543-4547.

136. Zeng, H.; Lee, Y.; Hilty, C. *Anal. Chem.* **2010**, *82*, 8897-8902.

137. Bowen, S.; Hilty, C. *Phys. Chem. Chem. Phys.* **2010**, *12*, 5766-5770.

138. Lee, Y.; Zeng, H.; Mazur, A.; Wegstroth, M.; Carlomagno, T.; Reese, M.; Lee, D.; Becker, S.; Griesinger, C.; Hilty, C. *Angew. Chem. Int. Ed.* **2012**, *51*, 5179-82.

139. Lee, Y.; Zeng, H.; Ruedisser, S.; Gossert, A. D.; Hilty, C. *J Am Chem Soc* **2012**, *134*, 17448-51.

140. Hajduk, P. J.; Meadows, R. P.; Fesik, S. W. *Q. Rev. Biophys.* **1999**, *32*, 211-240.

141. Dalvit, C.; Fagerness, P. E.; Hadden, D. T. A.; Sarver, R. W.; Stockman, B. J. *J. Am. Chem. Soc.* **2003**, *125*, 7696-7703.

142. Fielding, L. *Tetrahedron* **2000**, *56*, 6151-6170.

143. Shuker, S. B.; Hajduk, P. J.; Meadows, R. P.; Fesik, S. W. *Science* **1996**, *274*, 1531-1534.

144. Dalvit, C.; Flocco, M.; Knapp, S.; Mostardini, M.; Perego, R.; Stockman, B. J.; Veronesi, M.; Varasi, M. *J. Am. Chem. Soc.* **2002**, *124*, 7702-7709.

145. Jahnke, W.; Floersheim, P.; Ostermeier, C.; Zhang, X.; Hemmig, R.; Hurth, K.; Uzunov, D. P. *Angew. Chem. Int. Ed.* **2002**, *41*, 3420-3423.

146. Guan, H.-P.; Hu, C.-M. *Synthesis* **1996**, *1996*, 1363-1370.

147. van Beek, J. D. *J. Magn. Reson.* **2007**, *187*, 19-26.

148. Brownstein, S.; Bornais, J. *J. Magn. Reson.* **1980**, *38*, 131-133.

149. Harris, R. K.; Becker, E. D.; de Menezes, S. M. C.; Goodfellow, R.; Granger, P. *Pure Appl. Chem.* **2001**, *73*, 1795-1818.

150. Cavanagh, J.; Fairbrother, W. J.; Palmer Iii, A. G.; Rance, M.; Skelton, N. J., in *Protein NMR Spectroscopy (Second Edition)*. Academic Press: San Diego, CA, 2007.

151. Fielding, L. *Prog. Nucl. Magn. Reson. Spectrosc.* **2007**, *51*, 219-242.

152. Ismail, F. M. D. *J. Fluorine Chem.* **2002**, *118*, 27-33.

153. Müller, K.; Faeh, C.; Diederich, F. *Science* **2007**, *317*, 1881-1886.

154. *MDDR (Drug Data Report)*; San Leandro, CA, 2010.

155. Vulpetti, A.; Hommel, U.; Landrum, G.; Lewis, R.; Dalvit, C. *J. Am. Chem. Soc.* **2009**, *131*, 12949-12959.

156. Dalvit, C. *Prog. Nucl. Magn. Reson. Spectrosc.* **2007**, *51*, 243-271.

157. Vulpetti, A.; Schiering, N.; Dalvit, C. *Proteins: Struct., Funct., Bioinf.* **2010**, *78*, 3281-3291.

158. Carr, H. Y.; Purcell, E. M. *Phys. Rev.* **1954**, *94*, 630-638.

159. Meiboom, S.; Gill, D. *Rev. Sci. Instrum.* **1958**, *29*, 688-691.

160. Zhang, X.; Sänger, A.; Hemmig, R.; Jahnke, W. *Angew. Chem. Int. Ed.* **2009**, *48*, 6691-6694.

161. Ernst, R. R.; Bodenhausen, G.; Wokaun, A., *Principles of Nuclear Magnetic Resonance in One and Two Dimensions* Clarendon Press: Oxford, 1990; p 610.

162. Mayer, M.; Meyer, B. *J. Am. Chem. Soc.* **2001**, *123*, 6108-6117.

163. Sánchez-Pedregal, V. M.; Reese, M.; Meiler, J.; Blommers, M. J. J.; Griesinger, C.; Carlomagno, T. *Angew. Chem. Int. Ed.* **2005**, *44*, 4172-4175.

164. Reese, M.; Sánchez-Pedregal, V. M.; Kubicek, K.; Meiler, J.; Blommers, M. J. J.; Griesinger, C.; Carlomagno, T. *Angew. Chem. Int. Ed.* **2007**, *46*, 1864-1868.

165. Orts, J.; Tuma, J.; Reese, M.; Grimm, S. K.; Monecke, P.; Bartoschek, S.; Schiffer, A.; Wendt, K. U.; Griesinger, C.; Carlomagno, T. *Angew. Chem. Int. Ed.* **2008**, *47*, 7736-7740.

166. Orts, J.; Griesinger, C.; Carlomagno, T. *J. Magn. Reson.* **2009**, *200*, 64-73.

167. Bartoschek, S.; Klabunde, T.; Defossa, E.; Dietrich, V.; Stengelin, S.; Griesinger, C.; Carlomagno, T.; Focken, I.; Wendt, K. U. *Angew. Chem. Int. Ed.* **2010**, *49*, 1426-1429.

168. Ni, F. *Prog. Nucl. Magn. Reson. Spectrosc.* **1994**, *26*, 517-606.

169. Chen, H. Y.; Lee, Y.; Bowen, S.; Hilty, C. *J. Magn. Reson.* **2011**, *208*, 204-209.

170. Langer, T.; Vogtherr, M.; Elshorst, B.; Betz, M.; Schieborr, U.; Saxena, K.; Schwalbe, H. *ChemBioChem* **2004**, *5*, 1508-1516.

171. Zeng, H. Quantitative Determination of Chemical Processes by Dynamic Nuclear Polarization enhanced Nuclear Magnetic Resonance Spectroscopy. Ph. D. Thesis, Texas A&M University, College Station, 2012.

172. Ando, I.; Yamanobe, T.; Asakura, T. *Prog. Nucl. Magn. Reson. Spectrosc.* **1990**, *22*, 349-400.

173. So, Y.-H.; Heeschen, J. P.; Bell, B.; Bonk, P.; Briggs, M.; DeCaire, R. *Macromolecules* **1998**, *31*, 5229-5239.

174. Kricheldorf, H. R.; Kreiser-Saunders, I.; Stricker, A. *Macromolecules* **2000**, *33*, 702-709.

175. Pellecchia, C.; Grassi, A. *Top. Catal.* **1999**, *7*, 125-132.

176. Moad, G.; Rizzardo, E.; Solomon, D. H.; Johns, S. R.; Willing, R. I. *Macromol. Rapid Commun.* **1984**, *5*, 793-798.

177. Ragavan, M.; Chen, H.-Y.; Sekar, G.; Hilty, C. *Anal. Chem.* **2011**, *83*, 6054-6059.

178. Hilty, C.; Bowen, S. *Org. Biomol. Chem.* **2010**, *8*, 3361-3365.

179. Heimenz, P.; Lodge, T., *Polymer Chemistry, Second Edition*. Taylor&Francis: 2007.

180. Baskaran, D.; Müller, A. H. E. *Prog. Polym. Sci.* **2007**, *32*, 173-219.

181. Baskaran, D.; Müller, A., *Anionic Vinyl Polymerization*. Wiley-VCH: 2009.

182. Webster, O. W. *Science* **1991**, *251*, 887-893.

183. Szwarc, M. *Nature* **1956**, *178*, 1168-1169.

184. Szwarc, M.; Levy, M.; Milkovich, R. *J. Am. Chem. Soc.* **1956**, *78*, 2656-2657.

185. Stretch, C.; Allen, G. *Polymer* **1961**, *2*, 151-160.

186. Szwarc, M. *Pure Appl. Chem.* **1984**, *56*, 447-460.

187. Zierhut, M. L.; Yen, Y. F.; Chen, A. P.; Bok, R.; Albers, M. J.; Zhang, V.; Tropp, J.; Park, I.; Vigneron, D. B.; Kurhanewicz, J.; Hurd, R. E.; Nelson, S. J. *J. Magn. Reson.* **2010**, *202*, 85-92.

188. Montaudo, G.; Samperi, F.; Montaudo, M. S. *Prog. Polym. Sci.* **2006**, *31*, 277-357.

189. Ryu, J.; Im, K.; Yu, W.; Park, J.; Chang, T.; Lee, K.; Choi, N. *Macromolecules* **2004**, *37*, 8805-8807.

190. Stretch, C.; Allen, G. *Proc. Chem. Soc.* **1959**, 399.

191. Dainton, F.; East, G.; Harpell, G.; Hurworth, N.; Ivin, K.; LaFlair, R.; Pallen, R.; Hui, K. *Macromol. Chem. Phys.* **1965**, *89*, 257-262.

192. Matsuzaki, K.; Shinohara, Y.; Kanai, T. *Macromol. Chem. Phys.* **1980**, *181*, 1923-1934.

193. Hsieh, H.; Quirk, R. P., *Anionic polymerization: principles and practical applications*. CRC: 1996; Vol. 34.

194. Szwarc, M., in *Living Polymers and Mechanisms of Anionic Polymerization*. Springer Berlin Heidelberg, 1983, vol. 49, pp 1-177.

195. Beylen, M. v.; Bhattacharyya, D. N.; Smid, J.; Szwarc, M. *J. Phys. Chem.* **1966**, *70*, 157-161.

196. Bywater, S.; Worsfold, D. J. *Can. J. Chem.* **1962**, *40*, 1564-1570.

197. Doi, Y.; Ueki, S.; Keii, T. *Macromolecules* **1979**, *12*, 814-819.

198. Doi, Y.; Suzuki, S.; Soga, K. *Macromolecules* **1986**, *19*, 2896-2900.

199. Schugens, C.; Maquet, V.; Grandfils, C.; Jérôme, R.; Teyssie, P. *J. Biomed. Mater. Res., Part A* **1998**, *30*, 449-461.

200. Ray, S. S.; Maiti, P.; Okamoto, M.; Yamada, K.; Ueda, K. *Macromolecules* **2002**, *35*, 3104-3110.

201. Dechy-Cabaret, O.; Martin-Vaca, B.; Bourissou, D. *Chem. Rev.* **2004**, *104*, 6147-6176.

202. Csihony, S.; Culkin, D. A.; Sentman, A. C.; Dove, A. P.; Waymouth, R. M.; Hedrick, J. L. *J. Am. Chem. Soc.* **2005**, *127*, 9079-9084.

203. Dove, A. P.; Pratt, R. C.; Lohmeijer, B. G. G.; Waymouth, R. M.; Hedrick, J. L. *J. Am. Chem. Soc.* **2005**, *127*, 13798-13799.

204. Pratt, R. C.; Lohmeijer, B. G. G.; Long, D. A.; Waymouth, R. M.; Hedrick, J. L. *J. Am. Chem. Soc.* **2006**, *128*, 4556-4557.

205. Lohmeijer, B. G. G.; Pratt, R. C.; Leibfarth, F.; Logan, J. W.; Long, D. A.; Dove, A. P.; Nederberg, F.; Choi, J.; Wade, C.; Waymouth, R. M.; Hedrick, J. L. *Macromolecules* **2006**, *39*, 8574-8583.

206. Chuma, A.; Horn, H. W.; Swope, W. C.; Pratt, R. C.; Zhang, L.; Lohmeijer, B. G. G.; Wade, C. G.; Waymouth, R. M.; Hedrick, J. L.; Rice, J. E. *J. Am. Chem. Soc.* **2008**, *130*, 6749-6754.

207. Simón, L.; Goodman, J. M. *J. Org. Chem.* **2007**, *72*, 9656-9662.

208. Brown, H. A.; De Crisci, A. G.; Hedrick, J. L.; Waymouth, R. M. *ACS Macro Lett.* **2012**, *1*, 1113-1115.

209. Li, J.; Sha, Y. *Molecules* **2008**, *13*, 1111-1119.

210. Geen, H.; Freeman, R. *J. Magn. Reson.* **1991**, *93*, 93-141.

211. Warshel, A.; Naray-Szabo, G.; Sussman, F.; Hwang, J. K. *Biochemistry* **1989**, *28*, 3629-3637.

212. Hedstrom, L. *Chem. Rev.* **2002**, *102*, 4501-4524.